

Surface-induced Dissociation for Application in Mass Spectrometry

ACADEMISCH PROEFSCHRIFT

ter verkrijging van de graad van doctor aan de Universiteit van Amsterdam op gezag van de Rector Magnificus prof. dr. J.J.M. Franse, ten overstaan van een door het college voor promoties ingestelde commissie in het openbaar te verdedigen in de Aula der Universiteit op woensdag 30 juni 1999, te 11:00 uur.

door

Adriana de Maaijer-Gielbert

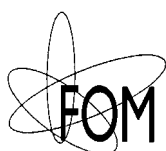
geboren te Rotterdam

Promotiecommissie

promotor	Prof. dr. P.G. Kistemaker
copromotor	Dr. T.L. Weeding
overige leden	Prof. dr. J.J. Boon Dr. W. Genuit Prof. dr. J. Haverkamp Prof. dr. A.W. Kleyn Dr. C.G. de Koster Prof. dr. P.W.N.M. van Leeuwen Prof. dr. N.M.M. Nibbering

Faculteit der Scheikunde

*Cover design in collaboration with H. Sodenkamp
Compartment C, Car 193, 1938, Edward Hopper
Armonk (NY), Collection IBM Corporation*



The work in this thesis was performed at the FOM-insituut voor Atoom- en Molecuulfysica, Kruislaan 407, 1098 SJ Amsterdam, The Netherlands. It is part of the research program of the Stichting voor Fundamenteel Onderzoek der Materie (FOM) and was made possible by financial support from the Stichting Technische Wetenschappen (STW).

*aan mijn ouders
aan Remco
aan Wendelien*

This thesis is based on the following papers:

Chapter 2:

Surface-induced dissociation of benzene on a PFPE liquid insulator in a time-of-flight mass spectrometer

J. de Maaijer-Gielbert, J.H.M. Beijersbergen, P.G. Kistemaker and T.L. Weeding

International Journal of Mass Spectrometry and Ion Processes 153 (1996) 119-128

Chapter 3:

Surface-induced dissociation of diphenyl ether

J. de Maaijer-Gielbert, Á. Somogyi, V.H. Wysocki, P.G. Kistemaker and T.L. Weeding

International Journal of Mass Spectrometry and Ion Processes 153 (1996) 119-128

Chapter 4:

ESI/SID of polypropylenamine dendrimers

J. de Maaijer-Gielbert, C. Gu, Á. Somogyi, V.H. Wysocki, P.G. Kistemaker and T.L. Weeding

Advances in Mass Spectrometry 14 (1998) ThOr09

Surface-induced dissociation of singly and multiple protonated POPAM dendrimers

J. de Maaijer-Gielbert, C. Gu, Á. Somogyi, V.H. Wysocki, P.G. Kistemaker and T.L. Weeding

Journal of the American Society for Mass Spectrometry 10 (1999) 414-422

Chapter 5:

J. de Maaijer-Gielbert, C. Gu, V.H. Wysocki, L. Drahos, R.M.A. Heeren, P.G. Kistemaker and T.L. Weeding

To be published

Table of Contents

Chapter 1: General Introduction	7
1.1 Mass Spectrometry and Ion Activation.....	7
1.2 Polyatomic Ion/Solid Interactions	8
1.3 Surface-Induced Dissociation in Mass Spectrometry	10
1.3.1 Instrumentation	10
1.3.2 The role of the collision surface	10
1.3.3 The fragmentation of ions of macromolecules by SID.....	12
1.4 Other activation methods for ions of high molecular weight	12
1.4.1 Activation by a single high-energy gas phase collision	12
1.4.2 Activation by multiple low-energy gas-phase collisions.....	13
1.4.3 Other methods	14
Chapter 2: Surface-induced dissociation of benzene on a PFPE liquid insulator in a time-of-flight mass spectrometer	15
2.1 Introduction	15
2.2 Experimental	16
2.3 Results and Discussion	19
2.3.1 Liquid insulator surface.....	19
2.3.2 Fragment mass spectra	20
2.3.3 Energy conversion efficiency	22
2.3.4 Width of SID-fragment peaks.....	23
Chapter 3: Surface-induced dissociation of diphenyl ether	25
3.1 Introduction	25
3.2 Experimental	27
3.3 Results and Discussion	28
3.3.1 Spectra and ER-SID diagrams.....	28
3.3.2 Estimate of energy conversion.....	35
3.3.3 Ion/surface reactions	38
3.4. Conclusions.....	42
Chapter 4: Surface-induced dissociation of singly and multiply protonated polypropylenamine dendrimers	43
4.1 Introduction	43
4.2 Experimental	46
4.3 Results and Discussion	48
4.3.1 SID spectra	48
4.3.2 Gas-phase basicity and Coulomb interactions.....	51
4.3.3 Fragmentation efficiency.....	54

4.4 Conclusions.....	56
Chapter 5: Activation of POPAM dendrimers by low-energy multiple collision CID in trapped ion mass spectrometers	57
5.1 Introduction	57
5.2 Experimental	59
5.2.1 ITMS experiments.....	59
5.2.2 FTMS experiments	60
5.2.3 sample preparation	61
5.2.4 Computational details	61
5.3. Results	62
5.3.1 ITMS experiments.....	57
5.3.2 Energy-resolved CID and SID.....	64
5.4. Discussion.....	67
5.4.1 Fragment ions.....	67
5.4.2 Internal energies and dissociation rates in SID.....	68
5.4.3 Dissociation rates calculated with RRKM theory.....	70
5.4.4 Internal energies and dissociation rates in FTMS CID.....	73
5.5. Conclusions.....	78
References.....	79
Summary.....	91
Samenvatting	95
Nawoord	99

General Introduction

1.1 Mass Spectrometry and Ion Activation

Mass spectrometry is a powerful analytical technique used for the identification of a compound or the components of a mixture. For this identification, the molecular weights of the components can be determined based on the mass-to-charge ratio of ions made from intact constituents of a sample. In addition, fragmentation of the constituents and/or their ions followed by mass spectrometric detection can be used. Fragmentation can be used to increase the selectivity and sensitivity of the identification, or to identify the structural units of an unknown compound. Fragmentation of molecules or ions from a sample can be achieved before or during the ionization process, or in a separate step after ionization. The extent to which fragmentation is observed depends on the combination of the mass spectrometric methods and the properties of the analyte. The internal energy before ionization and the ionization method influence the energy that is left above the ionization threshold of the analyte. The fragmentation rate is influenced by the available internal energy after ionization. The relation between internal energy and rate of a given fragmentation reaction is a property specific of the analyte. The time available for fragmentation reactions in the mass spectrometer determines the observed amount of fragmentation at a given fragmentation rate (see, for example, [1]). The ionization methods which deposit relatively large amounts of internal energy and therefore often induce fragmentation, are known as 'hot' ionization techniques, for example 70 eV electron ionization (EI) and ^{252}Cf plasma desorption (PD). Ionization methods which in principle allow low energy deposition are referred to as 'soft' or 'mild' processes, for example (multi) photon ionization ((M)PI), chemical ionization (CI), field desorption (FD), surface ionization (SI) and electrospray ionization (ESI). Fast atom bombardment (FAB) or fast ion bombardment, usually referred to as 'liquid' secondary ion mass spectrometry (LSIMS) and matrix-assisted laser desorption/ionization (MALDI) are regarded as intermediate.

Especially with soft ionization methods it is not always possible to obtain sufficient fragmentation in the ionization process to obtain information about both the molecular weight and fragment molecular weights in a single stage. It may also be desirable to

separate the fragmentation from the ionization step, for example in the analysis of mixtures. Tandem mass spectrometry or MS/MS is a method by which compounds are analyzed in multiple stages. In the first MS stage, a compound or mixture of compounds is ionized and ions of a given mass-to-charge ratio are selected. These ions are fragmented in a following stage, and a fragment mass spectrum is recorded. Another advantage of separating ionization and activation processes can be the ability to vary the degree of fragmentation without affecting the ionization efficiency, for example in MALDI.

Many methods which can be used for ionization can also be used to add energy to ions after the ionization process: irradiation by electrons or photons, collisions with atoms or collisions with solid surfaces. Collision induced dissociation (CID) utilizes energetic collisions of ions with a light gas such as He, Ar, Xe or N₂ to increase the internal energy of the ions, and is a common method in tandem mass spectrometry. Recently several authors have reported on the versatility of ion activation by means of energetic ion/surface collisions, referred to as surface-induced dissociation (SID) [2, 3]. SID has advantages such as unity collision probability, high kinetic-to-internal energy conversion efficiency and, possibly, better reproducibility of fragmentation which could improve fragment library matching. The utilization of SID in a mass spectrometer instead of CID reduces vacuum requirements and allows application with wider ion beams, facilitating instrument design. This thesis is intended to give prospects for the activation of ions by colliding them with a surface for mass spectrometric applications. In this thesis the possibilities and limitations of the implementation of SID are studied, SID results from different mass spectrometers are compared, SID is applied to study macromolecules and is compared to multiple low-energy CID.

1.2 Polyatomic Ion/Solid Interactions

The study and application of ion/solid collision phenomena have a long-standing history in physics and have been of importance for developments within the field of mass spectrometry. Processes occurring upon impact of ions with solids are scattering of the incident ions, charge exchange, sputtering of ions or neutrals from the surface, trapping, implantation, emission of electrons or photons, and chemical reactions (see, for example, [2, 4, 5]). Ion/solid interactions have been used for surface analysis by ion scattering (10^1 - 10^3 eV), surface modification by chemical reactions (10^1 - 10^3 eV), cleaning and lithography (10^2 - 10^4 eV), implantation (10^3 - 10^6 eV) and nuclear fission ($>10^7$ eV). In addition to ion activation by SID, mass spectrometric applications of ion/solid collisions include the detection of ions and ionization methods such as SI, ²⁵²Cf plasma desorption, SIMS and LSIMS.

The laboratory collision energy for SID is in the range of 10^1 - 10^3 eV (low-collision energy range). In this energy range also other processes occur, which can either obscure

or augment the information in the SID fragment spectra. Figure 1.1 shows a cartoon summarizing the processes known to be possible processes upon low-energy ion/surface collisions. An important process upon ion impact with a surface in the 10^1 - 10^3 eV energy range is neutralization of the incident ions. Since mass spectrometers commonly detect charged species, the fragments from the neutralized compound are not useful unless reionization takes place.

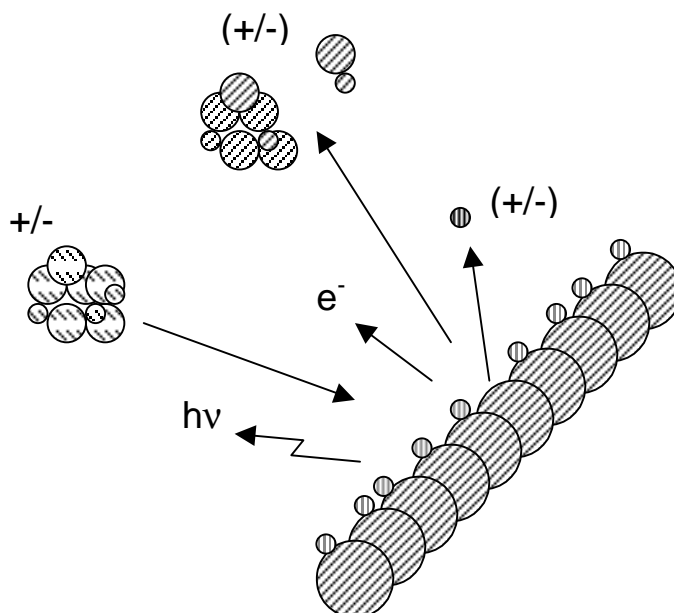


Figure 1.1: cartoon summarizing processes which can occur upon ion/solid collisions in the 10^1 - 10^3 eV laboratory collision energy range.

The most important mechanism for internal excitation of polyatomic ions upon their collision with a solid surface, in which the ion remains charged after the collision, is impulsive excitation. The first impulsive model developed for dissociative molecule/surface collisions was based on a diatomic molecule, in which the atoms were forced follow independent trajectories as a result of the collision. This involved different impact parameters for each atom and subsequently dissociation could occur [6]. More recently, models have been proposed inferring vibrational excitation occurring upon compression of one or more bonds in the collision process [7].

Processes besides ion activation which can occur upon low-energy collisions of polyatomic ions with a surface are secondary ion and secondary electron emission [8-12] photon emission [13] and ion/surface reactions [2, 14, 15]. These processes have been applied in studies both of fundamental and of analytical character. Ion/surface reaction phenomena are discussed in a following paragraph.

1.3 Surface-Induced Dissociation in Mass Spectrometry

1.3.1 Instrumentation

The possible employment of SID for mass spectrometric analysis was first suggested by Cooks et al. in 1975 [16, 17]. In 1977, Gandy et al. reported the use of a stainless steel collision device inserted in the acceleration region of a time-of-flight (TOF) mass spectrometer for collisional activation of parent ions, which were selected by an orthogonally coupled magnetic spectrometer [18]. In 1985, Cooks and coworkers implemented the SID technique in a hybrid magnetic sector-quadrupole (BQ) mass spectrometer and demonstrated the efficient fragmentation of small hydrocarbon cations on a stainless steel collision surface [19, 20]. In the following years, Cooks and coworkers demonstrated that SID could be implemented in various types of mass spectrometers, such as TOF [21, 22], 2D quadrupole [23] and quadrupole ion trap (IT) [24] mass spectrometers. SID has been implemented in a four-sector mass spectrometer by Jennings and coworkers [25-27], in a Fourier transform ion cyclotron mass spectrometer (FTMS) in the groups of Wilkins [28-30] and McLafferty [31, 32], and in a TOF mass spectrometer by Whetten and coworkers [9, 33-36] and Zare and coworkers [37, 38]. Tandem quadrupole mass spectrometers are employed by Wysocki and coworkers [39].

Time-of-flight mass spectrometers have an in principle unlimited mass range and are routinely combined with both MALDI and ESI as well as with many other ionization methods. This makes it very attractive to implement SID in a TOF mass spectrometer. Although good resolution can be obtained with TOF, SID-TOF spectra have been demonstrated with only low fragment ion resolution [21, 22, 37, 38, 40]. Various factors are responsible, such as the time distribution of the parent ions at the collision surface and the initial kinetic energy distribution of the fragment ions leaving the surface. In a tandem linear geometry, it is necessary that the parent ion beam be time-focused at the collision surface to have optimal starting conditions for the daughter ions. For optimal resolution in selection of the parent ions, their time-focusing at the selection device is also necessary. These two conditions are in conflict when parent ion selection and surface collision are spatially separate as in previous studies [21, 22, 37, 38, 40]. In Chapter 2 of this thesis, optimal resolution in parent ion selection has been combined with parent ion time-focusing at the collision surface by pulsing the voltage on the collision surface. Chapter 3 contains a comparison between the 90° arrangement of the quadrupole mass spectrometers in Wysocki's group [39] and the tandem linear TOF set-up at FOM.

1.3.2 The role of the collision surface

Charge retention. The collection of charged fragments is crucial for the use of SID

in mass spectrometry. In the early SID experiments by Cooks and coworkers, although the fragmentation was efficient, neutralization appeared also an efficient process. Fragment ion yields were found to improve significantly when a thin insulating layer was applied on top of a conducting surface, compared to yields from a bare conducting surface. Self-assembled monolayer (SAM) surfaces, consisting of alkanethiol compounds grown on vapor-deposited or single-crystal gold or silver surfaces, appeared useful [41-43]. Somogyi et al. have measured the ratio of the ion current before and after ion/ surface collision to determine the probability of charge retention by the analyte. For 30eV collisions of the benzene radical cation with C₄, C₁₂ and C₁₈ SAM surfaces this is 1.5, 11 and 12%, respectively, and 66% for a fluorinated (F-) C₁₀ SAM surface [15]. With these SAMs neutralization could be reduced for a conducting collision surface, which is preferred to prevent its charging, which could result in an undefined collision energy.

Pradeep et al. proposed a liquid perfluorinated polyether (PFPE) oil film applied to a conducting surface as an alternative to the F-SAM surface [44]. This surface has the same properties as the F-SAM surface with respect to fragment ion yield and absence of charging of the surface. In addition, the PFPE film appeared insensitive to damage by the incident ion beam or contamination from background hydrocarbon molecules and ions [44]. Koppers et al. have studied the dissociative scattering of CF₃⁺ ions from clean and barium-covered Ag(111) [45, 46] surfaces and from a liquid PFPE film [47, 48]. This research clearly showed that for the clean metal surface, neutralization and subsequent electronic excitation was responsible for observed dissociation products, whereas collisional excitation was dominant for the insulating liquid PFPE surface. The TOF-SID experiments described in Chapter 2 and 3 of this thesis have also been obtained with the use of a liquid PFPE film as the collision surface.

Reactivity. In the SID fragment mass spectra of various radical cations, products were observed which were ascribed to abstraction of groups from species present on the surface [2, 22, 41, 42, 49-54]. Ion/surface reaction spectra can be used both to characterize the reactivity and hence the condition of the collision surface [15, 55] or to characterize the reactivity of, for example, isomeric ions [56]. In Chapter 3 of this thesis the ion/surface reactions of (perdeuterated) diphenyl ether molecular and fragment ions with self-assembled monolayers are reported.

Conversion of kinetic to internal energy. Of fundamental interest for the application of SID in mass spectrometry is how efficiently the collisional energy is converted into internal energy of the incident ions. The composition of the collision surface influences the energy conversion. Several groups have studied collision-energy dependent SID fragment spectra to determine energy conversion efficiencies [2, 21, 23, 42, 44, 57]. In these studies ions of known fragment ion appearance energies are used, referred to as "thermometer ions". Examples are tetraethylsilane (Si(Et)₄⁺) [21, 23], butylbenzene (C₁₀H₁₄⁺) [2], iron pentacarbonyl (Fe(CO)₅⁺) [2] and tungsten hexacarbonyl (W(CO)₆⁺)

ions [42, 44]. Using these thermometer molecules, Cooks and coworkers found average efficiencies for conversion of kinetic into internal energy of 10-15% for stainless steel and alkanethiolate SAM surfaces [2] and 17-20% for fluorinated (F-SAM and PFPE) surfaces [42, 44]. The benzene radical cation was used as a thermometer ion by Vékey et al. [57]. The average conversion efficiency obtained by deconvolution of benzene SID spectra was higher than obtained from the carbonyl ion spectra: 17% for alkanethiolate SAM surfaces and 28% for F-SAM surfaces. In Chapter 2 of this thesis energy-resolved benzene SID spectra, obtained in the tandem linear TOF set-up with a PFPE covered stainless steel collision surface, are deconvoluted to estimate the internal energy distribution. In Chapter 3, a similar deconvolution of diphenyl ether SID spectra is used to estimate fragmentation efficiencies at laboratory energies higher than 80 eV. In addition, the energy conversion in the tandem linear TOF set-up and the tandem quadrupole set-up are compared.

1.3.3 The fragmentation of ions of macromolecules by SID

The efficient kinetic to internal energy conversion by SID makes it a promising technique for excitation of macromolecules. The more degrees of freedom over which internal energy can be distributed, the more energy is required to effect fragmentation of ions on the time scale of the mass spectrometer [1, 58]. The application of SID for macromolecule analysis was initiated simultaneously in the groups of Cooks [59], Wilkins [28-30] and McLafferty [31] for biological compounds in the range of 1-3 ku. Later McLafferty's group applied SID to peptides up to 29 ku in a FTMS [32]. The most extensive SID studies of macromolecules have been performed by Wysocki and coworkers, who used SID to investigate the influence of the composition of peptide ions on the ease of fragmentation [60-63]. The use of energy-resolved SID enabled them to demonstrate the dependence of the ease of fragmentation of protonated peptides on the gas-phase basicity of the amino acid residues present [62].

In Chapter 4 of this thesis energy-resolved SID is used to study a new class of macromolecules: dendrimers. The influence of the size and charge state of protonated polypropylenamine (POPAM) dendrimer ions on their fragmentation efficiency is investigated.

1.4 Other activation methods for ions of high molecular weight

1.4.1 Activation by a single high-energy gas phase collision

High-energy (3-20 keV) collision-induced dissociation (CID) is generally performed

with sector mass spectrometers. Application in a hybrid sector-TOF set-up is also reported [64]. A single keV collision can result in a transfer of kinetic to internal energy up to 10 eV [65], but the probability of truly high energy transfer (> 10 eV) remains low [66]. The total energy transferred to an ion can be increased by an increase of the gas pressure, which allows multiple collisions to occur, but this also results in ion loss through scattering. When low gas pressure is used to avoid multiple collisions, the fragment ion yield is $\sim 10\%$ of the parent ion current [67]. For application of high-energy CID to high molecular weight compounds, sector mass spectrometers are mostly used in conjunction with FAB for ionization.

1.4.2 Activation by multiple low-energy gas-phase collisions

Currently the most widely used instrumentation for MS/MS analysis of (bio) macromolecules is a triple quadrupole mass spectrometer operating with an ESI source, optionally coupled with liquid chromatography as a first separation method for a complex mixture. For example, proteins can be identified with the following sequence of methods: tryptic digestion, chromatographic separation of the resulting peptides and their detection by ESI/MS. This procedure is referred to as peptide mapping. For further characterization the peptides can be sequenced by means of low-energy CID in a triple quadrupole [68].

Other multiple collision CID methods that are used to obtain information about the structure of macromolecules are dissociation by acceleration of ions in the nozzle-skimmer interface of an ESI source and in-source decay (ISD) or post-source decay (PSD) of ions formed by MALDI. These methods are routinely used and available on commercially obtained instruments. They are referred to as pseudo-MS/MS since selection of the parent ion does not take place.

High-resolution low-energy CID fragment spectra can be obtained using a FTMS, either with on- or off-resonance excitation. McLafferty and coworkers have demonstrated low-energy CID of various high molecular weight compounds (29-67 kDa) [69, 70]. An additional advantage of trapped ion mass spectrometers for MS/MS of macromolecules is that they allow relatively long (10^{-3} -1 s) observation times. Hence dissociation can occur at a lower rate, and therefore less internal energy is needed for a given fragmentation channel to be observed [1].

In Chapter 5 of this thesis, the fragment spectra obtained by multiple collision low-energy CID are compared to those obtained by SID, in which the internal energy needed to fragment (quasi)molecular ions of macromolecules can be deposited in a single collision event. For this comparison, low-energy CID spectra of protonated POPAM dendrimers have been obtained in a FTMS and in a ITMS. The activation energies for fragmentation in the different time scales of observation are calculated by Rice-Rampsberger-Kassel-Markus (RRKM) methods.

1.4.3 Other methods

Another method by which (quasi)molecular ions of macromolecules can be dissociated is irradiation with photons obtained from a laser, ultraviolet [71] or infrared photons (infrared multiphoton dissociation (IRMPD) [72], or with photons obtained by heating of the ICR cell in a FTMS (black-body infrared dissociation (BIRD)) [73]).

Irradiation by electrons leading to capture and subsequent dissociation of the ion (electron capture dissociation (ECD)) can be used to dissociate multiply protonated peptides [74]. The current state of these methods is predominantly for research purposes.

Surface-induced dissociation of benzene on a PFPE liquid insulator in a time-of-flight mass spectrometer

Abstract

A perfluorinated polyether (PFPE) surface is used to enhance the fragment ion yield for surface-induced dissociation (SID) in a tandem time-of-flight mass spectrometer. Selection of the parent ion by separation of M^+ from $(M-H)^+$ is obtained with unit resolution by pulsing the voltage on the collision surface. The benzene radical cation is used as a model compound to characterise the instrument. Fragment ions are collected with a mass resolution of 100. The distribution of recoil energies of the SID-fragments leaving the collision surface is not sufficient to clarify the limited mass resolution. We estimate an average conversion efficiency of kinetic into internal energy of $30 \pm 7\%$ between 20 and 40 eV collision energy, by analysing the relative intensities of the SID-fragments as a function of collision energy.

2.1 Introduction

In search for methods to obtain more information on the composition of molecules, dissociation induced by ion/surface collision has been successfully employed in mass spectrometric analysis [2]. From the relative intensities of the resulting fragment ions it has been demonstrated that a much narrower distribution of internal energies can be deposited in the ions with activation by surface collisions than by a collision gas (CAD) [39]. One of the most challenging perspectives of surface-induced dissociation (SID) is the option of activating and fragmenting ions above m/z 1500, for which the information content of CAD spectra becomes less satisfactory [75]. The SID technique promises to yield fragmentation conveniently and efficiently for such compounds because the collision probability per ion is unity and the collision energy can be easily defined. However, the (quasi-)molecular ions often exceed the m/z limit of sector and quadrupole instruments. An apparatus with an in principle unlimited mass range is a time-of-flight mass spectrometer (TOF-MS). A few groups have already demonstrated the use of TOF-MS for SID. In the mid-eighties, a time-of-flight instrument provided Schey et al. [21] the possibility to reach collision energies over

100 eV to dissociate the relatively stable molecular ions of polycyclic aromatic hydrocarbons. In the early nineties, Whetten and coworkers showed that fullerenes are highly resilient with respect to collisional activation by a surface in a tandem linear TOF-MS even at collision energies up to 200 eV. At higher collision energies, fragmentation is observed, mainly through sequential C₂ loss [9, 36, 40, 76]. Williams et al. [37, 38] have obtained SID-fragment spectra of singly charged molecular ions in a tandem time-of-flight apparatus of a geometry similar to Whetten's. They also observed pick-up by the molecular ion of species unintentionally adsorbed on the collision surface. However, SID experiments in a TOF-MS have not yet extended far beyond 1000 Da, mainly because the TOF-MS has a relatively low mass resolution. The low duty cycle of a TOF-MS means that measuring times can be long. Therefore, the highly efficient but unwanted neutralisation of the parent ions upon collision with the surface must be minimised. Surfaces which reduce neutralisation that have been demonstrated for their usefulness are self-assembled monolayers of various compositions [15, 42, 56, 77], oxide surfaces [78] and, more recently, thin films of an inert polymer oil [44]. The latter compound, a perfluorinated polyether (PFPE), proved very efficient in reducing neutralisation and is easy to apply. This film was first used by Pradeep and coworkers in a sector/quadrupole tandem mass spectrometer [44].

In this chapter we discuss the combination of a tandem time-of-flight apparatus with a PFPE collision surface. In addition, we have combined parent ion selection with time-focusing of the selected ions on the collision surface. With this set-up, SID-fragment mass resolution has become comparable to that obtained when quadrupole mass spectrometers are employed to analyse the SID-fragment ions [56, 77, 79]. The benzene radical cation is used as a model system because it has been studied extensively with SID on several different collision surfaces: stainless steel [22, 35, 39, 79], hydrogenated and fluorinated self-assembled monolayers [15, 42, 56, 77] and rhenium oxide [78]. Its transitions for resonant multiphoton ionisation (REMPI) are known [80, 81] and its fragmentation as a function of internal energy distribution has been studied [57, 82]. With REMPI, a pulsed technique compatible with TOF-MS, the parent molecular ions can be made with very little internal energy, high selectivity and high yield. From spectra collected at several collision energies we constructed a 'breakdown' diagram and estimated the energy conversion efficiency.

2.2 Experimental

The tandem linear time-of-flight mass spectrometer used in the experiments is presented in Figure 2.1. It is a modified form of an apparatus described earlier (Bruker-Franzen) [83]. The original gridless reflector was replaced by one with grids (RM Jordan Co.), in which the collision surface is mounted on a feedthrough with a linear transfer

mechanism. The surface was moved close to the grids for the collision experiments. This set-up is comparable to those used in the groups of Whetten [9, 33, 36] and Zare [37, 38]. The parent ions are selected in the first stage, path length 1.15 m, of the tandem linear time-of-flight mass spectrometer. The SID-fragments are identified based on their flight times in the second stage, path length 0.74 m, between the surface and the detector. The angle defined by the source, the surface and the detector is about 6° . The collision energy is defined by the potential energy difference at the point of ionisation and at the surface. It can be tuned by varying the voltage on the surface. The potential energy of the ions at the

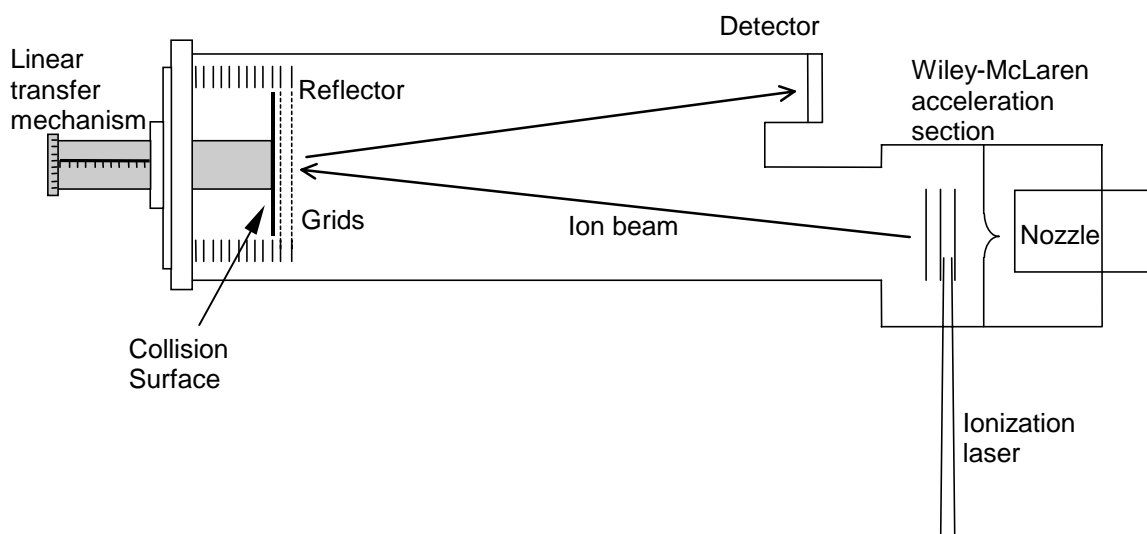


Figure 2.1: Set-up of the linear tandem time-of-flight mass spectrometer

laser focus is 830 ± 5 eV depending upon their position in the extraction field (30 V/cm); therefore, this contribution to the uncertainty in the collision energy is also ± 5 eV.

The gas-phase benzene molecules are introduced into the ionisation chamber through a skimmer, after cooling in a supersonic expansion from a pulsed nozzle. During sample inlet, the pressure in the ionisation chamber is typically between 10^{-4} and 10^{-5} Pa. Ionisation is performed in a 1+1 resonance enhanced multiphoton process, employing the $6_0^1 1_1^0$ intermediate state of benzene (253.31 nm, 4.89 eV). The total energy available in this two-photon process leaves a maximum of 0.54 eV for the internal energy of the benzene ions if the energy in excess of the ionisation threshold (9.25 eV) [82] were to remain in the ion. The laser light of about 3 mJ per pulse is focused into the ion source by a cylindrical lens (focal length 15 cm). Unintentional three-photon processes, probable at the maximum of the laser intensity distribution, can result in fragmentation of the molecular ion [84]. To avoid interference of these fragment ions formed in the source with those obtained by surface-induced dissociation of the molecular ion, the voltage on the collision surface is pulsed. As the molecular ion enters the deceleration region, the voltage on the collision surface is increased from ground to the desired potential. Fragment ions with a velocity

Figure 2.2: Effectiveness of parent ion selection by pulsing the deceleration field in front of the collision surface: (a) without pulsed selection, (b) with pulsed selection. Note that the $^{13}\text{CC}_5\text{H}_6^+$ can not be eliminated from the spectrum.

higher than that of the selected ions are thus removed from the beam. (M-H)⁺ fragments formed in the ion source can be separated from the parent M⁺ ion with unit resolution (Figure 2.2). The (M-H)⁺ ion, that has not yet reached the collision surface when the decelerating field is switched on, only partially experiences the field, and collides with the surface with a high collision energy (about 200 eV). Neutralisation is very efficient at these energies, and therefore the (M-H)⁺ fragments from the source, and their possible SID-fragments, do not contribute to the SID-fragment spectra. Metastable fragment ions formed in the first field-free region have the same velocity as the molecular ions and therefore the pulsed collision surface can not prevent their appearance in the SID-fragment spectra.

For optimal SID-fragment resolution and optimal performance of the pulsed ion selection, the parent ions should be time-focused at the collision surface [85, 86]. The position of the time-focus is a function of the various static electric fields. The electric field in front of the surface, used to decelerate the ions to the desired collision energy and to accelerate the SID-fragments towards the detector, acts as a diverging lens affecting the

position of the time-focus. We performed time-of-flight calculations to optimise the source potentials for time-focusing at the surface. In these calculations the initial kinetic energy of the molecules in the supersonic nozzle was neglected. The position of the time-focus obtained in a Wiley-McLaren type of ion source is a function of the ratio of the two fields. The lower the ratio of the extraction and acceleration fields, the further the distance of the time-focus from the ion source [85]. In our geometry, a ratio of about 1:30 is required for time-focusing of the parent ions at the surface. This results in relatively low extraction efficiency and consequently in a low signal-to-noise ratio for the mass spectra, but significantly improves resolution. Experimentally, after we applied the calculated potentials, the resolution $m/\Delta m$ of the SID-fragment spectra improved to 100 at m/z 50 (see Figure 2.3). The detector is an electron multiplier with an intrinsic time width of 10 ns.

To increase survival of the charged state, and therefore improve the signal-to-noise ratio, the stainless steel collision surface was covered with a high molecular weight PFPE [44], sold under the trade name Krytox 16256 with structural formula $F[CF(CF_3)CF_2O]_{63(ave)}CF_2CF_3$. Its average molecular weight is 11000 and its vapour pressure at room temperature is approximately 10^{-12} Pa. We obtained a smooth thin film by allowing the liquid to sheet across a stainless steel surface of 98 by 35 mm.

2.3 Results and Discussion

2.3.1 Liquid insulator surface

Neutralisation is a highly efficient process upon impact of radical cations with a conductor surface. In mass spectrometers only charged particles are detectable and, therefore, neutralisation must be reduced. Several groups have shown that adding a thin layer to the surface that acts as a barrier for electron transfer greatly improves survival of the charged state [15, 42, 44, 56, 77, 78, 87]. Because of its apparent ease in application and demonstrated usefulness [44], our choice was to apply a PFPE film to the stainless steel collision surface. To determine the difference in yield of positively charged SID-fragments, we compared the results obtained with a stainless steel surface with those of the PFPE surface. The spectra for this comparison were measured with SID-fragment mass resolution $m/\Delta m$ of about 5 to obtain higher intensity of the fragment ions from the stainless steel surface. The intensity of the detected SID-fragment ions after collision with the PFPE surface was about 10 times higher than that after collision with the stainless steel surface (measured between 30 and 70 eV collision energy). Insight in the reduction in neutralisation efficiency for the PFPE-film is provided by evaluation of the ionisation energies of the surface species. The work function of a clean metal surface is at most 6 eV [88], while the ionisation energy of benzene to form a radical cation is 9.25 eV [82].

Therefore, transfer of an electron from a clean metal surface to the ion is a highly exothermic process. In a UHV study, Wu and Hanley [87] demonstrated that the thicker the organic adsorbate layer (up to a thickness of 3 monolayers pyridine) on a clean Ag(111) surface, the greater the survival of scattered pyridine radical cations after collision with the surface. They explained this behaviour by the decreased probability of direct charge transfer from the metal to the colliding ions. Under the vacuum conditions under which most mass spectrometers operate, the collision surface is not clean but presumably covered with hydrocarbon adsorbates (pump oil) [2]. However, neutralisation under these poorly defined circumstances is still significant. This can be explained by either the thickness of the layer or the ionisation energy of the adsorbate, or a combination of the two. The PFPE was applied in macroscopically thick layers, i.e. thicker than 3 monolayers, and ionisation energies of (per)fluorinated ethers are above 12 eV [88]. This is several eV higher than that of comparable hydrocarbon compounds, making neutralisation by direct electron transfer from such surface molecules to the incident benzene radical cation endothermic. Pradeep et al. demonstrated the tendency of the PFPE surface to remain relatively clean from adventitious hydrocarbons by demonstrating the absence of hydrogen adducts after colliding pyrazine and benzene molecular ions with the PFPE surface compared to their presence after collision with a fluorinated self-assembled monolayer [44]. Though the liquid PFPE surface is considered an insulator, we found no evidence for charging of this surface: (i) the spectra were well reproducible and (ii) the voltage required to decelerate the ion beam so that collisions with the surface are just prevented showed no significant changes in the course of our experiments. These observations are in agreement with the findings of Pradeep et al. [44] who, even with a much higher ion current than our estimated 10^{-16} A, did not see charging of the surface.

2.3.2 Fragment mass spectra

To calibrate the mass scale, we calculated the flight times for the assumed elemental compositions of eight SID-fragments of benzene, assuming equal flight times for the parent ions and dissociation at the surface in less than 1 ns. In these calculations, the instrument is taken to be linear and all fields to be defined by grids. The influence of the Einzel lens and the X and Y deflection plates on the flight times is neglected. The average absolute difference between calculated and experimentally observed flight times can be minimised to below the width of the peaks for only one of several possible ways of assigning the hydrogen compositions to the chosen eight SID-fragment peaks. For this minimisation the ion optical parameters used in the calculation are iteratively varied within about 5% of their values. The mass scale, as shown in Figure 2.3, is calibrated using a first-order polynomial through the peaks at mass 26 and 63.

Most SID-fragment spectra of benzene reported by other groups [15, 22, 36, 39, 42, 44, 56, 77-79] show the same fragment mass peaks as our spectra. Differences in relative

intensities are observed as different collision geometries and energies are used. In Figure 2.3, the SID-fragment spectrum of the benzene molecular ion after a 40 eV collision with the PFPE covered surface is shown. In this spectrum, the peaks of the molecular ion and the (M-H)⁺ ion are not well resolved, despite selection and time-focusing of the parent ions at the collision surface. This is attributed to the overlap with the signal of fragments from metastable decay in the first field-free region, expected to appear around m/z 75 in the SID-fragment mass spectrum, which could not be eliminated from the parent ion beam. As reported by Somogyi et al. [15, 56] the spectra show the same fragment mass peaks as found in mass spectra of benzene from EI, MPI and CAD [84, 89-91]. The peak at m/z 63 is abundant in SID-fragment spectra of benzene on the reported surfaces [15, 36, 39, 42, 50, 56, 77-79] and is assigned as C₅H₃⁺ since Wysocki et al. observe SID-fragment mass 66 upon collision of deuterobenzene with an ethanethiol self-assembled monolayer (SAM) surface [77]. It is also commonly observed in EI [89] and CAD [91] mass spectra, but with much lower intensity relative to the other fragments. The route to this fragment remains unclear. For collisions of benzene radical cations with perfluorinated SAM surfaces, several groups have observed peaks at m/z 95 and 96, reported to result from pick-up of fluorine and subsequent hydrogen loss [15, 42, 56]. However, the small signal at m/z 95 in our spectrum can not be interpreted as resulting from a product of a pick-up reaction, due to the low signal-to-noise ratio.

Figure 2.3: Fragment ion mass spectrum obtained upon 40±5 eV collisions of benzene molecular ions with a PFPE surface, with time-focusing of the primary ions at the surface. This spectrum was obtained from 1250 laser shots and processed with a three-point smoothing routine. Calibration was obtained by fitting a first-order polynomial once the hydrogen composition of the fragments had been determined.

2.3.3 Energy conversion efficiency

The internal energy of ions acquired in a collision with a surface has been studied experimentally [39, 42, 44, 57] and theoretically [92]. The internal energy is frequently expressed as a percentage of the collision energy and values between 15% and 33% have been reported for various systems. For organic molecules, published breakdown curves can be used to derive the internal energy by comparison with the relative fragment intensities in the SID spectra. Although the internal energy distribution is relatively narrow in SID, both the mean value and the width of the distribution must be taken into account for a meaningful interpretation. The accuracy of the comparison depends strongly on unique fragment ions characteristic for the particular energy domain being investigated. For this purpose, transition metal hexacarbonyl ions are very useful because of the sequential loss of carbonyl groups with increasing internal energy. Recently, Vékey et al. [57] developed an analogous procedure for benzene ions. With this method, a conversion efficiency of 28% was derived for benzene radical cations colliding with a surface covered with a perfluorinated self-assembled monolayer [57].

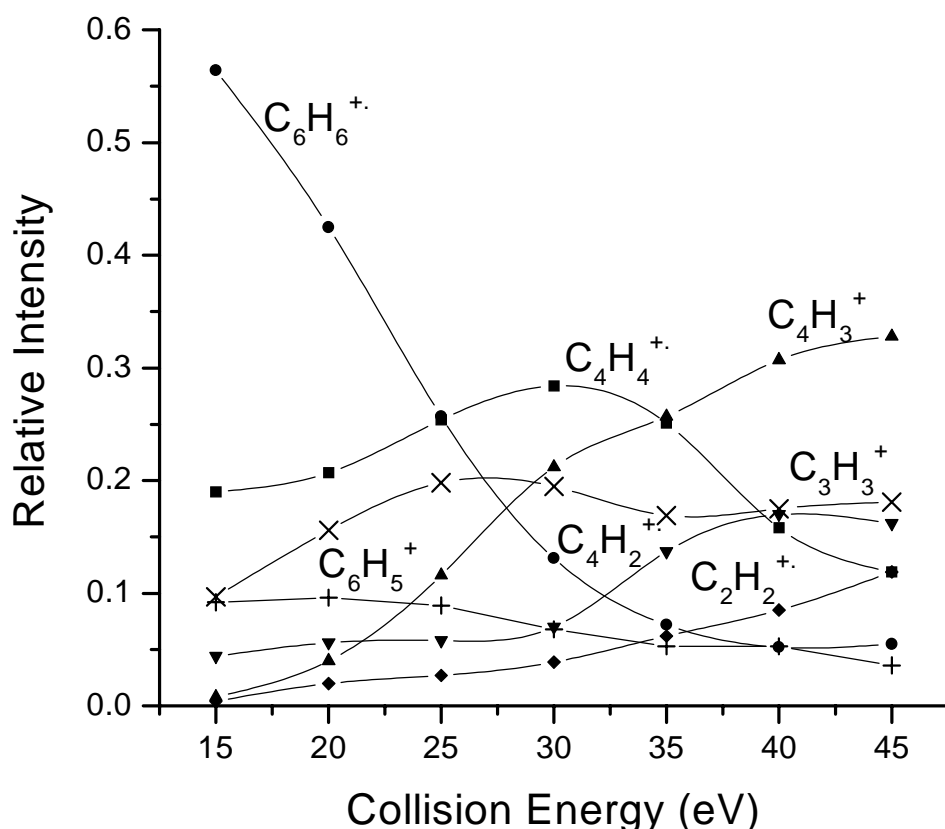


Figure 2.4: Energy-resolved SID diagram of selected fragmentations of the benzene molecular ion. The uncertainty in the relative intensity is about 5%, except for the fragment at m/z 77, for which it is about 20%.

In Figure 2.4, the diagram of the relative fragment ion intensities measured for the range of 15 to 45 eV collision energy is displayed. The uncertainty in the collision energy is ± 5 eV and the uncertainty in the intensities is in the order of 20%. Application of the deconvolution method described by Vékey allows us to calculate the internal energy distribution. The mean energies, estimated from the first moments of the distribution, scale with $(0.30 \pm 0.07) \cdot E_{\text{coll}}$. The widths are approximated by twice the second moment of the distributions and are 4.6 to 6.0 eV. The conversion efficiency of 30% is relatively high compared to values reported for metal hexacarbonyls (15-20%) [42] and peptides (13%) [31], but within the error of determination, the same as the value of 28% reported by Vékey et al. for benzene [57]. In their experiment, the molecular ions collide with the surface at an angle of 45° and are detected at an angle of 45° , while in our experiment, the ions collide nearly normal to the surface. These results indicate that the conversion efficiency is not very sensitive to the angle of impact. This is confirmed by scattering experiments of CF_3^+ ions on a PFPE surface [47], which show that the relative intensities of the fragment ions are independent of the angle of incidence of the parent ions, as long as the total scattering angle is held constant.

2.3.4 Width of SID-fragment peaks

The time widths of the fragment peaks in the SID mass spectrum displayed in Figure 2.3 vary from 60 ns at m/z 26 to 90 ns at m/z 78, full width at half maximum (FWHM), limiting the mass resolution $m/\Delta m$ to 100. In search of improvements in mass resolution, we investigated the influence of a number of parameters on the distribution in fragment ion flight times. The results of varying one parameter at a time, while holding the others fixed at their mean values, were calculated. For simplicity, all variations, except the angular dependence of the recoil energies, were assumed to follow a Gaussian distribution. The calculated flight times were segmented into bins of 5 ns, the time resolution of the acquisition system used. Fixed instrument parameters were set to the values determined from the optimisation of the mass scale described above.

First we focus on the ionisation and flight times in the first linear TOF. The REMPI pulse leads to a 5 ns spread in flight times of the parent molecular ions at the surface. The Gaussian laser intensity profile with $\sigma_{\text{laser}}=1$ mm similarly leads, for the instrument parameters concerned, to a 10 ns distribution of arrival times of the molecular ions at the surface. A difference in flight paths caused by a 6° opening angle of the parent ion beam would result in a time width of 10 ns at the collision surface. Combining these three independent effects, we calculate a distribution of arrival times at the surface of 15 ns.

Second we consider the flight time distributions after collision with the surface which are caused by the spread in kinetic energy of the fragments, by the spread in scattering angle and the detector response time. Neither the energy nor the angular distribution of the fragment ions is known. Based on the observations of Wu and Hanley [14], Morris et

al. [42] and Winger et al. [93], we estimate that 20% of the collision energy is retained as kinetic energy. This energy is shared over neutral and ionic fragments, proportional to their masses. In our case, this leads to a mean value of the 'recoil' energy of 0.13 eV/Da. However, the width of the distribution about this mean is very poorly known. Morris et al. [42] measured a FWHM value of 4 eV for fragment ions and deduced a molecular ion distribution width of 5 eV. Adopting this value, we take $\sigma_{\text{recoil}} = 25 \text{ meV/Da}$. The angular distribution is approximated by a cosine squared distribution. The finite size of the detector (1 cm radius) leads to an acceptance angle of only 6° . This severely limits the combinations of energies and angles with which the fragment ions can reach the detector. Therefore, the combined influence of these distributions has to be evaluated. The convolution of recoil energy and angular distribution leads to FWHM values of 10 ns and 50 ns for fragment ions of 26 Da and 78 Da, respectively. Also, there is a, mass dependent, effect of flight path differences due to the angle of the detector relative to the surface (3°), resulting in broadening of 10 ns for ions at m/z 26 and 20 ns at m/z 78. Combining the effects from the first and second stages of the tandem TOF-MS, assuming all broadening effects are independent of one another, the FWHM at m/z 26 and at m/z 78 are 35 ns and 75 ns, respectively. It is clear that the recoil energy is the dominant factor for the larger fragments, while for m/z 26, the different contributions are of comparable magnitude. The experimental width for m/z 26 (60 ns) can not be explained by any reasonable value for the recoil energy. Therefore, the discrepancy between experimental and calculated widths must be due to parameters which have been misinterpreted or neglected in the calculations. Two possibilities are readily apparent: time focusing of the molecular ion at the surface could not be tested experimentally. A width of 30 ns of the parent ion beam at the surface can explain the discrepancy. Although on one hand we calculated that to obtain a 30 ns width of the parent ion beam by misfocusing the Wiley-McLaren ion source, the voltages on the source plates would have to be about 50 V off, on the other hand we did not include the influences of the Einzel lens, the X and Y deflection plates, and the absence of grids in the ion source. A second possibility is that the ion optical elements are not well-aligned. If the last grid before the surface is not parallel to the surface, off by 0.5 mm for example, a flight time difference of 30 to 40 ns (m/z 26 to 78) would also be observed.

To meet the resolving power required for the study of larger molecular systems, the contribution of the misalignment factors to the time width of the fragment peaks must be decreased. The contribution of recoil energy alone would theoretically limit $m/\Delta m$ to about 500 at m/z 50. This is acceptable only for the study of small bio- and synthetic polymers. An ion reflector is required to energy-focus the SID-fragment ions onto the detector for larger molecular systems. If different ionisation methods are used to create the parent ions, there will be different experimental requirements to time-focus the ions at the collision surface, and other adaptations of the TOF-MS will be necessary to obtain sufficient mass resolution in the SID-fragment spectra.

Surface-induced dissociation of diphenyl ether

Abstract

The primary fragmentation of diphenyl ether and further secondary dissociation of its fragments have been studied by surface-induced dissociation (SID). In a tandem linear time-of-flight mass spectrometer, the dissociation of ions is studied as a function of the collision energy with a liquid perfluorinated polyether (PFPE) surface. In a tandem quadrupole instrument, an alkyl terminated (C_{18}) and a perfluoroalkyl terminated (FC_{10}) self-assembled monolayer surface have been used. The differences in the spectra obtained with the TOF and quadrupole instruments are attributed to the different time frames available for observation of the fragments. Deconvolution of the collision energy resolved SID spectra of diphenyl ether shows that above 50 eV collision energy the energy conversion efficiency is similar in the two experimental set-ups, in spite of the different geometries.

Ion/surface reactions are observed upon collisions of the diphenyl ether radical cation with the C_{18} surface but not with the FC_{10} surface. The rearrangement fragments, obtained from perdeuterated diphenyl ether, $C_{11}D_{10}^+$ and $C_{11}D_9^+$, react with both the C_{18} and FC_{10} surface. Hydrogen exchange with the surface combined with hydrocarbon loss from $C_{12}D_{10}O^+$, $C_{11}D_{10}^+$, and $C_{11}D_9^+$ is observed.

3.1 Introduction

During the last 10-15 years, surface-induced dissociation (SID) has been employed as a tool in analytical mass spectrometry to deposit a well-defined amount of energy into many different types of ions [19, 39, 44, 57, 60]. For recent reviews, see [2, 3, 36, 44]. For SID, low-energy (0-200 eV, but usually below 100 eV) collisions are sufficient to overcome the activation energies for fragmentation of most types of ions. Different types of mass spectrometers have been used in which SID is implemented, in varying geometries. Examples are sector, [20, 26], quadrupole [23, 39], time of flight [21, 36, 38], ion trap [94] and Fourier-transform mass spectrometers [29, 31, 95].

An important characteristic of SID is the defined kinetic-to-internal energy conversion of the ion, which can be tuned by varying the collision energy. Many of the "thermometer molecules" which have been employed to quantify the energy conversion in

ion/surface collisions are small ions such as metal carbonyls [39, 42, 44] and benzene radical cations [57, 96]. These ions show their most informative fragments between 10 and 80 eV collision energies. Kinetic into internal energy conversion efficiencies of 12-18% for hydrocarbon covered surfaces [39, 42], and 18-30% for fluorinated surfaces [42, 44, 57, 96] have been reported. Systematically, the lower value corresponds to the metal carbonyl ion method, the higher value to the benzene deconvolution method. For the fragmentation of large or especially stable species, such as peptides [3] and buckminsterfullerenes [36], the required collision energies may extend to 100 eV or more. In this paper ion/surface collisions of the diphenyl ether radical cation and two of its fragments are investigated. Diphenyl ether is small enough to show distinct fragments at collision energies lower than 30 eV, but on the other hand is stable enough to show informative changes in fragmentation at collision energies higher than 100 eV. In addition to hydrogen atom loss, the diphenyl ether radical cation ($C_{12}H_{10}O^+$) shows two main fragmentation channels: a rearrangement reaction that involves CO loss, presumably leading to a benzotropylium radical cation ($C_{11}H_{10}^+$), and a direct cleavage, presumably leading to a phenyl cation ($C_6H_5^+$), both of which can in turn fragment further [97, 98]. The appearance energies for the $C_{11}H_{10}^+$ and $C_6H_5^+$ fragments have been reported previously to be 12.69 and 14.88 eV, respectively [98]. The secondary fragmentation of $C_6H_5^+$ is expected to show several fragments which also occur in the fragment spectra of benzene. Benzene has been employed to quantify the kinetic-to-internal energy conversion by alkyl and fluoroalkyl collision surfaces, for up to 80 eV kinetic energy of the projectile ions [39, 57, 96]. Since diphenyl ether is larger than benzene and several eV are required to form $C_6H_5^+$, it is expected that relatively high internal energies will be required to show similar fragments as benzene.

In addition to fragmentation, ion/surface reactions have been observed for a wide variety of colliding ions, and on different types of surfaces [15, 41, 42, 50, 53-56, 77, 79, 99]. The kind of and extent of the ion/surface reactions observed depends strongly on the nature of the colliding ion and the composition of the surface. For example, upon collisions with a hydrocarbon surface, acetone, DMSO and pyridine radical cations give extensive H addition reactions and can be used to probe surface damage and/or surface contamination [55]. It has been shown that benzene radical cations give a higher abundance of methyl adducts than doubly charged benzene ions, while they give about the same abundances of ions corresponding to F additions [56]. For isomeric $C_6H_6^+$ ions, Hayward et al. have shown that the benzene radical cation gives more extensive methyl adducts upon collision with a stainless steel surface covered with pump-oil residues, than 1,5-hexadiyne or 2,4-hexadiyne radical cations [79]. Extensive ion/surface reactions with respect to alkyl addition are obtained from collisions of pyrene radical cations with a stainless steel or alkyl self-assembled monolayer surfaces [42, 93]. Diphenyl ether as an aromatic radical cation is expected to show some reactivity towards an alkyl collision surface.

In this paper we show the use of diphenyl ether as a probe to estimate the kinetic-to-internal energy conversion efficiency at collision energies of more than 100 eV.

Furthermore, we have compared the SID fragment spectra of the diphenyl ether radical cation acquired on two different instruments: a tandem TOF and a tandem quadrupole mass spectrometer. These instruments differ in geometry and in the time frame during which fragmentation can be probed. In addition, we have investigated the ion/surface reactions of the diphenyl ether radical cations and of the CO loss rearrangement fragments with C₁₈ and FC₁₀ surfaces.

3.2 Experimental

The tandem linear time-of-flight mass spectrometer has been described in detail earlier [96]. The ions are selected in the first time-of-flight section which is approximately normal to the collision surface, the SID-fragments are identified based on their flight times in the second stage between the surface and the detector. The collision energy is defined by the potential energy difference between the point of ionization and the collision surface, and can be tuned by varying the voltage on the surface. The potential energy of the ions at the laser focus is approximately 3 keV and depends on the start position in the extraction field (0.3 kV/cm). This position is known within ± 0.5 mm, which leads to an uncertainty of ± 15 eV. The potential energy is verified experimentally by lowering the voltage on the collision surface until the signal of the parent ions starts to decrease, due to the onset of ion/surface collisions. We estimate the uncertainty in the collision energy scale as ± 10 eV. The width of the ionizing laser beam at the focal point of the lens is about 90 μ m, which results in a kinetic energy distribution of ± 1.5 eV in the parent ion beam.

The gas-phase diphenyl ether molecules are introduced into the ionization chamber through a skimmer, after cooling in a supersonic expansion from a pulsed nozzle which is heated to about 40°C. Ionization is performed in a 1+1 resonance enhanced multiphoton process with 4.46 eV photons. The total energy available in this two-photon process leaves a maximum of 0.89 eV for the internal energy of the radical cations if the energy in excess of the ionization threshold, determined from the photoelectron spectrum as 8.03 ± 0.15 eV [100] were to remain in the ion. The laser light of about 2 mJ per pulse is focused into the ion source by a cylindrical lens (focal length 15 cm). For the SID experiments, formation of the C₆H₅⁺ fragment ions is accomplished upon absorption of two additional photons by the diphenyl ether radical cation. This leaves the fragment with a maximum of 1.5 eV internal energy, if upon ionization of diphenyl ether all the excess energy were to remain in the diphenyl ether radical cation, and if upon photodissociation the excess energy were equally distributed among the degrees of freedom (DOF) of the fragment ion and the neutral. Interference of other ions than the intended parent ion created in the ion source, with fragments obtained by surface-induced dissociation, is avoided by pulsing the voltage on the collision surface [96]. The collision surface consists of a stainless steel plate covered by a thin film of high molecular weight liquid

perfluorinated polyether (PFPE), as described earlier [96]. The geometrical angle defined by the ion source, collision surface and detector is about 6° , resulting in a geometrical angle of incidence of the ions with respect to the surface normal of 3° . Yeretian et al. have discussed how the angle of incidence of the ions changes because the ratio of the parallel and perpendicular velocity of the ions is changed by the deceleration at the surface, but they have observed little change in fragmentation patterns by varying this angle [36].

The tandem quadrupole instrument used has been described earlier [39]. Briefly, it consists of two 4000 u quadrupoles (Extrel, Pittsburgh, PA, USA) arranged in a 90° geometry with the surface positioned to intersect the ion optical path of each quadrupole. The angle between the ion beam and the surface normal is kept at $45 \pm 5^\circ$. The diphenyl ether molecules are brought into the ion source by heating the sample vessel and inlet tube (about 40°C) and ionized by 70 eV electron ionization (EI). The collision surfaces utilized are self-assembled monolayers (SAMs) from alkyl thiols grown on clean vapour-deposited gold surfaces. The experiments described below utilize SAM-surfaces consisting either of hydrogen terminated alkyl chains with 18 carbon atoms (C_{18} surface) or of fluorine-terminated alkyl chains, $\text{CF}_3\text{-(CF}_2)_7\text{-(CH}_2)_2\text{-S-Au}$, (FC_{10} surface). The efficiency of charge retention at these surfaces has been reported previously [54] and is higher for the fluorocarbon surface than for the hydrocarbon surface (65% vs. 12%, respectively, with benzene projectile).

3.3 Results and Discussion

3.3.1 Spectra and ER-SID diagrams

Figure 3.1 shows the SID spectrum that results from 20 eV collisions of diphenyl ether radical cation (m/z 170) with a PFPE surface in the tandem TOF mass spectrometer, an instrument in which the resolution is limited to about 100 at m/z 100 [96]. Figure 3.2 shows a plot of the relative fragment ion intensities of diphenylether as a function of the collision energy in the tandem TOF mass spectrometer. Energy-resolved SID diagrams (ER-SID) of this type are useful to monitor dissociation pathways as a function of collision energy. Note that ER-SID diagrams should be distinguished from breakdown diagrams which show relative fragment ion intensity as a function of the (univalue) internal energy.

As indicated by the spectrum (Figure 3.1) and the ER-SID diagram (Figure 3.2), at collision energies lower than 50 eV the dominant fragment ion is the direct cleavage product C_6H_5^+ at m/z 77. Further fragmentation of C_6H_5^+ (see discussion below) accounts for the dominant ions in the low m/z range (lower than m/z 77) at higher collision energies.

Figure 3.1: 20 eV SID spectrum of the radical cation of diphenyl ether on a PFPE surface in the tandem TOF instrument. This spectrum is acquired from 1250 laser shots.

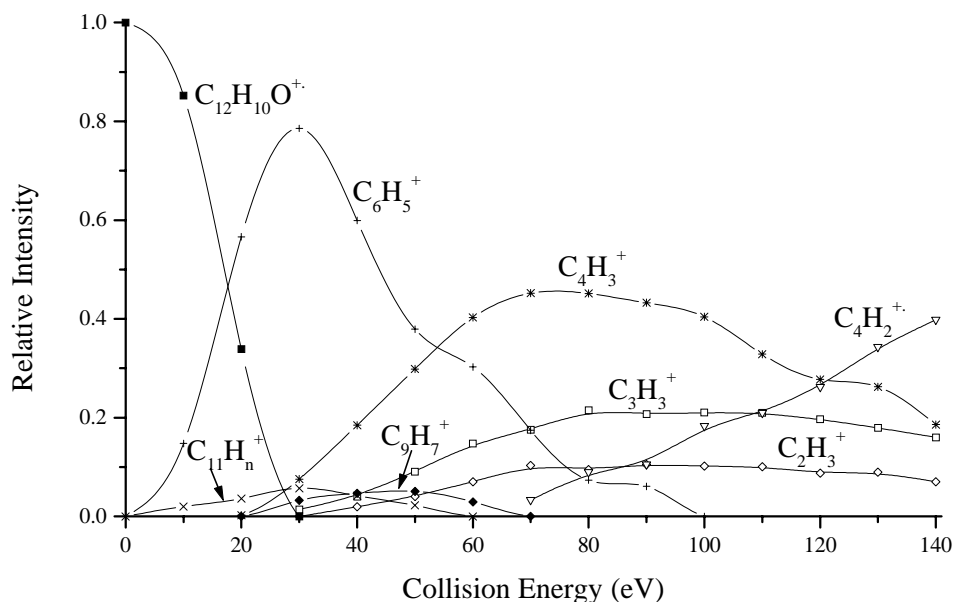


Figure 3.2: ER-SID diagram of the radical cation of diphenyl ether on the PFPE collision surface. Only the fragments with an abundance of more than 10% at any collision energy are indicated. The spectra on which this diagram is based are acquired from 1250 laser shots.

In contrast to the high intensity of the direct cleavage product, the expected CO loss rearrangement product, $C_{11}H_{10}^+$ (m/z 142), is of low intensity even at low collision energies. Also notable in Figure 3.1 is the signal of fragments from metastable decay in the first field free region. These fragments appear around m/z 165 in the SID spectrum and inhibit the accurate determination of the intensity of the SID fragment ions in this mass range.

Figure 3.3 shows a 20 eV SID spectrum of diphenyl ether colliding with a FC_{10} surface in the tandem quadrupole instrument [101]. The acquisition time of this spectrum is comparable to the time required to obtain the TOF SID spectrum in Figure 3.1, which is about 10 minutes. From a comparison of the spectra in Figure 3.1 and Figure 3.3 it is clear that the tandem quadrupole instrument yields a much better signal-to-noise ratio than the tandem TOF. This is expected based on the difference in parent ion current, estimated as 10^4 ions/s for the tandem TOF, and 10^9 for the tandem quadrupole. Furthermore, the tandem quadrupole yields a better resolution above m/z 100. Figure 3.4 shows the ER-SID diagrams recorded with the tandem quadrupole instrument. Some ER-SID curves look similar obtained with the tandem TOF and the tandem quadrupole experiments with the fluorinated surfaces, e.g., compare the curves of $C_6H_5^+$ and $C_4H_3^+$ in Figure 3.2 with those in Figure 3.4(a). Other curves are clearly different, especially those related to the CO loss rearrangement products. Due to the limited resolution we use the summed signal of the rearrangement fragments $C_{11}H_n^{+(\cdot)}$ ($n = 7-10$, m/z 139-142) for the ER-SID diagram in Figure 3.2. The rearrangement fragment $C_{11}H_{10}^+$ should have its maximum intensity at SID collision energies between 15 and 25 eV when one assumes that the time frame for dissociation is of the same order of magnitude as that used to measure the appearance energy for this fragment. This is based on estimates of the efficiency of conversion of collision energy into internal energy (about 30% for the PFPE surface [96]), and the 4.66 eV difference between the known ionization energy (IE) (8.03 eV [100]) for the parent ion and appearance energy (12.69 eV [97]) for the fragment ion. For the direct cleavage product $C_6H_5^+$, the appearance energy (AE) has been established as 14.88 eV [97] leading to a AE-IE value of 6.85 eV. Although the rearrangement fragments are present at collision energies between 15 and 25 eV, in the TOF-SID spectra their abundance is never higher than the abundance of the fragment formed by direct cleavage, $C_6H_5^+$, even at 10 eV collision energy. We attribute this to a combination of the width of the distribution of the obtained internal energy, and the short time frame for observation of the rearrangement reaction in the TOF-SID instrument. The length of the acceleration region after the collision surface is 10 mm in the TOF-SID instrument. Combined with an acceleration voltage of 3 kV, this results in a time spent in the acceleration section of only 0.2 ms for a particle of m/z 100. In the tandem quadrupole instrument this time frame is about 2 ms and therefore the relative intensity of the fragments connected with CO loss is higher. It is difficult to tune the tandem quadrupole instrument at a collision energy lower than 10 eV, so that $C_{11}H_{10}^+$ ions are never the most abundant fragments in the experiments performed with the FC_{10} surface.

Figure 3.3: 20 eV SID spectrum of the radical cation of diphenyl ether on a FC_{10} surface in the tandem quadrupole instrument.

When the C_{18} surface is used, the $C_{11}H_{10}^+$ ions are the most abundant fragments between 10 and 20 eV collision energy (Figure 3.4(b)), which is consistent with the smaller kinetic-to-internal energy conversion efficiency for the C_{18} surface [42, 57]. These results show that the differences in the ER-SID curves are related to the differences in the observation time for the two instruments. In its current configuration, the tandem TOF instrument can not be used to study fragmentation processes which occur on a microsecond time scale. This could be advantageous for systems in which rearrangements complicate interpretation of the mass spectrum. A possible improvement to allow investigation of slower dissociations would involve delayed extraction of the fragments after the collision surface. Since the ER-SID curves of the fragments from the direct cleavage reaction are very similar, we conclude that for the higher-energy collisions (> 50 eV), the difference in geometry between the instruments (6° vs. 90° , collisions at 90° vs. 45°) does not greatly influence the kinetic-to-internal energy conversion by the fluorinated alkyl surface. This has already been indicated by experiments with benzene [96] and scattering experiments of CF_3^+ [47].

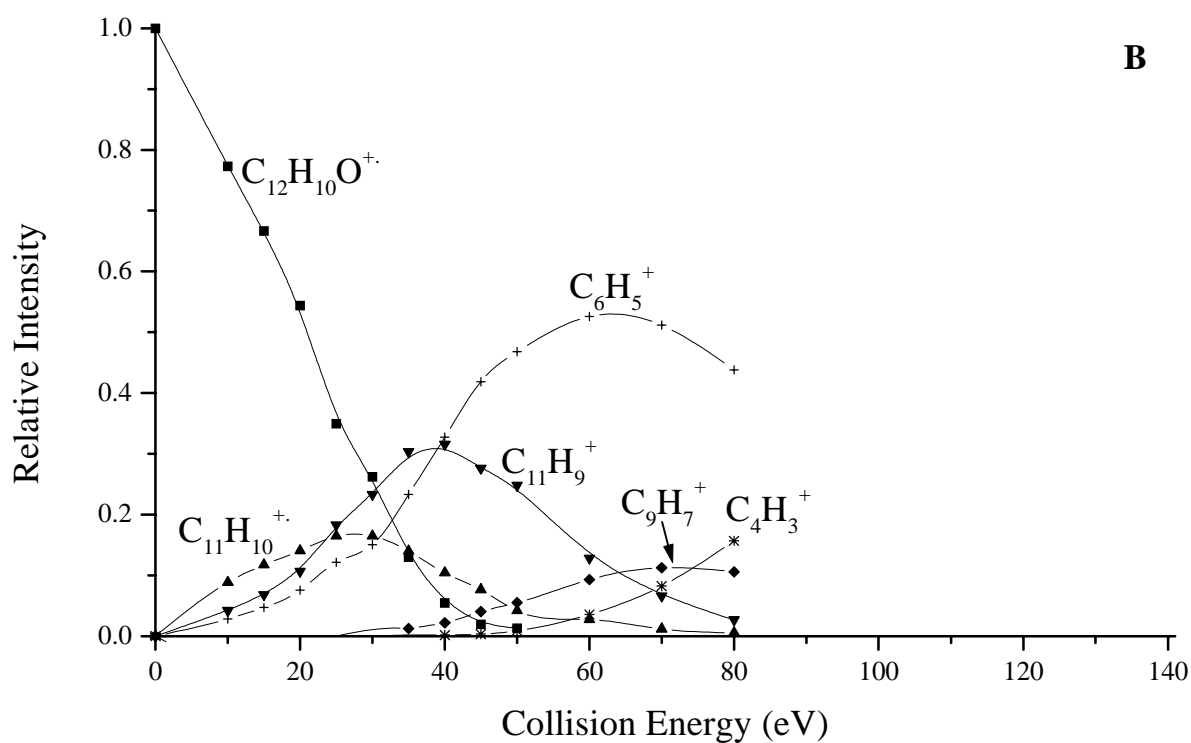
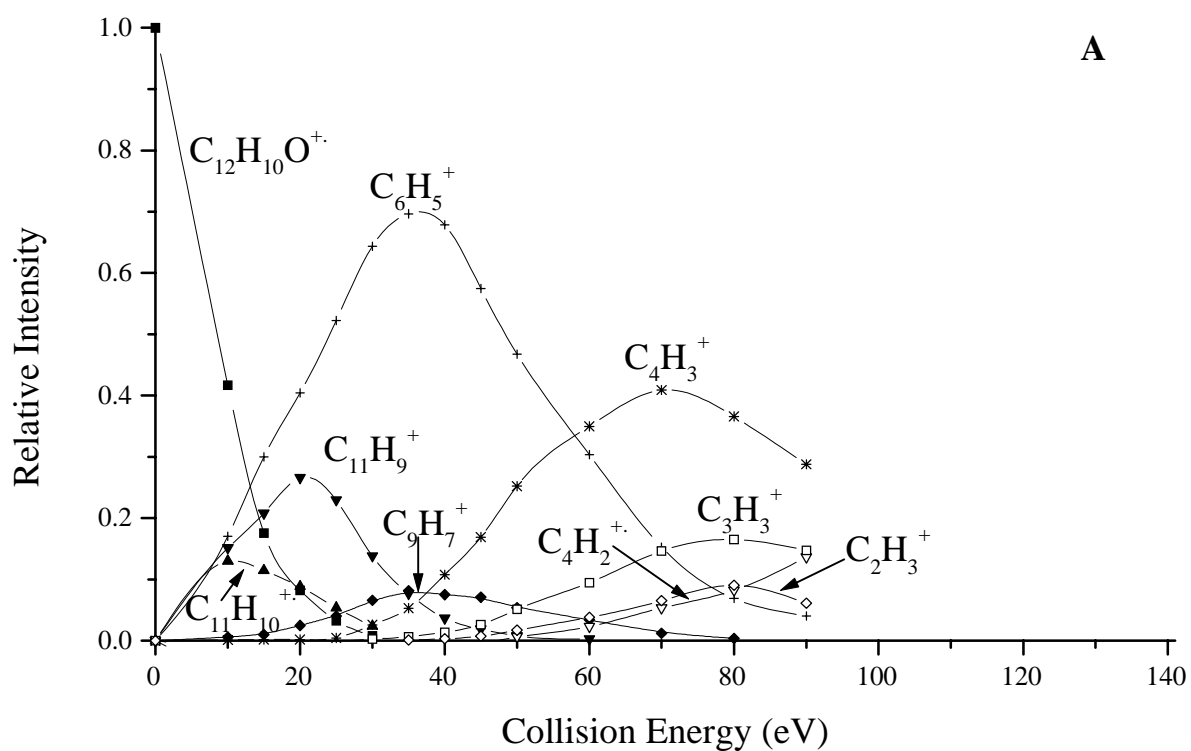
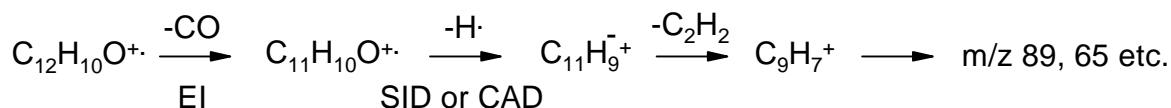


Figure 3.4: (a) ER-SID diagram of the radical cation of diphenyl ether on the FC10 surface showing only fragments with an abundance > 10%. (b) ER-SID diagram of the radical cation of diphenyl ether on the C18 surface. Only with use of the surface with the lower energy conversion efficiency, C_{18} , and at low collision energies, the fragment $C_{11}H_{10}^+$ is the most abundant fragment.

SID experiments with the $C_{11}H_{10}^+$ and $C_{11}H_9^+$ ions are performed in the tandem quadrupole instrument. To improve the mass selection of the parent ion, and to investigate possible ion/surface reactions, perdeuterated diphenyl ether is used for these experiments. These experiments were compared with keV CAD experiments of selected $C_{11}H_{10}^+$ formed from $C_{12}H_{10}O^+$, as summarized below:



$C_{11}D_9^+$ ($C_{11}H_9^+$) is a dominant product of $C_{11}D_{10}^+$ ($C_{11}H_{10}^+$). This is in contrast to the CAD results reported by Stiller and Johnston [98] who found that $C_{11}H_9^+$ was not formed from $C_{11}H_{10}^+$. Acetylene loss from $C_{11}D_{10}^+$ ($C_{11}H_{10}^+$) resulting in $C_9D_8^+$ ($C_9H_8^+$) (m/z 124 (116)) is observed only in small (<2%) amounts from SID on FC10 or the CAD experiments.

Table 3.1 contains a list of all fragments of the diphenyl ether radical cation which appear with a peak height of at least 0.1% in any of the tandem quadrupole and 1% in the tandem TOF SID spectra, along with a proposal for their formation. SID experiments with the (perdeuterated) rearrangement fragments have been used to confirm the composition of some of the fragments. The relative peak height of a fragment at the collision energy (below 140 eV) corresponding to its maximal abundance, is qualified with S (strong) when between 5 and 100%, with M (medium) when between 1 and 5% and with W (weak) when between 0.1 and 1%. Table 1 shows, for example, that if sufficient energy is imparted in the rearrangement fragments $C_{11}D_{10}^+$ and $C_{11}D_9^+$, a small amount of $C_6H_5^+$ is formed. This reaction however is not expected to contribute to the amount of $C_6H_5^+$ formed from the diphenyl ether radical cation, due to the competitive shift.

Table 3.1: Summary of fragments observed upon SID of the diphenyl ether radical cation. The second column (I) indicates the maximum intensity at any collision energy between 10 and 140 eV: S (strong) when between 5 and 100%, M (medium) when between 1 and 5%, W (weak) when between 0.1 and 1%. The third and fourth columns show the atomic composition and a proposal for the origin of the fragment. The fifth column shows the mass-to-charge ratio at which the equivalent fragment from perdeuterated diphenyl ether is observed upon collisions with a fluorinated alkyl surface. The last column shows which primary fragment of diphenyl ether was used to confirm the composition of the fragment in the second column. [†]: tandem TOF SID spectra, ^q: tandem quadrupole SID spectra, [‡]: only observed with C₁₈ surface, [†]: not expected.

m/z	I	Formula	Process	H -> D (m/z)	confirmed by SID of:
170 ^{†,q}	S	C ₁₂ H ₁₀ O	M	180	C ₁₂ D ₁₀ O
169 ^{†,q}	M	C ₁₂ H ₉ O	M - H	178	C ₁₂ D ₁₀ O
168 ^q	M	C ₁₂ H ₈ O	M - H ₂	176	C ₁₂ D ₁₀ O
155 ^q	M	C ₁₁ H ₇ O	M - CH ₃	162	C ₁₂ D ₁₀ O
153 ^q	W	C ₁₁ H ₅ O	155 - H ₂	158	C ₁₂ D ₁₀ O
152 ^q	W				
151 ^q	W				
144 ^q	W				
142 ^{†,q}	S	C ₁₁ H ₁₀	M - CO	152	C ₁₁ D ₁₀
141 ^{†,q}	S	C ₁₁ H ₉	142 - H, 169 - CO	150	C ₁₁ D ₁₀ , C ₁₁ D ₉
140 ^q	W	C ₁₁ H ₈			
139 ^q	M	C ₁₁ H ₇	141 - H ₂	146	C ₁₁ D ₁₀ , C ₁₁ D ₉
131 ^q	W	C ₉ H ₇ O	M - C ₃ H ₃	138	C ₁₂ D ₁₀ O
129 ^q	W	C ₉ H ₅ O	155 - C ₂ H ₂	134	C ₁₂ D ₁₀ O
129 ^q	W	C ₁₀ H ₇	142 - CH ₃	136	C ₁₁ D ₁₀ , (C ₁₁ D ₉ [*])
128 ^q	W	C ₁₀ H ₆	141 - CH ₃	134	C ₁₁ D ₁₀ , C ₁₁ D ₉
127 ^q	W				
126 ^q	W				
116 ^q	M	C ₉ H ₈	142 - C ₂ H ₂	124	C ₁₁ D ₁₀
115 ^{†,q}	M	C ₉ H ₇	141 - C ₂ H ₂	122	C ₁₁ D ₉ (S), C ₁₁ D ₁₀ (S)
103 ^q	W	C ₈ H ₇	142 - C ₃ H ₃	110	C ₁₁ D ₁₀
102 ^q	M	C ₈ H ₆	141 - C ₃ H ₃	108	C ₁₁ D ₁₀ , C ₁₁ D ₉
94 ^{†,q}	M	C ₆ H ₆ O	M - C ₆ H ₄		
93 ^q	W	C ₆ H ₅ O	M - C ₆ H ₅ , 94 - H		
92 ^q	W	C ₆ H ₄ O	94 - H ₂		
92 ^q	W	C ₇ H ₈	142 - C ₄ H ₂	100	C ₁₁ D ₁₀ (W), C ₁₁ D ₉
(W) [†]					
91 ^q	M	C ₇ H ₇	141 - C ₄ H ₂	98	C ₁₁ D ₁₀ , C ₁₁ D ₉
90 ^q	W	C ₇ H ₆	116 - C ₂ H ₂	96	C ₁₁ D ₁₀ (M), C ₁₁ D ₉ (W) [†]
89 ^q	M	C ₇ H ₅	115 - C ₂ H ₂	94	C ₁₁ D ₁₀ , C ₁₁ D ₉

Table 3.1
(continued)

78 ^q	W	C ₆ H ₆	116 - C ₃ H ₂ ,	84	C ₁₁ D ₁₀ (M), C ₁₁ D ₉ (W) [†]
77 ^{t,q}	S	C ₆ H ₅	M - C ₆ H ₅ O	84	C ₁₂ D ₁₀ O
77 ^{t,q}		C ₆ H ₅	116 - C ₃ H ₃ , 115 - C ₃ H ₂		82
76 ^q	W	C ₆ H ₄	77 - H		C ₆ H ₅
76 ^q	M	C ₆ H ₄	115 - C ₃ H ₃	80	C ₁₁ D ₁₀ (M), C ₁₁ D ₉ (M)
75 ^q	M	C ₆ H ₃	77 - H ₂	78	C ₁₁ D ₁₀ , C ₁₁ D ₉
74 ^q	W	C ₆ H ₂	126 - C ₄ H ₂	76	C ₁₁ D ₁₀ , C ₁₁ D ₉
70 ^q	W				
66 ^q	M	C ₅ H ₆	116 - C ₄ H ₂	72	C ₁₁ D ₁₀
65 ^{t,q}	S	C ₅ H ₅	115 - C ₄ H ₂ , 91 - C ₂ H ₂		70
64 ^q	W	C ₅ H ₄	90 - C ₂ H ₂	68	C ₁₁ D ₁₀
63 ^{t,q}	M	C ₅ H ₃	89 - C ₂ H ₂	66	C ₁₁ D ₁₀ , C ₁₁ D ₉
62 ^q	W				
55 ^q	W				
53 ^q	W				
52 ^q	W				
51 ^{t,q}	S	C ₄ H ₃	77 - C ₂ H ₂		
50 ^{t,q}	S	C ₄ H ₂	77 - C ₂ H ₃		
41 ^q	W				
40 ^q	W				
39 ^{t,q}	S	C ₃ H ₃	94 - C ₃ H ₃ O	42	C ₁₁ D ₁₀ , C ₁₁ D ₉ , C ₆ H ₅
(W)					
38 ^{t,q}	M				
37 ^{t,q}	W				
27 ^{t,q}	S	C ₂ H ₃	77 - C ₄ H ₂		C ₆ H ₅
26 ^{t,q}	M	C ₂ H ₂	77 - C ₄ H ₃		C ₆ H ₅

3.3.2 Estimate of energy conversion

Vékey et al. have determined the kinetic-to-internal energy conversion for benzene radical cations upon SID in the collision energy range of 10-70 eV. The ER-SID diagram was deconvoluted with the use of a breakdown diagram for benzene, as obtained by photodissociation experiments [57]. However, to our knowledge, no breakdown diagrams have been published for diphenyl ether which extend to the high internal energies as deposited by the ion/surface collisions. Brown has obtained ratios of the rearrangement and cleavage reactions of diphenyl ether as a function of the EI energy [97]. At collision energies higher than 50 eV, the fragment ion spectrum of diphenyl ether is dominated by

the primary fragment $C_6H_5^+$ (m/z 77) and the secondary products of this fragment $C_4H_3^+$ (m/z 51) and $C_4H_2^+$ (m/z 50). This opens the possibility to use these secondary fragment ions to estimate the kinetic-to-internal energy conversion for the diphenyl ether radical cation. The other fragments on which the deconvolution of the ER-SID diagram of benzene is based, C_3H^+ (m/z 37) and $C_2H_2^+$ (m/z 26), appear with such low abundances in the TOF-SID spectra of diphenyl ether, that they are not included. Furthermore it can be argued that other fragmentation pathways give only minor contributions to the formation of $C_4H_3^+$ and $C_4H_2^+$ ions from diphenyl ether. It is assumed that after the primary fragmentation the residual internal energy is distributed over the secondary fragments in proportion to their degrees of freedom (DOF). On the basis of this assumption, the energy deposited into the parent diphenyl ether ion can be calculated from the internal energy of the primary fragment ion $C_6H_5^+$, as calculated from the relative intensities of the secondary fragments $C_4H_3^+$, $C_4H_2^+$, C_3H^+ and $C_2H_2^+$. To do so, the activation energy for the primary fragmentation of $C_{12}H_{10}O^+$ to $C_6H_5^+$ has to be used. This value is taken to be 6.85 eV, the difference of the appearance energy of $C_6H_5^+$ (14.88 eV) and the ionization energy of $C_{12}H_6O^+$ (8.03 eV).

$$E_{\text{int}}(C_{12}H_{10}O^+) = 6.85 + 63/27 \times E_{\text{int}}(C_6H_5^+)$$

Note that our present approach is similar to that of Meot-Ner (Mautner) et al. who have compared the SID fragmentation of protonated leucine-enkephalin (YGGFL) and its proton-bound dimer by correcting for the DOF ratio and hydrogen bond energy [102].

We have applied this adapted deconvolution both to the SID spectra of the diphenyl ether radical cation obtained with the tandem TOF and to those obtained with the tandem quadrupole SID instruments. Furthermore, to verify whether the deconvolution of fragment spectra of $C_6H_6^+$ can be applied to $C_6H_5^+$, we have obtained and deconvoluted SID spectra of $C_6H_5^+$. The results are shown in Figure 3.5 in which the mean internal energy is plotted versus the collision energy. The uncertainty in the data points obtained for the tandem TOF is somewhat larger than for the tandem quadrupole: due to signal/noise limitations we estimate an uncertainty of about 10% in the determination of the peak area in the TOF spectra, leading to an uncertainty in the calculated average energy deposited of ± 0.3 eV.

From Figure 3.5 it appears that the data points from $C_6H_5^+$ and those from the diphenyl ether fragmentation observed with the quadrupole, are on one line. The TOF data appear to level off at collision energies higher than 80 eV. For the collision energies of 80 eV and lower the estimated deposited energies are similar to those obtained from the tandem quadrupole spectra. The leveling off may be a consequence of the omission of the high energy fragments C_3H^+ and $C_2H_2^+$ for the deconvolution, which is also shown to occur for benzene by Vékey et al. [57]. A linear fit through the data points for $C_{12}H_{10}O^+$ has a slope of 0.27 for the tandem quadrupole and 0.24 for the linear part of the tandem TOF data, implying kinetic-to-internal energy conversion efficiencies of 27% and 24%,

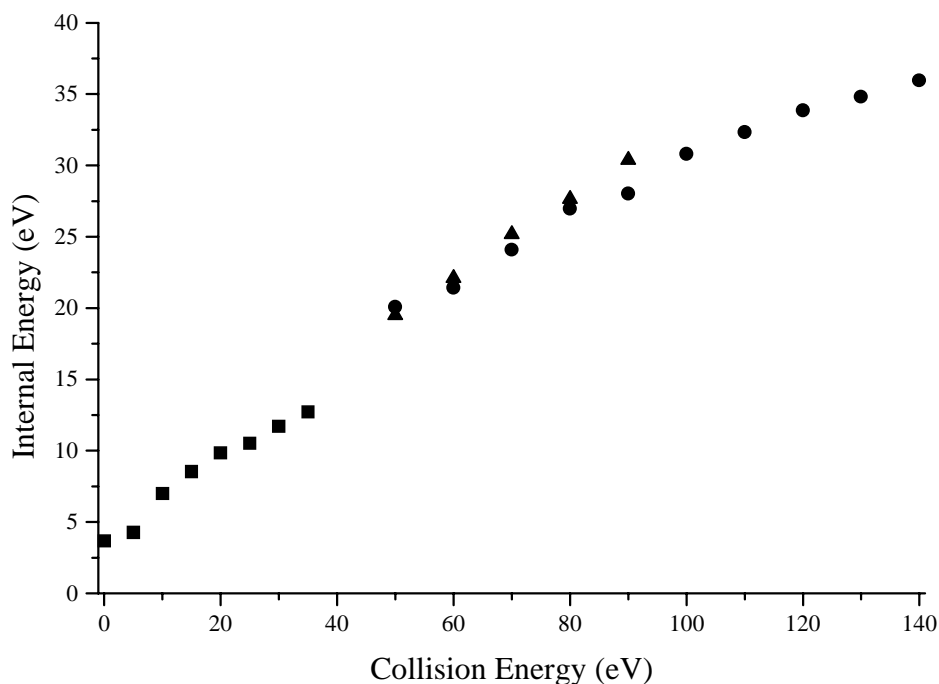


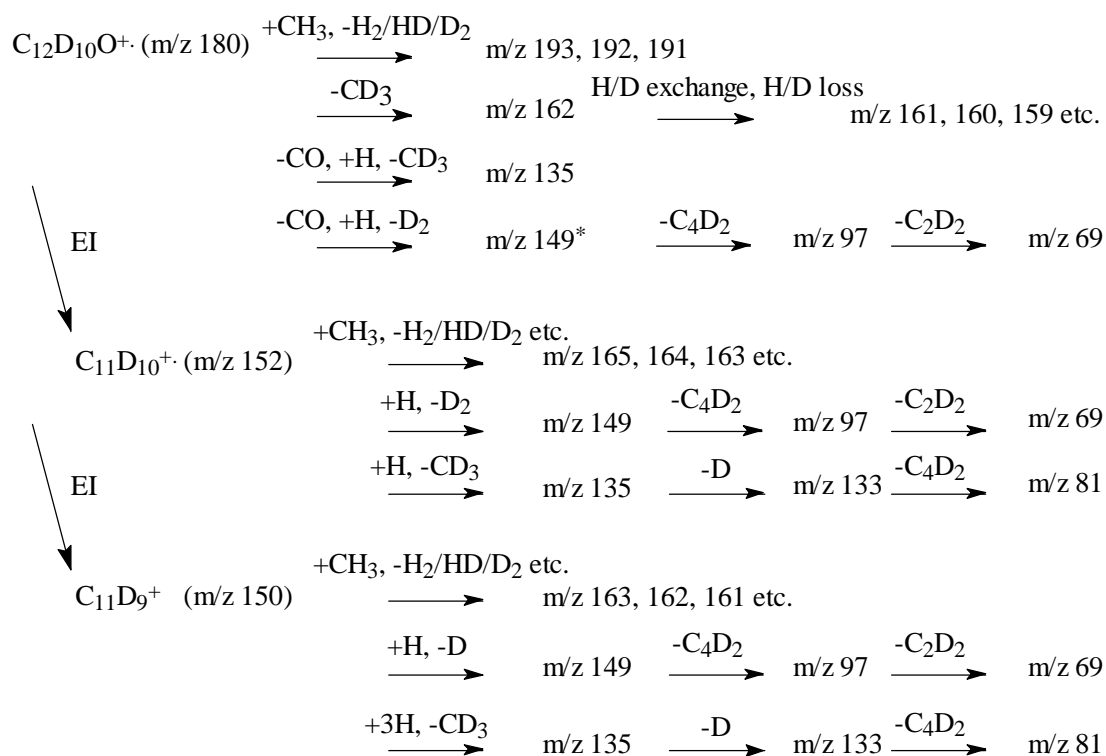
Figure 3.5: plot of average energy deposited into the parent ions, calculated by deconvolution of the (further) fragments of $C_6H_5^+$ versus collision energy. ■: $C_6H_5^+$, ●: $C_{12}H_{10}O^+$ in tandem TOF, ▲: $C_{12}H_{10}O^+$ in tandem quadrupole.

respectively. For SID spectra obtained for $C_6H_5^+$ also an energy conversion efficiency of 27% is obtained. This value is comparable to the 28% obtained by deconvolution of the SID spectra of the benzene radical cation for the tandem quadrupole by Vékey et al. [57] and the $(30\pm 7)\%$ for the tandem TOF [96]. The result for $C_6H_5^+$ gives us confidence that, within the assumptions made, the derived energy conversion for diphenyl ether shows the correct tendency. Further work is required to understand the value of the y-intercept in Figure 3.5.

Note that the results of this adapted deconvolution are not reliable when a large part of the distribution of internal energies deposited is lower than the formation energy of $C_6H_5^+$ from $C_{12}H_6O^+$. The internal energy distribution curves obtained by Vékey et al. for benzene show that at 50 eV collision energy, only a few percent of the ions obtain an internal energy lower than about 7 eV [57]. For 30 eV collisions the amount is significantly higher. Therefore we have restricted ourselves to SID spectra acquired at collision energies of 50 eV and higher for our estimate of the average energies deposited. To accurately calculate the internal energy distribution deposited into the diphenyl ether radical cations and hence the conversion efficiency of kinetic into internal energy, comparison with a breakdown diagram of diphenyl ether radical cations would be required, or another method or molecule could be used to compare the average energy conversion for the two instruments.

3.3.3 Ion/surface reactions

Collision of the diphenyl ether radical cation with the C₁₈ surface results in peaks at m/z 183 (C₁₂H₁₀O⁺ +CH₃ -H₂) and at m/z 197 (+CH₂CH₃ -H₂), reactions which have also been observed for benzene [15]. However, for the FC₁₀ surface, no reaction products have been observed at m/z 187 (+F -H₂), where they are expected in analogy with the behaviour of benzene radical cations [15]. The reaction products formed upon collision with the C₁₈ surface are confirmed by experiments with the perdeuterated compound. The ion/surface reactions observed are shown in Scheme 3.1. In addition, ion/surface collisions of the perdeuterated radical cation with the C₁₈ surface leads to odd-mass peaks at m/z 161, 159, 135, 97 and 69 (Figure 3.6(a)), while in the SID spectra on the FC₁₀ surface only the even mass fragment peaks around these m/z values are present (Figure 3.6(b)). For formation of the odd-mass products we propose a mechanism which involves hydrogen pick-up followed by the loss of a hydrocarbon neutral.



Scheme 3.1: ion/surface reactions of perdeuterated diphenyl ether and its CO loss rearrangement fragments with the C₁₈ collision surface.

^{*}): can not be distinguished in spectrum.

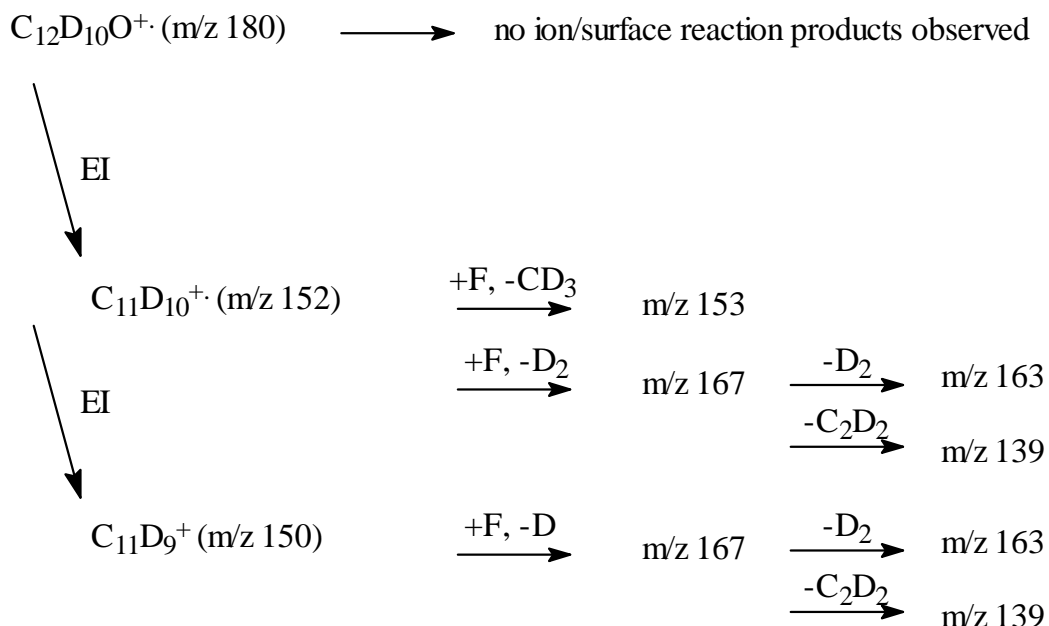
Figure 3.6: (a) 40 eV deuterated diphenyl ether on C₁₈, (b) 30 eV deuterated diphenyl ether on FC₁₀ surface, (c) 40 eV rearrangement fragment C₁₁D₁₀⁺ on C₁₈ surface,

Figure 3.6 (continued): (d) 30 eV rearrangement fragment C₁₁D₁₀⁺ on FC10, (e) 40 eV rearrangement fragment C₁₁D₉⁺ on C18 surface, (f) 30 eV rearrangement fragment C₁₁D₉⁺ on FC10 surface. The arrows indicate products of ion/surface reactions. Note that these spectra are 10x magnified.

To compare the reactivity of the diphenyl ether radical cation with that of its primary fragments towards these surfaces, we have obtained SID spectra of the perdeuterated rearrangement fragments, produced by EI of diphenyl ether (Figure 3.6(c-f)). In the spectra of both $C_{11}D_{10}^+$ and $C_{11}D_9^+$, colliding with the C_{18} surface, pick-up products at m/z 165 (+CH₃ -H₂), 164, 163 etc., are observed. Methyl loss from $C_{11}D_{10}^+$ and $C_{11}D_9^+$ is accompanied by ion/surface reactions with the C_{18} -surface, yielding products at m/z 135, 133 and further fragments, depending on the collision energy. The peaks at m/z 135, 97 and 69 are also present in the C_{18} SID spectrum of $C_{12}D_{10}O^+$.

The abundance of hydrogen exchange products around m/z 135 is lower for $C_{11}D_9^+$ than for $C_{11}D_{10}^+$, while for the SID spectra on the FC_{10} surface, the abundance of the methyl loss fragments (m/z 136, 134 and 132) are comparable. This indicates that the reactivity of the odd-electron $C_{11}D_{10}^+$ towards direct hydrogen exchange and methyl loss is higher than of the even-electron ion $C_{11}D_9^+$.

$C_{11}D_{10}^+$ and $C_{11}D_9^+$ show ion/surface reactions with the FC_{10} surface (Figures 3.6(d) and 3.6(f)), while none are observed for diphenyl ether radical cation (Figure 3.6(b)). These reactions are summarized in Scheme 3.2. While the reactivity with the C_{18} surface is different for the odd and even electron rearrangement fragments, such differences are not so clear for the FC_{10} surface. It must be noted that the overall abundance of ion/surface reaction products is much lower for the FC_{10} surface compared to the C_{18} surface, which makes it more difficult to detect possible differences in reactivity.



Scheme 3.2: ion/surface reactions of perdeuterated diphenyl ether and its CO loss rearrangement fragments with the FC_{10} collision surface.

3.4. Conclusions

In spite of the different instrument geometries and collision angles, the tandem linear TOF and the dual quadrupole instruments give similar energy-resolved SID plots for fragmentation of diphenyl ether. The tandem linear TOF has a short time frame (ca. 10^{-7} s) available for observation of fragmentation reactions. This results in general in lower relative intensities of rearrangement fragments than for the tandem quadrupole SID instrument, for which fragments with decay times of microseconds can be observed. Deconvolution of energy-resolved SID spectra show that the conversion efficiency of kinetic into internal energy (24-27%) is similar for the two instruments for collisions higher than 50 eV.

Ion/surface reactions of the diphenyl ether radical cation involve hydrocarbon addition combined with hydrogen loss on one hand, and hydrogen addition combined with alkyl loss on the other. The $C_{11}D_{10}^+$ and $C_{11}D_9^+$ fragment ions show more abundant ion/surface reaction products with both the C_{18} and the FC_{10} collision surface, than the perdeuterated diphenyl ether radical cation.

Surface-induced dissociation of singly and multiply protonated polypropylenamine dendrimers

Abstract

The ease of fragmentation of various charge states of protonated polypropylenamine (POPAM) dendrimers is investigated by surface-induced dissociation (SID). Investigated are the protonated diaminobutane propylenamines (DAB(PA)_n) DAB(PA)₈ (1+ and 2+) DAB(PA)₁₆ (2+ and 3+) and DAB(PA)₃₂ (3+ and 4+). These ions have been proposed to fragment by charge-directed intramolecular nucleophilic substitution (S_Ni) reactions. Differences in relative fragment ion abundances between charge states can be related to the occupation of different protonation sites. These positions can be rationalized based on estimates of Coulomb energies and gas-phase basicities of the protonation/fragmentation sites. The laboratory collision energies at which the fragment ion current is *ca.* 50% of the total ion current were found to increase with the size, but to be independent of charge state of the protonated POPAM dendrimers. It is suggested that intramolecular Coulomb repulsion within the multiply protonated POPAM dendrimers selected for activation does not readily result in easier fragmentation, which is in accordance with the proposed fragmentation mechanism.

4.1 Introduction

The introduction of electrospray ionization (ESI) [103, 104] has greatly facilitated the production of multiply charged ions. ESI has made it possible to analyze high molecular weight compounds, provided they can carry the required number of charges, in a *m/z* range accessible with most mass analyzers. Tandem mass spectrometry (MS/MS) has been applied successfully for increasingly large systems. Most of the MS/MS investigations concerning multiply charged ions have focused on protonated peptides or small proteins. For example, complete sequencing of multiply charged biopolymers < 3 ku has been demonstrated [105, 106], while sequence information has also been obtained for larger biopolymers such as carbonic anhydrase (29 ku) [70] and serum albumins (66 ku)

[107]. An important aspect of the dissociation of multiply protonated ions is the often observed easier fragmentation with increasing charge state [105]. This is favorable for example when the MS/MS set-up is limited to low-energy collisional activation [105, 108]. In many studies, the influence of peptide composition and charge state on the ease of fragmentation have been investigated [3, 62, 106, 108-113]. In most of these studies either gas-phase collision-induced dissociation (CID) [106, 109-111, 114] or surface-induced dissociation (SID) [3, 62, 112, 113] were employed, and the peptide results from both indicate that fragmentation is often facilitated for a higher charge state. An exception is reported by Jockush et al. who determined an increase in the fragmentation energy of ubiquitin 6+ to 11+ in black-body infrared dissociation experiments. The authors propose that the influence of multiple charges in ubiquitin is by changing the ion conformation and/or charge distribution rather than by lowering bond dissociation energies [115].

Several authors have proposed an explanation for the easier fragmentation of multiply charged peptides. Gaskell and co-workers use the term 'increased charge heterogeneity' [110, 116]. Wysocki and co-workers have proposed the 'mobile-proton' model [3, 112, 113]. The similar models state that factors that allow protons to access less basic sites in the molecules lead to enhanced non-selective cleavage that provides sequence information. The participation of amide nitrogens, which have a relatively low gas-phase basicity within the peptide, in the protonation is assumed to be required to initiate the relatively low-energy charge-directed fragmentations [61, 117, 118]. Although proton migration to the less basic amide nitrogen is an endothermic process, the significant weakening of the amide bonds in these forms 'drives' the amide bond cleavages faster than in other protonated forms [61, 117]. Separate from these explanations, multiply charged ions have also been proposed to be inherently less stable than singly charged ions [119, 120]. Rockwood et al. predict a lower activation energy for dissociation of a linear polymer with higher charge state, as a result of the Coulomb interactions [119]. Vékey and Gömöry have calculated potential energy profiles using semi-empirical and *ab initio* methods for doubly protonated tetraglycine and conclude that the presence of multiple charge sites in a peptide may lead to further weakening of the amide bond [120]. However, this result has not been verified experimentally, because a doubly protonated ion is not obtained in an ESI source for such a small non-basic peptide.

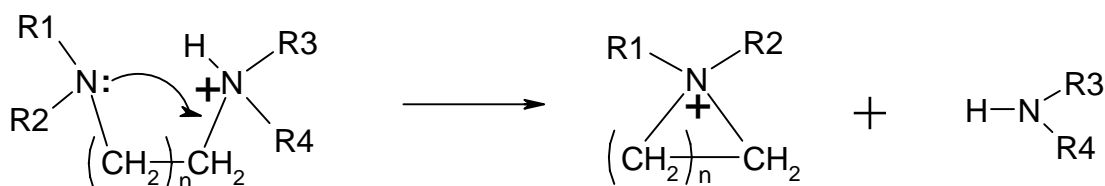
To further study the charge-state dependence of the fragmentation efficiencies, we have looked for compounds which can be multiply protonated, but in which the gas-phase basicity of various sites in the molecule does not vary as greatly as in peptides. In the present work the size and charge state dependence of the fragmentation efficiency of protonated POPAM dendrimers DAB(PA)₈, DAB(PA)₁₆ and DAB(PA)₃₂ is investigated. These dendrimers consist of a 1,4-diaminobutane (DAB) core group in which the amine hydrogens have been replaced by propylenamine (PA) groups. Therefore, they contain tertiary amine 'inner' nitrogens and primary amine end-groups [121]. The presence of many amine nitrogens in a POPAM dendrimer makes internal solvation possible, resulting in a high gas-phase basicity. In general, a protonation site in a polyamine compound is

assumed to consist of several amine nitrogens to which the proton is hydrogen-bound. Experimental data by Yamdagni and Kebarle indicate that proton-bound cyclic structures are formed in singly protonated polyamines [122].

The proposed fragmentation mechanism for polytertiary alkylamines is a charge-directed intramolecular nucleophilic substitution (S_{Ni}) [123]. A generalization of the S_{Ni} fragmentation mechanism for these compounds, based on earlier publications for singly protonated POPAM dendrimers [124, 125], is shown in Scheme 4.1. In the POPAM dendrimers the protonation of the sites which have the highest gas-phase basicity within the molecule, the tertiary amine nitrogens, can give rise to the S_{Ni} fragmentation reactions, and therefore prior mobilization of the proton is not necessary. This is different from the situation in peptides, where the proton may reside at a basic site where it can not readily initiate fragmentation, e.g. at the side chain of a basic amino acid residue or a free N-terminal amino group. In protonated dendrimers, the activation energies for the S_{Ni} reactions may not differ significantly and do not depend significantly on the protonation site. A nucleophilic attack by a non-protonated amine nitrogen is required: the proton primarily determines the preferred position of the attack but not the bond dissociation energy of the C-N bonds. For protonated peptides, the activation energy for fragmentation is determined by both the activation energy for intramolecular proton transfer and the C-N bond dissociation energy. In this case the addition of a second proton has a pronounced effect [112] besides possible Coulomb destabilization.

SID, pioneered by Cooks and co-workers [2], has proved to be a valuable tool in the energy-resolved fragmentation of many different compounds [2, 3]. With SID up to 30% of the laboratory collision energy (kinetic energy) can be converted into internal energy of the projectile ions, and the energy conversion efficiency is shown to be approximately constant up to 80 eV collision energy [57, 126]. The SID studies on the effects of peptide composition and charge state utilize fragmentation efficiency curves, which relate the percent fragmentation to the laboratory collision energy. For a peptide with a given amino acid sequence, lower characteristic fragmentation energies (E_{chr}) have been observed for the multiply protonated species [112]. E_{chr} is defined as the laboratory collision energy at the inflection point of the fragmentation efficiency curve.

In the first part of this paper we present the ESI/SID spectra for various charge states of the dendrimers. In the second part we present SID fragmentation efficiency curves of protonated dendrimers to demonstrate the effects of size and charge state on the ease of fragmentation.



Scheme 4.1

4.2 Experimental

The ESI/SID experiments have been performed in a tandem quadrupole instrument which has been described in detail earlier [39], and is based on an instrument designed by Cooks and co-workers [23]. Briefly, it consists of two Extrel 4000 u quadrupoles (now ABB Extrel, Pittsburgh, PA, USA) arranged in a 90° geometry with the SID surface positioned to intersect the ion optical path of each quadrupole. The angles between the incoming or outgoing ion beams and the surface normal are 45±5°. Ions are produced by ESI and introduced into vacuum via a stainless steel heated inlet capillary (about 400 K) which is positioned in front of a skimmer [127, 128].

In the ESI source, there was a 30 V difference between the capillary and the skimmer to improve ion extraction; this difference was maintained for all MS and MS/MS experiments and results in a relatively low level of excitation of the ions prior to the surface collision [62]. The SID collision energy is defined by the voltage difference between the skimmer and the collision surface multiplied by the charge state of the ion. The skimmer potential was kept constantly at 90 V and the surface potential was varied (e.g., 40 V applied to the surface for a doubly charged ion gives $2e \times (90-40) \text{ V} = 100 \text{ eV}$ collision energy). The parent ions are selected by the first quadrupole, and after the collision with the surface the fragment ions are analyzed by scanning the second quadrupole. We utilized a self-assembled monolayer (SAM) of fluoroalkanethiols on a gold surface, i.e. $\text{CF}_3\text{-(CF}_2)_7\text{-(CH}_2)_2\text{-S-Au}$ (hereafter, referred to as FC_{10} surface) for all SID spectra reported in this paper. To maximize sensitivity, the quadrupole mass analyzers are routinely set to a resolution of 3-5 mass units (FWHH). Some experiments have been performed with unit resolution to confirm the accuracy of peak assignment.

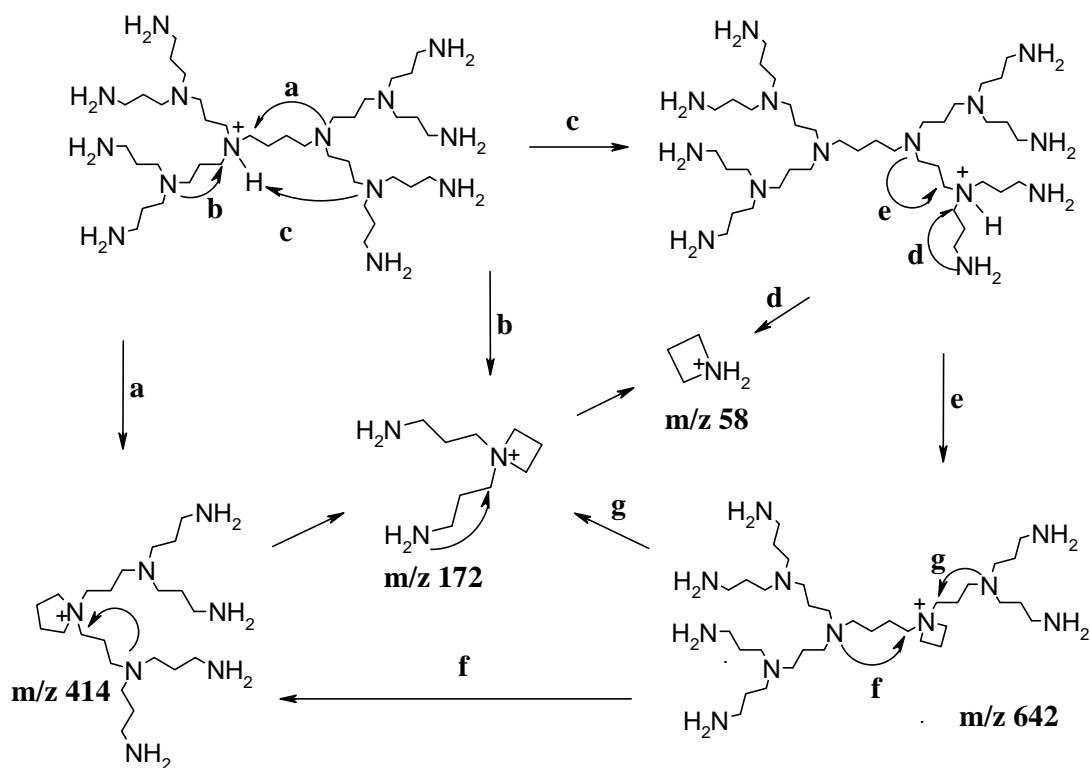
The dendrimers DAB(PA)_8 , DAB(PA)_{16} and DAB(PA)_{32} have been obtained from DSM (Geleen, The Netherlands). For ESI, 75-150 μM solutions in a 3:1 methanol:water mixture are used. To enhance multiple protonation, acetic acid is added to a concentration between 0.1-2%, to optimize the intensity of a specific charge state to be selected for SID.

Figure 4.1: 45 eV SID spectrum upon collision with a FC₁₀ surface of (a) DAB(PA)₈H⁺ (b) DAB(PA)₈H₂²⁺.

4.3 Results and Discussion

4.3.1 SID spectra

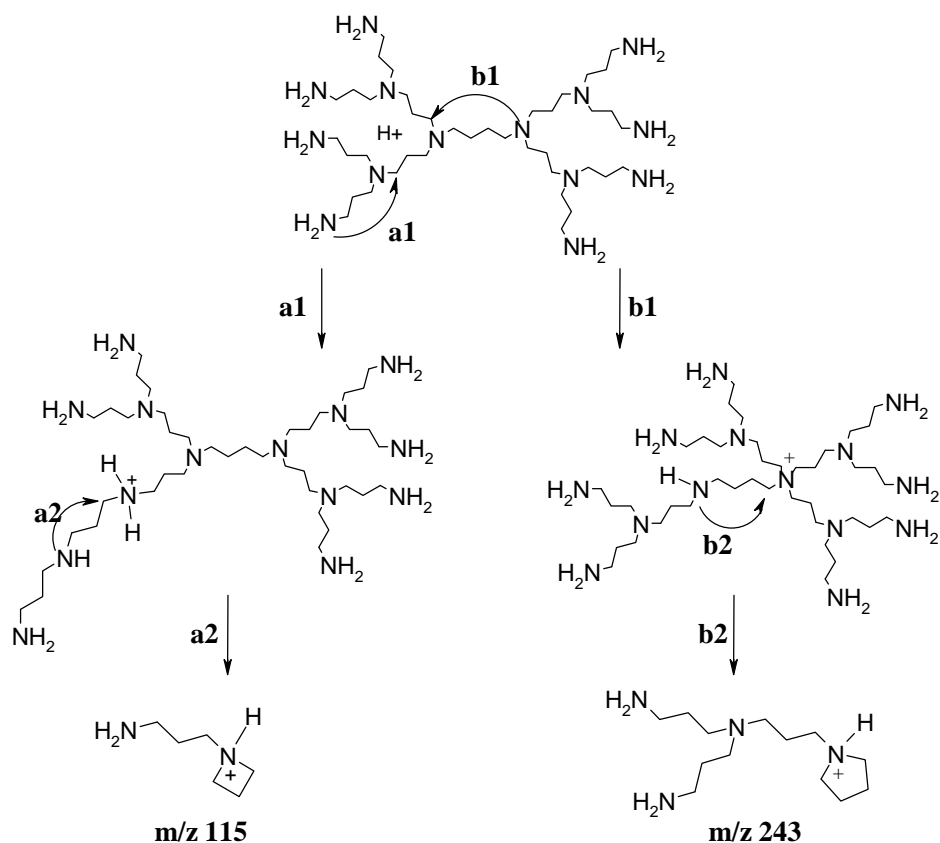
Figure 4.1(a) shows the SID spectrum resulting from 45 eV collisions of singly charged $\text{DAB}(\text{PA})_8\text{H}^+$ ions with the FC_{10} surface. The formation of most fragments, such as m/z 58, 172, 243, 414, and 642, can be explained by the S_{Ni} reactions shown in Schemes 4.2 and 4.3. In the 45 eV SID spectrum, m/z 172 is the base peak. The fragment at m/z 414 has been identified as the lowest-energy fragmentation channel, and m/z 172 to the next-lowest, by both thermal decomposition experiments and low energy CID experiments in an ion trap mass spectrometer [129]. The possibility of sequential fragmentation, such as the formation of m/z 172 out of m/z 414 (see Scheme 4.2), has been confirmed by CID MS^3 experiments in an ion trap mass spectrometer [129] and in a triple quadrupole mass spectrometer [124]. The abundance of the fragment at m/z 58 is low in Figure 4.1(a) but it increases with increasing collision energy. At collision energies higher than 100 eV the spectrum is dominated by m/z 58. The fragment at m/z 642 is of low intensity at all collision energies utilized with a maximum (10% of the base peak) around 30-35 eV collision energy (not shown). Other minor fragments in the 45 eV SID spectrum of $\text{DAB}(\text{PA})_8\text{H}^+$ are observed at m/z 70, 72, 84, 101, 112, 115, 144 and 243 (unit



Scheme 4.2

resolution experiments). These can be explained by sequential S_{Ni} rearrangement reactions in the ion, terminated by a S_{Ni} fragmentation. Examples are shown in Scheme 4.3 for formation of the fragments m/z 115 and 243.

Figure 4.1(b) shows a 45 eV SID spectrum obtained by collision of doubly charged $DAB(PA)_8H_2^{2+}$ with a FC_{10} surface. The base peak is the precursor (doubly charged) ion. The ratio of the total fragment ion current to the total ion current is the same for the spectra in Figure 4.1(a) and (b). This indicates that at the collision energy of 45 eV, the doubly charged ion is not more fragile than the singly charged one. The ease of relative fragmentation of different charge states will be further discussed below. The most abundant fragment is again the ion at m/z 172, the complementary ion of which appears only as a minor peak in the spectrum at m/z 602. Fragments at lower masses, such as at m/z 127, 115, and 58, are more intense in the SID spectrum of the doubly charged ion than in that of the singly charged ion. This is attributed to the distribution of the protonation to different sites caused by Coulomb repulsion, and is discussed in the following section. Scheme 4.4 shows a proposal for the S_{Ni} reactions leading to the fragments observed for $DAB(PA)_8H_2^{2+}$. Almost any structure in Scheme 4.4 can fragment further into m/z 172 and 58.



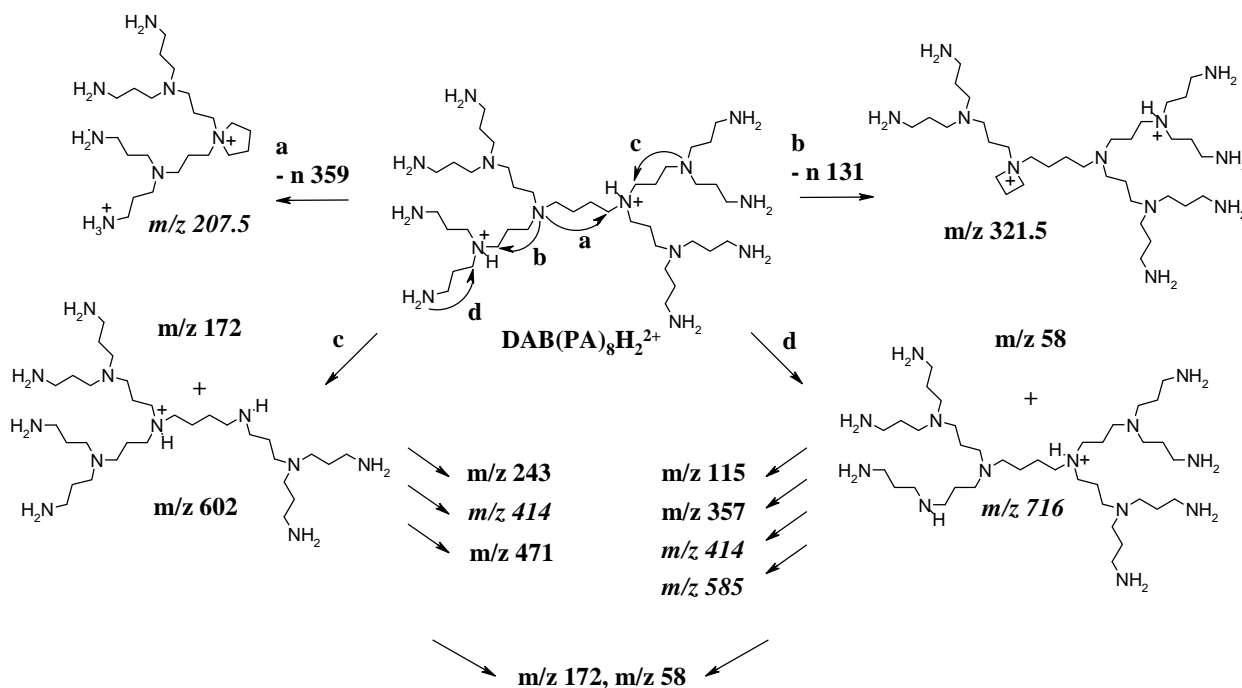
Scheme 4.3

Figure 4.2: 90 eV SID spectrum upon collision with a FC₁₀ surface of (a) DAB(PA)₁₆H₂²⁺ (b) DAB(PA)₁₆H₃³⁺.

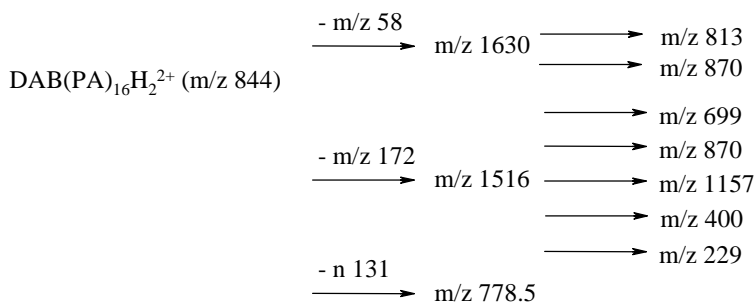
In the SID spectra of triply charged DAB(PA)₈H₃³⁺ the abundance of m/z 58 is higher than that of m/z 172 at all SID collision energies investigated. This indicates that the S_{Ni} reactions involving the outer groups are relatively facilitated (see discussion below).

Figure 4.2(a) shows the 90 eV SID spectrum of doubly charged DAB(PA)₁₆H₂²⁺ (m/z 844) on the FC₁₀ surface. Below m/z 200 this spectrum shows the same fragments as observed for DAB(PA)₈H_nⁿ⁺ (n=1,2). The base peak corresponds again to the ion at m/z 172. Most fragments of DAB(PA)₁₆H₂²⁺ can be explained based on the S_{Ni} fragmentation mechanism (Scheme 4.5). We can not provide a logical explanation for the abundant fragment at m/z 285 in the 90 eV SID spectrum of DAB(PA)₁₆H₃³⁺ (m/z 563) (Figure 4.2(b)). The SID spectra of DAB(PA)₃₂H₃³⁺ and DAB(PA)₃₂H₄⁴⁺ (not shown) also show mostly S_{Ni} fragmentation products: for example complementary ion pairs such as m/z 58

SID of singly and multiply protonated POPAM dendrimers



Scheme 4.4



Scheme 4.5

and $[MH_n-58]^{(n-1)+}$, m/z 172 and $[MH_n-172]^{(n-1)+}$, m/z 400 and $[MH_n-400]^{(n-1)+}$, and, upon loss of a 131 u neutral fragment, $[MH_n-131]^{n+}$ ($n=3,4$).

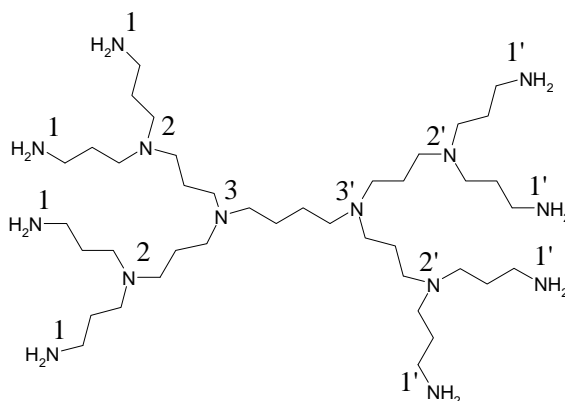
4.3.2 Gas-phase basicity and Coulomb interactions

As indicated in Scheme 4.2, the formation of m/z 414 and 172 from $DAB(PA)_8H^+$ (Figure 4.1(a) and (b)) can follow upon protonation at either of the innermost tertiary amines (N-3 and N-3') (see Scheme 4.6 for numerical designation of different amine nitrogens). The protonation at these inner tertiary nitrogens is favored by the relatively high proton affinity values of tertiary amines. Table 4.1 summarizes proton affinities for various diamines, which we consider to be representative for the amine groups in the POPAM

dendrimers [130]. We assume that in $\text{DAB}(\text{PA})_8\text{H}^+$ at low internal energy the proton is solvated between at least the two central tertiary nitrogens because these nitrogens have the largest substituents and therefore the highest gas-phase basicity. In addition the resulting structure is a proton-bound 'cyclicized' diaminobutane, which has a relatively small ring strain enthalpy [131].

When the collision (internal) energy is increased, both fragmentation and transfer of the proton to sites with a lower proton affinity can take place. This can in turn lead to fragmentation reactions at different sites, by which the low-mass fragments such as m/z 58 and m/z 115 can be formed (see Scheme 4.2 and 4.3).

In multiply protonated dendrimers the distribution of the charge sites is governed both by the gas-phase basicity of the site and by the Coulomb interactions of the charges in the ion. Schnier et al. have proposed that for a multiply protonated molecule, the lowest-energy configuration of the charges is such that the relative free energy of a given charge



Scheme 4.6

molecule	proton affinity (kJ/mol)	proton affinity (eV)
$\text{NH}_2(\text{C}_3\text{H}_6)\text{NH}_2$	979	10.1
$\text{NH}_2(\text{C}_4\text{H}_8)\text{NH}_2$	994	10.3
$\text{NH}_2(\text{C}_5\text{H}_{10})\text{NH}_2$	996	10.3
$\text{NH}_2(\text{C}_6\text{H}_{12})\text{NH}_2$	994.4	10.3
$(\text{CH}_3)_2\text{N}(\text{C}_3\text{H}_6)\text{NH}_2$	1006	10.4
$(\text{CH}_3)_2\text{N}(\text{C}_3\text{H}_6)\text{N}(\text{CH}_3)_2$	1017	10.5
$(\text{CH}_3)_2\text{N}(\text{C}_4\text{H}_8)\text{N}(\text{CH}_3)_2$	1029	10.7
$(\text{CH}_3)_2\text{N}(\text{C}_6\text{H}_{12})\text{N}(\text{CH}_3)_2$	1023	10.6

Table 4.1: Gas-phase proton affinities of several primary and tertiary diamines, as obtained from ref. [130].

configuration is minimized [132]. This relative free energy is minimized when

$$\sum_{\substack{i,j \\ i>j}}^n \frac{q^2}{4\pi\epsilon_0\epsilon_r r_{ij}} - \sum_{i=1}^n \text{GB}_i^{\text{intr}} \quad (4.1)$$

is minimized, where q is the charge, ϵ_0 is the vacuum permittivity, ϵ_r the relative permittivity of the medium and r_{ij} the distance between the charges, and $\text{GB}_i^{\text{intr}}$ the intrinsic gas-phase basicity of a protonation site. This and related expressions have been helpful in predicting the maximum charge state and proton transfer reactivity of multiply protonated compounds [132, 133]. The relative free energies associated with the charge distribution in a multiply protonated dendrimer can in principle be determined from expression 4.1. It is clear that the Coulomb interactions decrease when the charge sites are more widely separated. Although the exact determination of the lowest-energy proton distribution is complicated by the absence of values for the gas-phase basicity of the protonation sites in the POPAM dendrimer and for the distances in the lowest-energy geometry, we can estimate the magnitude of these effects. For the Coulomb interactions in $\text{DAB}(\text{PA})_8\text{H}_2^{2+}$ we assume that the maximum possible distance between the charges is realized when NH_2 groups on opposite sides of the dendrimer are protonated. Using C-C and C-N bond lengths of 1.54 Å and 1.47 Å, respectively, and assuming average bond angles of 110°, the distance is about 25 Å giving 0.6 eV Coulomb energy (using $E_{\text{Coulomb}}(\text{eV}) = 14.4/r(\text{Å})$). The displacement of one of the protons from the 'outer' shell one layer inward (by one propyl group) leads to an increase in the Coulomb energy of 0.1-0.3 eV. The proton affinity of the tertiary amine nitrogens is higher than that of the primary nitrogens of the outer shells by 0.1-0.3 eV. Thus the changes in gas-phase basicity and Coulomb repulsion are comparable, such that a single lowest-energy proton distribution can not be predicted. However, it is reasonable to say that for higher charge states there is increased participation of the 'outer' amine nitrogens (N-2 and N-1 in Scheme 4.6) in the solvation of the protons, compared to that for $\text{DAB}(\text{PA})_8\text{H}^+$ where at low internal energy the proton is solvated by central tertiary nitrogens (N-3 and N-3'). This assumption is supported by the higher relative abundance of fragments from the periphery of the ion for higher charge states of the dendrimers (compare Figure 4.1(a) with 4.1(b), and Figure 4.2(a) with 4.2(b)). However, the probability that two of the outer primary amines are simultaneously protonated in a doubly charged dendrimer is low. For example, proton transfer from sites N-2 and N-2' to N-1 and N-1' in $\text{DAB}(\text{PA})_8\text{H}_2^{2+}$ decreases the Coulomb repulsion with only 0.3 eV, but the gas-phase basicity with 0.6 eV. Similarly, we assume that the probability of simultaneous protonation of inner nitrogens (N-3 and N-2 as well as N-3 and N-3') is low due to strong Coulomb repulsion, as supported by the absence of m/z 414 from the SID spectra of $\text{DAB}(\text{PA})_8\text{H}_2^{2+}$. Such fragments containing the 5-membered ring are also absent from the SID fragment spectra of the other multiply protonated dendrimers. For example, there is no peak at m/z 870 in the spectra of $\text{DAB}(\text{PA})_{16}\text{H}_2^{2+}$, whereas it has been observed in the SID fragment spectra of the singly protonated form, $\text{DAB}(\text{PA})_{16}\text{H}^+$.

4.3.3 Fragmentation efficiency

Figure 4.3 shows the ESI/SID fragmentation efficiency curves obtained for $\text{DAB}(\text{PA})_8\text{H}^+$, $\text{DAB}(\text{PA})_8\text{H}_2^{2+}$, $\text{DAB}(\text{PA})_{16}\text{H}_2^{2+}$, $\text{DAB}(\text{PA})_{16}\text{H}_3^{3+}$, $\text{DAB}(\text{PA})_{32}\text{H}_3^{3+}$ and $\text{DAB}(\text{PA})_{32}\text{H}_4^{4+}$. The fragmentation efficiency curves clearly show the independence of the characteristic fragmentation energy, E_{chr} , on the dendrimer charge state and the increase of E_{chr} with dendrimer size. The obtained values of E_{chr} are given in Table 4.2, which also gives the number of DOF for each of the ions. Previously an approximately linear correlation between the number of degrees of freedom (DOF) and E_{chr} for a series of singly protonated oligopeptides has been suggested [102, 112]. However, for the dendrimers investigated in this study, we do not find a linear relationship between E_{chr} and DOF. The approximate doubling of E_{chr} of $\text{DAB}(\text{PA})_{16}$ compared to E_{chr} of $\text{DAB}(\text{PA})_8$ is not followed by another doubling of E_{chr} for $\text{DAB}(\text{PA})_{32}$. Under assumption of statistical distribution of the internal energy on the time scale of the SID experiments, a possible explanation for this non-linearity can be an influence of the size or shape of the parent ion on the energy conversion efficiency. This effect has been suggested by Beck et al. for fullerenes [134]. On the other hand, non-statistical behaviour, as suggested to occur for ions with a high number of DOF by Schlag et al. [135] can not be excluded. In a forthcoming publication the internal energies for fragmentation on the time scale of the SID experiments will be determined by RRKM model calculations, and compared to fragmentation energies determined from the experimental data.

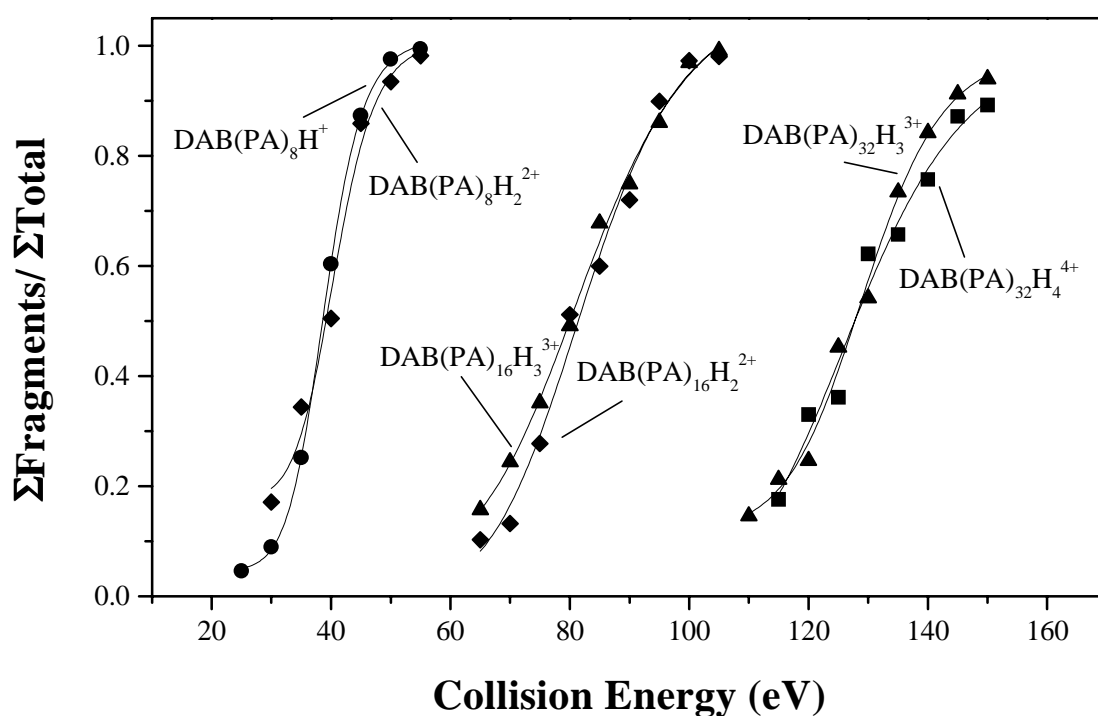


Figure 4.3: fragmentation efficiency curves of various charge states of POPAM dendrimers upon collisions with a FC_{10} surface.

parent ion	E_{chr} (eV)	number of DOF
DAB(PA) ₈ ⁺	39.0	447
DAB(PA) ₈ ²⁺	40.7	450
DAB(PA) ₁₆ ²⁺	82.6	966
DAB(PA) ₁₆ ³⁺	82.7	969
DAB(PA) ₃₂ ³⁺	129.4	2121
DAB(PA) ₃₂ ⁴⁺	127.3	2124

Table 4.2: The collision energy values at the inflection points of the fragmentation efficiency curves (characteristic collision energy, E_{chr}) for the investigated POPAM dendrimers.

From Figure 4.3 it is seen that the measured E_{chr} does not depend on the charge state for these dendrimer ions. In general, E_{chr} can be determined with a reproducibility of 1-2 eV (see also ref. [136]) due to statistical variations in the data. Additionally, there can be systematic, charge dependent errors in the measured E_{chr} . First, the higher the charge state of the ions the more internal energy they can gain by activation in the nozzle-skimmer region. Consequently, less SID collision energy is needed for the multiply charged ions to have the same internal energy as a lower charge state. Hence there can be a systematic underestimation of E_{chr} for a higher charge state. A second systematic error comes from the fact that a multiply charged parent ion can give more than one charged fragment per unimolecular dissociation. Consequently, at a comparable fragmentation rate, the multiply charged ion can give a higher fragment ion abundance compared to a singly charged ion. This could also introduce a shift in E_{chr} to lower values for the higher charge states. Thus, although the experimental values of E_{chr} are charge state independent, a small increase in the characteristic activation energy with charge state might be present.

The charge-state independent E_{chr} of POPAM dendrimers contrasts with the results for protonated peptides, for which lower E_{chr} have been observed for higher charge states [3, 112]. This contrast can be explained in terms of the 'mobile proton' model for the fragmentation of protonated peptides. As described in the previous section, the probability of protonation of the sites at which the S_{Ni} fragmentation occurs is high at low internal energies for the charge states of the POPAM dendrimers used in this study. Hence it is not necessary to 'mobilize' protons to cause fragmentation, and therefore there is no benefit of multiple charging. The observed independence of E_{chr} on the charge state of protonated POPAM dendrimers also suggests that there is no significant destabilization by Coulomb repulsion within the multiply charged ions selected for activation. Experiments with higher charge states would be interesting because stronger Coulomb effects may affect the fragmentation efficiency more distinctly. Larger destabilizing effects for sufficiently high charge states might lead to an observable decrease of E_{chr} . Alternatively, a higher activation energy for the S_{Ni} fragmentation of higher charge states may be required, when

the charges are driven to primary amine sites (N-1) by Coulomb repulsion. However, we have not been able to obtain sufficient highly charged dendrimers in our ESI source to test this hypothesis. In this case additional activation energy may be needed, to mobilize the protons to the tertiary sites (N-2 and N-3), which could increase E_{chr} .

4.4 Conclusions

The origin of most of the fragment ions from singly and multiply protonated POPAM dendrimers can be explained based on charge-directed S_{Ni} reactions. Observed trends in relative abundances of fragments for different charge states of the dendrimers can be explained based on competition between minimization of the Coulomb repulsion and proton occupation of the sites with the highest gas phase basicities.

The characteristic fragmentation energy is found to increase with the size of the dendrimers. However, in contrast to previous results for multiply protonated peptides of comparable size and charge states, no dependence of the characteristic fragmentation energy on the charge state of the POPAM dendrimers is observed. Apparently, for the charge states produced in the ESI source, Coulomb forces due to multiple protonation do not lead to sufficient bond weakening to influence the ease of fragmentation. The charge-state independence of the fragmentation efficiency is in contrast with previous results for multiply protonated peptides. In the protonated dendrimers, S_{Ni} fragmentation reactions are possible from almost any positioning of the protons. Hence proton transfers do not result in significant decrease in the activation energy of the S_{Ni} processes, and therefore increasing the charge state does not result in easier fragmentation. This is a characteristic difference between protonated dendrimers and protonated peptides: for the latter ions the mobilization of proton(s) from more basic sites to amide nitrogens leads to a significant decrease in the dissociation energy of the amide bond.

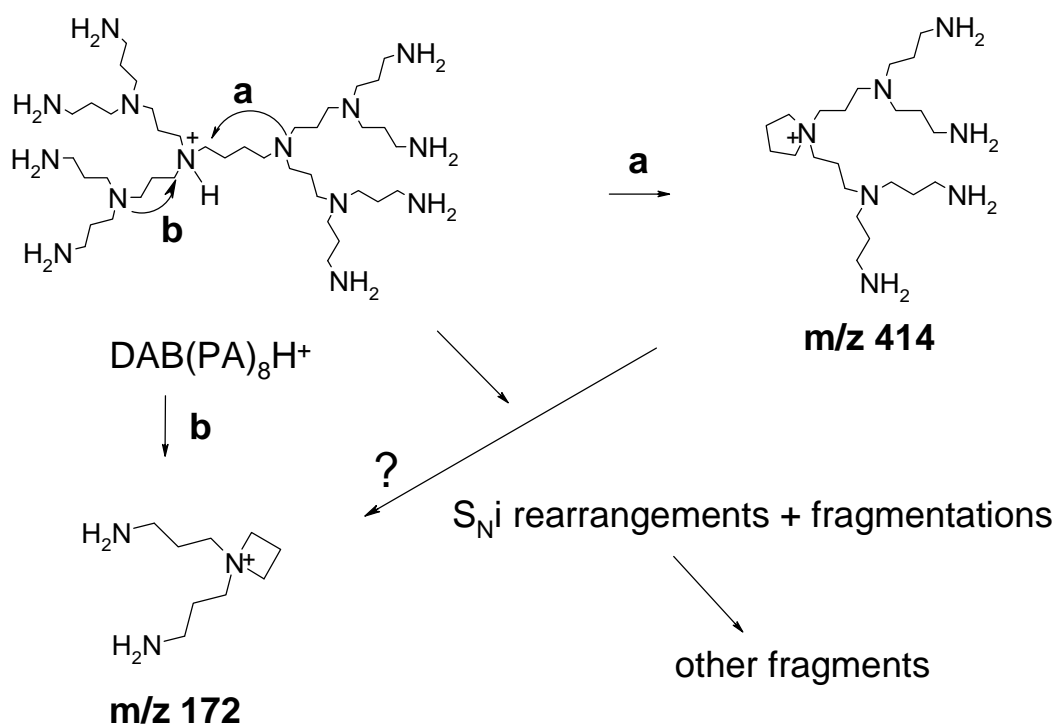
Activation of POPAM dendrimers by low-energy multiple collision CID in trapped ion mass spectrometers

Abstract

To determine the order of appearance energies of fragments of protonated polypropylenamine dendrimers, MS^2 experiments are performed in quadrupole ion trap (ITMS) and Fourier transform ion cyclotron resonance (FTMS) mass spectrometers. ITMS³ experiments show that fragmentation of $DAB(PA)_8H^+$ to m/z 172 can occur via m/z 414. Energy-resolved fragment spectra of POPAM dendrimers obtained with low-energy collision induced dissociation (CID) in a FTMS are compared with surface-induced dissociation (SID) fragment spectra obtained in a tandem linear quadrupole mass spectrometer. The internal energies needed for fragmentation of the POPAM dendrimers in these CID and SID experiments are estimated and compared. RRKM calculations are performed to help interpretation of the experimental results. Critical energies for the S_{Ni} reactions leading to fragments m/z 414 and 172 from $DAB(PA)_8H^+$ in the range of 1.4-1.6 eV give $k(E)$ curves approximately in agreement with the experimental results, the critical energy for formation of m/z 172 being larger than for formation of m/z 414.

5.1 Introduction

In the previous chapter, results were shown obtained by surface-induced dissociation (SID) of protonated polypropylenamine (POPAM) dendrimers [137]. Almost all fragment ions could be rationalized by single or sequential intramolecular nucleophilic substitution (S_{Ni}) reactions (Scheme 5.1). However, several questions could not be answered based on the SID data. First, it was difficult to determine the order in which the low-energy fragments of a selected parent ion appear as a function of internal energy [137]. Multiple fragment ions appeared simultaneously at all collision energies. Second, it was proposed that various reaction pathways could lead to the same fragment ion [137]. However, sequential fragmentation could not be demonstrated in spite of an attempt to use nozzle-skimmer dissociation to create dendrimer fragment ions in the electrospray ionization (ESI) source for pseudo- MS^3 studies. The intensity of these fragments



Scheme 5.1

individually was not sufficient to give SID spectra when selected.

A possible cause for the difficulty in determining the order of appearance of the low-energy fragments by SID is the instantaneous acquisition of a wide internal energy distribution by the parent ions, limiting the energy resolution of our studies. The kinetic-to-internal energy conversion by SID occurs in 10^{-12} - 10^{-14} s and can therefore be regarded as instantaneous compared to fragmentation rates, which are, depending on the internal energy of the ion, usually lower than 10^{12} s⁻¹ [2]. In addition, the internal energy distribution obtained by ions upon activation with SID is known to be wide. Vékey et al. have determined the full width at half maximum of the internal energy distribution upon SID as approximately half the mean internal energy deposited, using benzene as the probe ion [57]. Hence energetically close processes, as assumed for the fragmentation reactions of the diaminobutane (DAB) propylenamine (PA) dendrimer $\text{DAB(PA)}_8\text{H}^+$ into m/z 414 and m/z 172 , may not be separated by energy-resolved (ER-)SID. The internal energy distribution of ions activated by gas phase collision-induced dissociation (CID) with multiple low-energy collisions also has a considerable width. For the range between 5 and 28 eV laboratory kinetic energy, Wysocki et al. found widths of internal energy distributions approximately equal to or larger than the average internal energy using metal carbonyl probe ions [66]. During CID in a quadrupole ion trap mass spectrometer (ITMS) kinetic energy is converted to internal energy by multiple low-energy collisions, which typically involve laboratory kinetic energies of the parent ions lower than 15 eV [138]. Since in multiple low-energy collision CID the energy is converted in small steps over a longer

period of time, distinction of the order of appearance of the fragments as a function of energy may be easier, compared to when energy conversion is instantaneous. We have performed ITMS CID experiments to determine the lowest-energy fragmentation of $\text{DAB(PA)}_8\text{H}^+$ and to test the previously proposed sequential fragmentation mechanisms [137] with MS^n . We have investigated the fragmentation obtainable for the POPAM dendrimer $\text{DAB(PA)}_8\text{H}^+$ in ITMS CID as a function of the excitation amplitude and buffer c.q. collision gas composition and pressure.

Heeren and Vékey have determined energy conversion efficiencies for CID of protonated leucine-enkephalin upon resonant excitation in FTMS [139]. Assuming that the same energy conversion efficiency can be used for ions of similar size and composition, being organic polymers of 500-1000 u, we can estimate the internal energy corresponding to fragmentation of the dendrimers on the time scale of the FTMS experiments. To help the interpretation of these experimental results, we have calculated fragmentation rates of the POPAM dendrimers by RRKM methods.

5.2 Experimental

5.2.1 ITMS experiments

The ITMS experiments have been performed on an instrument described previously [140]. Briefly, it consists of a Bruker Esquire ion trap mass spectrometer with a home-built external matrix-assisted laser desorption/ionization (MALDI) source the same as that described previously in a combination with the FTMS instrument [141]. The ion trap is equipped with a direct gas inlet for the buffer gas which also functions as the collision gas. The pressure is measured outside the ion trap. Hence the pressure inside the ion trap is approximately 10 times higher than the measured pressure [142].

Frequency-tripled laser light (354 nm) produced from a Nd:YAG laser (Quanta-Ray GCR-11) is focused onto a single sample MALDI probe with an incident angle of approximately 45° . The ion beam is transported by an electrostatic lens system over a 0.2 m distance and focused onto the entrance of the ion trap [140]. Mass spectra are recorded by scanning the amplitude of the rf voltage on the ring electrode and the voltage over the two end-caps. This way the m/z values at which ions come in resonance and therefore are ejected, increases as a function of time. Between the firing of the laser and the recording of the mass spectrum, a delay of approximately 70 ms is used to allow the ions to travel from the source to the cell (several microseconds flight time) and to cool the ions to the center of the trap. For CID experiments, ions created by MALDI are accumulated and after a 25 ms delay the parent ions are selected by resonant ejection of all ions outside a 20 u window from the selected m/z value. After a 5 ms delay the selected parent ions are

kinetically excited by a rf voltage applied to the end-cap electrodes. We assume that the delay of 30 ms total between ion accumulation and resonant excitation in the ion traps is sufficient for equilibration of the ion temperature to that of the buffer gas [143]. The bandwidth of the rf excitation voltage corresponds to a window of 10 mass units around the parent ion m/z value. The internal energy of the parent ions is varied by varying the amplitude of the rf excitation voltage, for a fixed duration of 60 ms.

5.2.2 FTMS experiments

The ESI/FTMS experiments are performed on a Bruker Apex 7T FTMS equipped with a home-built external ESI source, described previously [139]. The ESI source is operated with a nozzle-skimmer voltage difference of 20 V to prevent collisional activation in the nozzle-skimmer region. The ions are transported from the ESI source into the ICR cell through an electrostatic ion guide in a 5-stage differential pumping system. The ions are accumulated during 400 ms after which the electrostatic gate is closed. The ions are left to equilibrate to the ICR cell temperature (293 K) for 10 s. For CID, Ar gas is introduced in the ICR cell through a pulsed valve which is kept open for 1 second upon which the pressure rises to 10^{-7} mbar. In the presence of the collision gas, the kinetic energy of the parent ions under study is increased by application of a resonant dipolar rf excitation field, but without prior isolation of these parent ions. The rf is switched on 100 ms after opening of the collision gas valve. The kinetic energy of the ions upon resonant excitation in the FTMS is given by

$$E_{\text{lab}} = \frac{q^2 \alpha^2 \Delta V^2 t_{\text{exc}}^2}{8md^2} \quad (5.1)$$

where α is the geometry factor for the InfinityCell (0.897) [139, 144], ΔV the amplitude of the voltage applied to the cell plates, t_{exc} the time during which the excitation field is applied, m the mass of the ion, q its charge, and d the diameter of the ICR cell (6 cm). The center-of-mass collision energy E_{cm} is defined by

$$E_{\text{cm}} = \{m_{\text{g}}/(m_{\text{i}}+m_{\text{g}})\} \times E_{\text{lab}} \quad (5.2)$$

where m_{g} is the molecular weight of the collision gas and m_{i} the molecular weight of the parent ions.

In our CID experiments the ion kinetic energy is varied by varying the duration of the rf excitation field, typically between 100 and 300 μs . The rf amplitude is maintained 36.0 V peak-to-peak for all experiments described. No parent ion isolation was used to prevent unintentional off-resonant excitation [145]. After closing of the Ar valve, a pump-down delay of 10 s is used before the ions are excited for detection. The pressure in the ICR cell during ion detection is lower than 10^{-9} mbar.

5.2.3 sample preparation

The POPAM dendrimers DAB(PA)₈, DAB(PA)₁₆ and DAB(PA)₃₂ have been obtained from DSM (Geleen, The Netherlands). For MALDI, a solution of DAB(PA)₈ : 2,5-dihydroxy benzoic acid (DHB) of 1:1000 in ethanol was applied to the stainless steel MALDI probe, and allowed to dry in air. For ESI, 75-150 μ M solutions in a 3:1 methanol:water mixture are used. To enhance multiple protonation, acetic acid is added to a concentration between 0.1-2%, depending on the charge state to be obtained.

5.2.4 Computational details

RRKM calculations on DAB(PA)₈ and DAB(PA)₁₆ have been performed with the 'Mass Kinetics' program written by Drahos and Vékely [146-148]. Vibrational frequencies of propylamine have been calculated by ab initio methods (B3LYP/6-31G(d)) using the Gaussian '94 package. The first 15 frequencies are 129, 232, 260, 294, 454, 768, 864, 882, 931, 1039, 1063, 1095, 1175, 1255 and 1311 cm^{-1} . These have been applied to calculate $k(E)$ values for DAB(PA)₈H⁺ and DAB(PA)₁₆H₂²⁺ by scaling up to the number of degrees of freedom of the dendrimer ions. The transition state frequencies have been estimated, based on the vibrational model described previously by Vékely et al. [136]. In this model, it is assumed that during a simple bond cleavage 1 rotation, 4 rocking and 1 stretching mode are converted into 3 rotation and 3 translation modes. The stretching mode at 1255 cm^{-1} is arbitrarily selected as the reaction coordinate. For the rotation the mode at 129 cm^{-1} is selected, for the 4 rocking modes 768, 864, 882 and 931 cm^{-1} are used. The transition state frequencies used are the ground state frequencies divided by two. In the cyclic transition state, the number of atoms in the transition state minus one rotations are frozen, so these rotations are converted into stretching and rocking frequencies. These frequencies are 232, 260, 294 and 454 cm^{-1} each frozen 5 times for the 5-membered ring transition state, and so on.

The relation between $\log(k)$ and E has been approximated by fitting an exponential decay function to the RRKM calculated $\log(k(E))$ values with Microcal Origin Version 5.0. Calculations of breakdown diagrams based on the fitted $\log(k(E))$ relations have been performed with Microsoft Excel 97.

5.3. Results

5.3.1 ITMS experiments

Figure 5.1(a) shows the MALDI spectrum of $\text{DAB}(\text{PA})_8$ in 2,5-DHB obtained with the ITMS set-up. Only the singly protonated form is observed. The peaks at m/z 137 and 273 are assigned to products formed from the 2,5-DHB matrix. The fragment ions of $\text{DAB}(\text{PA})_8\text{H}^+$ at m/z 414 and 172 are also observed in the MALDI spectrum. The abundance of these fragment ions varies with the laser intensity. However, when the laser

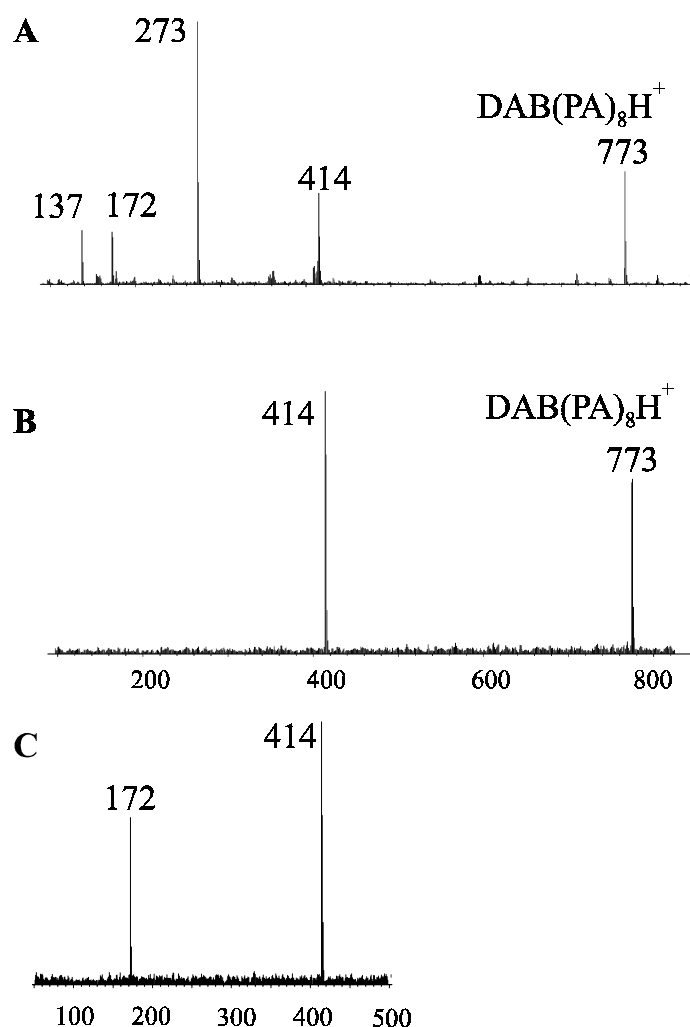


Figure 5.1: (a) MALDI-ITMS spectrum of $\text{DAB}(\text{PA})_8\text{H}^+$; (b) ITMS^2 spectrum of isolated $\text{DAB}(\text{PA})_8\text{H}^+$ upon collisions with He, pressure = 2.4×10^{-5} mbar, excitation duration = 60 ms, resonant excitation amplitude = 2.7 V; (c) ITMS^3 spectrum of isolated fragment m/z 414, excitation duration = 60 ms, resonant excitation amplitude = 1.8 V.

intensity is lowered such that the dendrimer fragment ions have disappeared from the spectra, the signal of $\text{DAB}(\text{PA})_8\text{H}^+$ is insufficient for MS/MS experiments. The laser power used for the MS^n experiments gives about 50% fragmentation of the parent ion $\text{DAB}(\text{PA})_8\text{H}^+$ in the MALDI spectra. Computer simulations by Goeringer et al. indicated that the equilibration time of peptide ions of 1 kDa molecular weight is approximately 0.5 ms at 10^{-3} mbar He buffer gas pressure in the trap [143]. In our experiments the buffer gas pressure is lower ($1.7\text{--}3.5 \times 10^{-5}$ mbar He, measured outside the trap) and therefore longer equilibration times are required. We assume that the parent ions have obtained the temperature of the buffer gas (300 K) during the 30 ms delay between ion accumulation and excitation, and therefore that the use of high laser power does not influence the fragmentation efficiency. Figure 5.1(b) shows a MS/MS spectrum of $\text{DAB}(\text{PA})_8\text{H}^+$ obtained by resonant excitation for 60 ms, with an excitation rf amplitude of 2.7 V and He buffer gas pressure of 2.4×10^{-5} mbar. The only fragment observed is m/z 414. The MS^3 spectrum of m/z 414 obtained by selection and resonant excitation for 60 ms at 1.8 V is shown in Figure 5.1(c). The only fragment observed is m/z 172. This confirms the possibility of formation of m/z 172 from m/z 414.

By varying the excitation amplitude in the multiple collision ITMS² experiments we could vary the fragmentation efficiency, defined as the total fragment ion current divided by the fragment plus parent ion current, of the $\text{DAB}(\text{PA})_8\text{H}^+$ ions between 0 and 100%, but

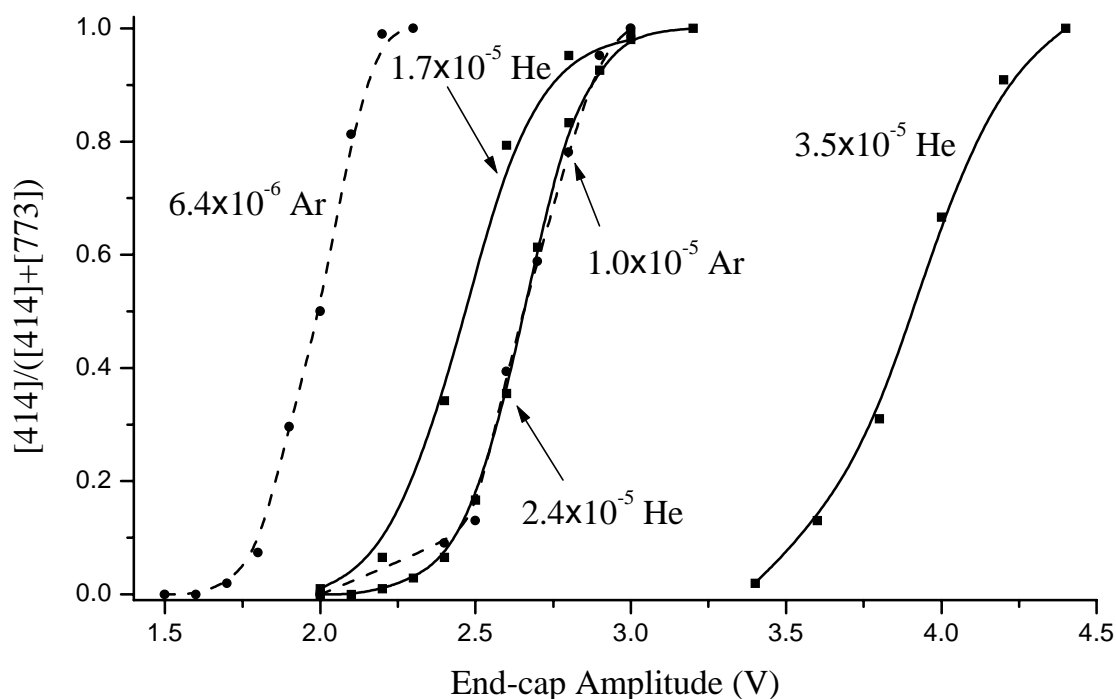


Figure 5.2: Fragmentation efficiency curves of $\text{DAB}(\text{PA})_8\text{H}^+$ fragmentation in ITMS upon resonant excitation at various pressures. For all curves the duration of the rf excitation pulse is 60 ms.

m/z 414 remained the only fragment observed. To test further if other fragments, for example m/z 172, could be formed by excitation of $\text{DAB}(\text{PA})_8\text{H}^+$ in ITMS² experiments, we have varied the buffer gas pressure and composition. The internal energy of the ions at a given excitation amplitude is known to increase with decreasing buffer gas pressure and to increase with the molecular weight of the buffer gas [149]. Figure 5.2 shows the fragmentation efficiency curves obtained with He (1.8 , 2.4 and 3.5×10^{-5} mbar) or Ar (6.4×10^{-6} and 1×10^{-5} mbar) buffer gas. However, fragment ions other than m/z 414 were not observed upon resonant excitation of $\text{DAB}(\text{PA})_8\text{H}^+$ under any of these conditions.

5.3.2 Energy-resolved CID and SID

Figure 5.3 shows ER-CID diagrams of $\text{DAB}(\text{PA})_8\text{H}^+$ and $\text{DAB}(\text{PA})_{16}\text{H}_2^{2+}$ obtained with resonant excitation of the parent ions in the FTMS. In all dendrimer spectra with and without excitation a small but not very reproducible signal (on average 3%) is observed at m/z 172. These ions are assumed to be responsible for the signal of m/z 172 observed below 80 eV collision energy, and leads to an uncertainty in the ER-CID curves in Figure 5.3(a) of 5%. In the FTMS CID experiments with $\text{DAB}(\text{PA})_8\text{H}^+$ fragmentation efficiency approaches unity at sufficiently high collision energy. However, the parent ions of $\text{DAB}(\text{PA})_{16}\text{H}_2^{2+}$ do not disappear from the CID spectra even at laboratory kinetic energies approaching 1 keV, but remains 10-20% of the initial ion abundance. In this particular experiment this is possibly caused by leaking of parent ions from the ESI source into the ICR cell during the waiting time after excitation. Because of this and the small current of m/z 172 at low energies as in the experiments with $\text{DAB}(\text{PA})_8\text{H}^+$, we assume an uncertainty of 20% of the ER-CID curves in Figure 5.3(b). In the FTMS ER-CID spectra of $\text{DAB}(\text{PA})_8\text{H}^+$ the fragment at m/z 414 is more abundant than m/z 172 between 80 and 150 eV laboratory kinetic energy. Above 150 eV, m/z 172 dominates the fragment spectra. For $\text{DAB}(\text{PA})_{16}\text{H}_2^{2+}$ m/z 172 is the dominant fragment at any collision energy above threshold (~ 200 eV laboratory kinetic energy), whereas also the abundance of fragment m/z 400 increases with the kinetic energy of the parent ion. The two most abundant fragments, m/z 414 and m/z 172 for $\text{DAB}(\text{PA})_8\text{H}^+$ and m/z 172 and m/z 400 for $\text{DAB}(\text{PA})_{16}\text{H}_2^{2+}$ constitute more than 95% of the total fragment ion current at any collision energy used (spectra not shown). The most abundant other fragment, with an abundance of 2-3%, is m/z 115 for both $\text{DAB}(\text{PA})_8\text{H}^+$ and $\text{DAB}(\text{PA})_{16}\text{H}_2^{2+}$.

Figure 5.4 shows ER-SID diagrams of $\text{DAB}(\text{PA})_8\text{H}^+$ and $\text{DAB}(\text{PA})_{16}\text{H}_2^{2+}$ obtained with SID in a tandem quadrupole set-up, based on the same data as the fragmentation efficiency curves shown in Chapter 4 (Figure 4.3). Note that the appearance energies of m/z 414 and 172 for $\text{DAB}(\text{PA})_8\text{H}^+$ can not be distinguished, both fragments appear at a collision energy of 30 eV. In the dendrimer SID spectra the abundance of fragments other than m/z 414 and 172 ($\text{DAB}(\text{PA})_8\text{H}^+$) or m/z 172 and 400 ($\text{DAB}(\text{PA})_{16}\text{H}_2^{2+}$) is much larger compared to the CID spectra: up to 30% of the total ion current at 100% fragmentation

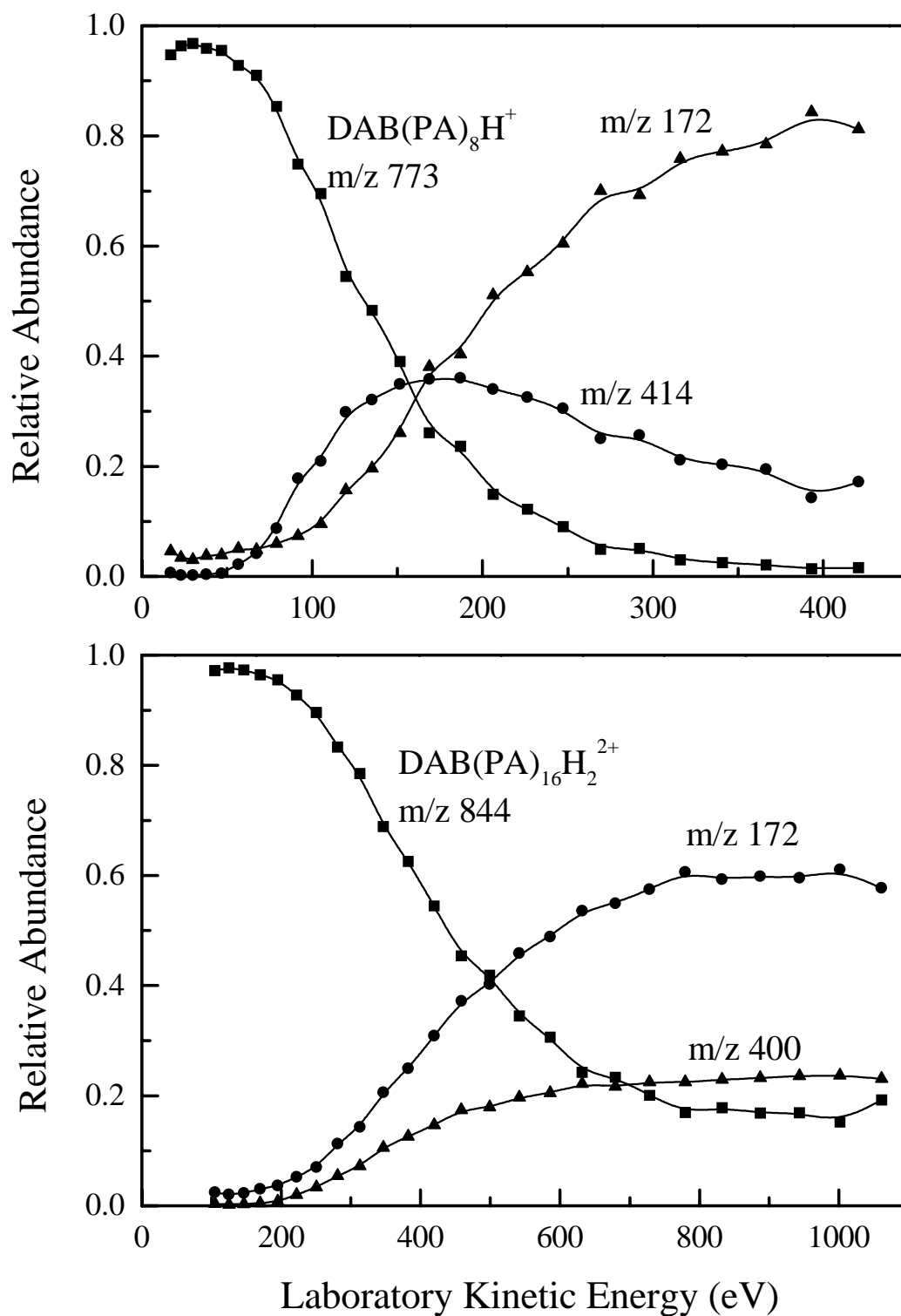


Figure 5.3: Energy-resolved CID diagrams obtained in the FTMS set-up, with 10^{-7} mbar Ar collision gas upon resonant excitation of (a) $\text{DAB(PA)}_8\text{H}^+$ and (b) $\text{DAB(PA)}_{16}\text{H}_2^{2+}$.

efficiency of $\text{DAB}(\text{PA})_8\text{H}^+$ (55 eV) and 50% at 100% fragmentation efficiency of $\text{DAB}(\text{PA})_{16}\text{H}_2^{2+}$ (100 eV). The majority of these fragments are in the m/z region below 172, for example m/z 127, 115, and 58. The mechanism proposed for their formation is discussed in a previous paper [137]. Experiments with higher collision energies (data not shown) indicate that the abundance of these low- m/z fragment ions continues to increase as the ion/surface collision energy is increased even after the parent ion has disappeared from the spectra. This is in contrast to observations in similar FTMS CID experiments (data also not shown), where the fragment ion relative abundances remain approximately constant above a certain collision energy (approximately 400 eV laboratory kinetic energy for $\text{DAB}(\text{PA})_8\text{H}^+$, 800 eV for $\text{DAB}(\text{PA})_{16}\text{H}_2^{2+}$). Possible causes for these differences between the SID and CID fragment spectra are discussed in section 5.4.3.

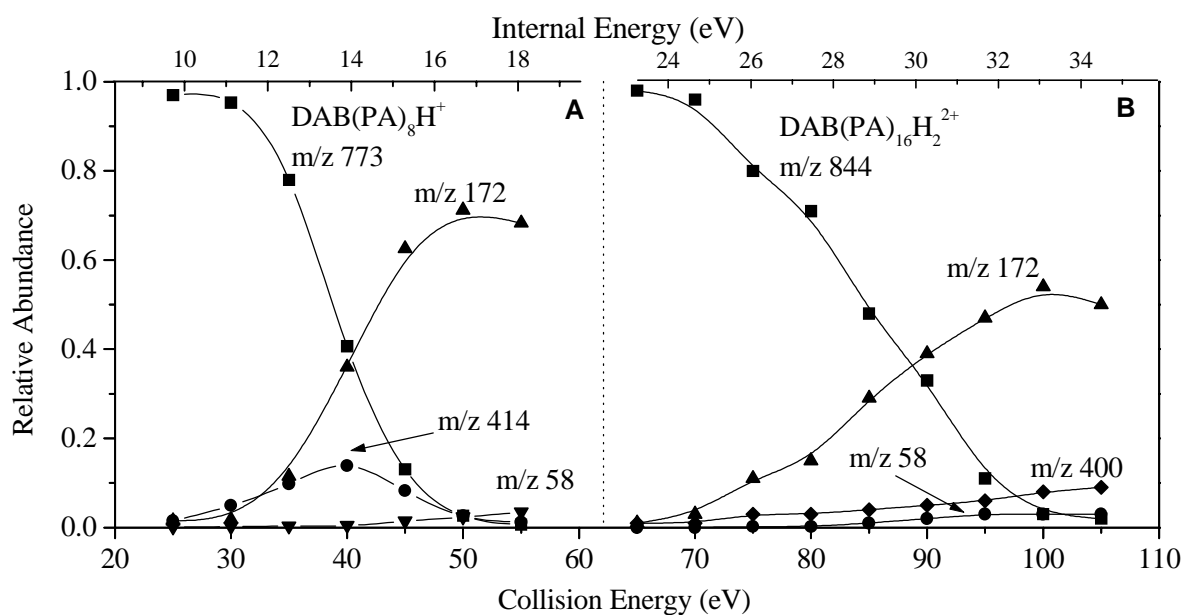


Figure 5.4: Energy-resolved SID diagrams obtained in the tandem quadrupole set-up with a fluorinated self-assembled monolayer collision surface (FC_{10} surface) of (a) $\text{DAB}(\text{PA})_8\text{H}^+$ and (b) $\text{DAB}(\text{PA})_{16}\text{H}_2^{2+}$. In the upper x-axis the internal energy scale is indicated as determined according to eq. 5.3.

5.4. Discussion

5.4.1 Fragment ions

The conclusion from the ITMS experiments, that m/z 414 has the lowest appearance energy of all $\text{DAB}(\text{PA})_8\text{H}^+$ fragments, can be explained based on the structures of the proposed fragment ions. In the fragmentation into m/z 414 a 5-membered ring is proposed to be formed, which has lower ring strain and hence lower activation energy than the 4-membered ring proposed for m/z 172. This is illustrated by Table 5.1, which shows data for heats of formation for 4- and 5-membered ring cyclic amines in comparison to those of linear systems of the same composition, obtained from [130]. Five-membered ring fragments, for example m/z 870 (1+) or m/z 435 (2+), were never observed in either SID or CID spectra of $\text{DAB}(\text{PA})_{16}\text{H}_2^{2+}$, although in principle these can be formed by reactions equivalent to the formation of m/z 414 from $\text{DAB}(\text{PA})_8\text{H}^+$. This observation with low-energy CID is in agreement with the proposal in Chapter 4 that the Coulomb

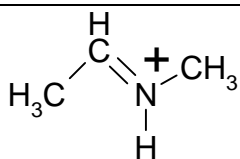
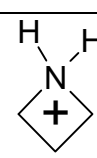
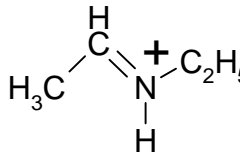
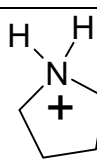
ion	ΔH_f (kJ/mol)	ΔH_f (eV)
$\text{C}_3\text{H}_8\text{N}^+$		
	618	6.4
	689	7.1
$\text{C}_4\text{H}_{10}\text{N}^+$		
	616	6.4
	585	6.1

Table 5.1: comparison formation enthalpies of cyclic and linear ions of the same atomic composition, obtained from Lias et al. [130].

repulsion between the charge sites in a multiply protonated dendrimer increases the activation energy for the formation of a 5-membered ring fragment, since the appropriate configuration of the protons is hindered [137].

Surprisingly in the FTMS CID experiments of $\text{DAB(PA)}_{16}\text{H}_2^{2+}$ no fragments have been observed which can be assigned to the complementary ions of the singly charged m/z 172 or m/z 400. In the SID experiments, a fragment at m/z 1516 has been observed with low abundance, constituting about 2% of the total fragment ion current (80-90 eV collision energies). This is much lower than that of its possible complement at m/z 172, which constitutes about 50% of the total fragment ion current. In resonant FTMS CID experiments the complementary fragments may have sufficient kinetic energy to undergo further collisional activation leading to fragmentation, which may explain their absence from the fragment spectra. Off-resonance CID experiments are planned to further investigate this.

5.4.2 Internal energies and dissociation rates in SID

The internal energy E_{int} of an ion upon activation by SID can be related to the laboratory collision energy E_{lab} by:

$$E_{\text{int}} = E_{\text{ini}} + \epsilon_{\text{SID}} \times E_{\text{lab}} \quad (5.3)$$

where E_{ini} represents the initial, pre-activation, internal energy of the ion and ϵ_{SID} the conversion efficiency of kinetic to internal energy. Vékey et al. have previously used this relation to estimate internal energies of protonated peptides upon SID [136]. The value of ϵ_{SID} has been characterised by various studies [57, 126]. For benzene ions colliding with a FC_{10} surface, the value $\epsilon_{\text{SID}}=0.28$ has been determined. Vékey et al. and de Maaijer-Gielbert et al. have shown that ϵ_{SID} is nearly constant for kinetic energies between 10 and 80 eV, as studied for benzene and diphenyl ether radical cations [57, 126]. In the following we will estimate the internal energy of POPAM dendrimers upon activation by SID on a FC_{10} surface adopting the value of $\epsilon_{\text{SID}}=0.28$ and assuming ϵ_{SID} to be constant over the studied laboratory kinetic energy range, 10 to 110 eV. To determine the internal energy of the ions before activation, we consider two terms: the thermal energy $E_{\text{int}}(T)$ gained by the ions in the heated ESI capillary (400 K) and the energy E_{ns} gained by collisional activation in the nozzle-skimmer interface. The thermal energy is calculated from:

$$E_{\text{int}}(T) = \sum_i n_i h \nu_i (1/\exp[h\nu_i/kT] - 1) \quad (5.4)$$

where n_i is the number of oscillators of frequency ν_i , h is Planck's constant, k the Boltzmann constant and T the absolute temperature. Using the set of vibrational frequencies as given in paragraph 5.2.4, $E_{\text{int}}(400\text{K})=1.95$ eV for $\text{DAB(PA)}_8\text{H}^+$. We estimate the accuracy of this calculated thermal energy about 1% [146-148]. A crude estimate for $E_{\text{ns}}=0.75$ eV is taken from Vékey et al. for $\text{N(CH}_3)_4^+$ ions [136]. With these approximations

the laboratory energy scale of the energy resolved SID diagram of $\text{DAB}(\text{PA})_8\text{H}^+$ in Figure 5.4 can be converted to an internal energy scale, which is given in the top of the figure.

We have determined overall dissociation rates Σk_i at different internal energies of $\text{DAB}(\text{PA})_8\text{H}^+$ from the ER-SID diagram. Here it is assumed that the ion abundances obtained in the quadrupole SID experiments are the integrated values over the observation time window t_{obs} :

$$\Sigma k_i = \frac{-\ln[M]}{t_{\text{obs}}} \quad (5.5)$$

For the SID experiments t_{obs} is assumed to be $6\mu\text{s}$. Hence the overall reaction rate must be $\geq 1.6 \times 10^5 \text{ s}^{-1}$ to lead to an observable degree of dissociation. From Figure 5.4 it appears that this condition is met at $E_{\text{int}} \sim 15 \text{ eV}$. The resulting values of Σk_i for different internal energies, derived from the ER-SID diagrams in Figure 5.4, are plotted in Figure 5.5.

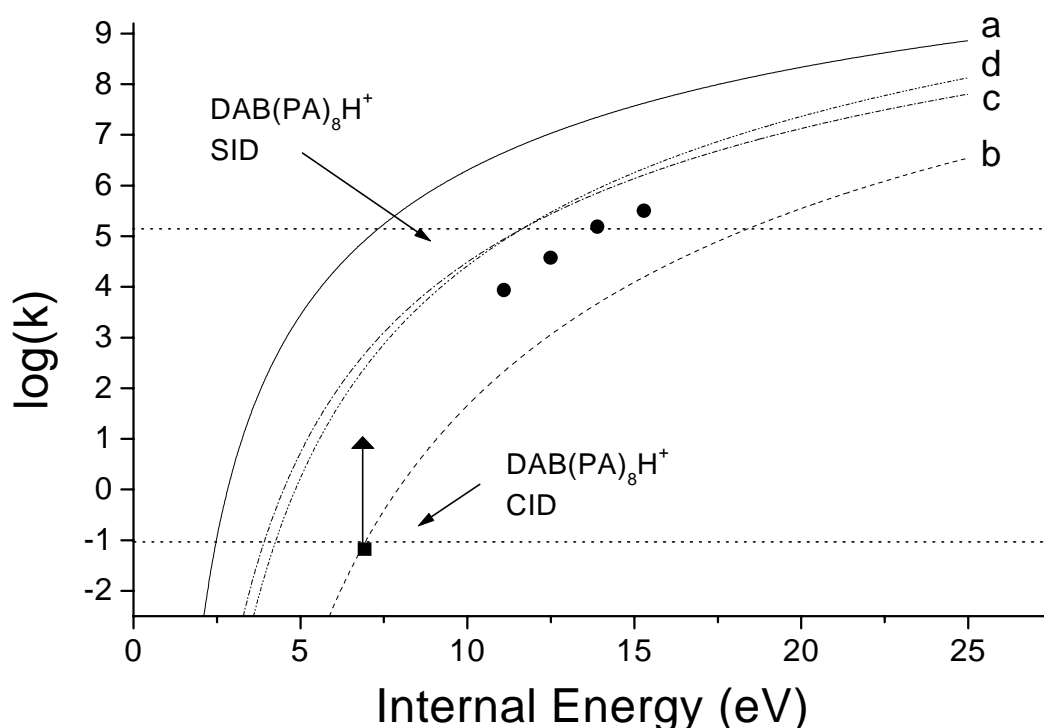
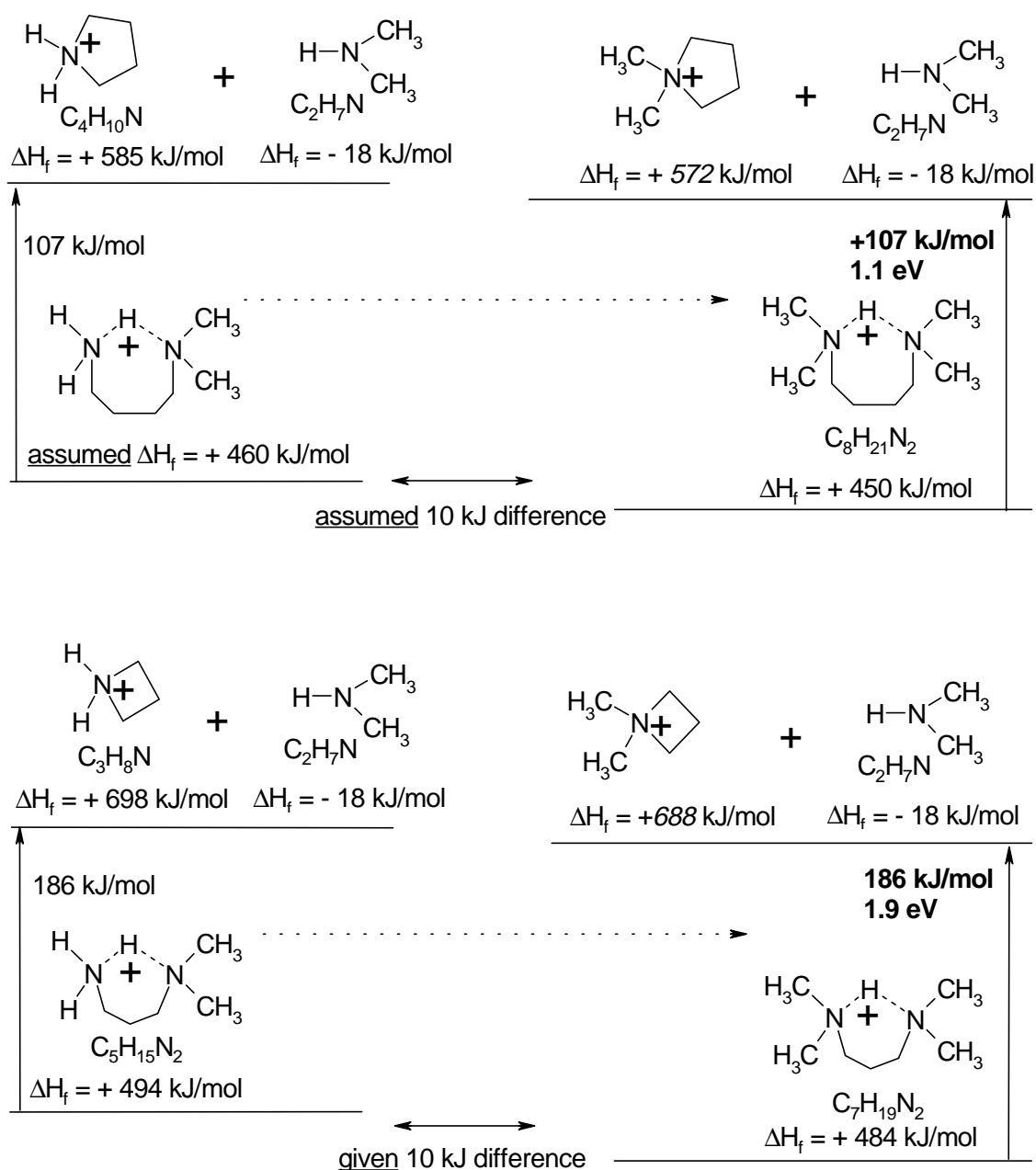


Figure 5.5: calculated $k(E)$ curves of fragmentation of $\text{DAB}(\text{PA})_8\text{H}^+$ (a) $E_{0414}=1.11 \text{ eV}$ and $A_{414} (=2.14 \times 10^{12})$ (b) $E_{0172} = 1.93 \text{ eV}$ and $A_{172} (= 9.72 \times 10^{12})$ (c) $E_{0414}=1.4 \text{ eV}$ and A_{414} (d) $E_{0172}=1.5 \text{ eV}$ and A_{172} . The dotted straight lines denote the rate associated with 50% fragmentation efficiency ($k=\ln 2/t_{\text{obs}}$) for the quadrupole SID experiments with $\text{DAB}(\text{PA})_8\text{H}^+$ ($t_{\text{obs}}=6 \mu\text{s}$) and FTMS CID experiments ($t_{\text{obs}}=10.4 \text{ s}$). Also in this graph quadrupole SID and FTMS CID experimental data are indicated.

5.4.3 Dissociation rates calculated with RRKM theory

To obtain $k_i(E_{int})$ values over the full range of E_{int} values we have performed RRKM theory calculations for the dissociation of $\text{DAB}(\text{PA})_8\text{H}^+$. The two dominant fragmentation pathways for the formation of m/z 414 and of m/z 172 are expected to have different critical energies E_{0i} and transition state configurations, as expressed by the Arrhenius factors A_i . Based on the set of frequencies given in the Experimental section 5.2.4 and using the same model for the transition state frequencies as described in [136], values of



Scheme 5.2

$A_{414}=2.14 \times 10^{12}$ and $A_{172}=9.72 \times 10^{12}$ are obtained. The values for the critical energies are not known on forehand. A first guess is based on an analysis of reaction enthalpies for the formation of a cyclic aminoalkane and dimethylamine from linear diaminoalkanes. We have determined reaction enthalpies based on differences in formation enthalpies obtained from ref. [130]. Scheme 5.2 shows the used formation enthalpies and the assumptions made to deduce the reaction enthalpies. From this analysis the values $E_{0414}=1.1$ eV (107 kJ/mol) and $E_{0172}=1.9$ eV (186 kJ/mol) are obtained. Using these values in the RRKM calculations leads to the dissociation rate curves labeled (a) and (b) in Figure 5.5. At the reaction rates where $\Sigma k_i \sim 10^5 \text{ s}^{-1}$, as studied in the SID experiments, the ratio of the abundances of m/z 414 and m/z 172 as obtained from the RRKM calculations is about 10^3 (compare curves (a) and (b) in Figure 5.5). This does not correspond to the observations from the SID experiments, as shown in Figure 5.4, where the ratio varies between 1 and 10^{-1} . The experimental data point to a much smaller difference between the critical energies and that both should have values around 1.5 eV. Therefore as a second guess we took the values $E_{0414}=1.4$ eV and $E_{0172}=1.5$ eV, which results in curves (c) and (d) in Figure 5.5. These curves cross around $E_{\text{int}} \sim 12$ eV, which indicates that at lower energies m/z 414 is dominant, while at higher energies m/z 172 is the most abundant ion. This is generally supported by the quadrupole ion trap and FTMS CID results on one hand and the quadrupole SID results on the other.

To investigate further how accurately the relative abundances of m/z 414 and m/z 172 are predicted by the RRKM calculated $k(E)$ values, we have reconstructed the ER-SID diagram of $\text{DAB(PA)}_8\text{H}^+$, shown in Figure 5.6(a), based on the $k(E)$ values represented by curves (c) and (d) in Figure 5.5 for an observation time window of 6 μs . In this reconstruction the internal energy of $\text{DAB(PA)}_8\text{H}^+$ was calculated according to eq. 5.3. From a comparison with the experimental SID diagram in Figure 5.4 we can make the following three remarks with respect to the RRKM calculated rates.

Firstly, it can be seen that the abundance of m/z 414 is overestimated in the RRKM calculations at the cost of the abundance of m/z 172. Thus the competitive shift in the dissociation rates takes place at lower internal energies than indicated in Figure 5.5. This means that the difference in critical energies should be somewhat smaller than the estimated 0.1 eV.

Secondly, the calculated collision energies needed to obtain a given fragmentation efficiency are lower by about 5 eV compared to the experimental observations. This implies that the critical energies of 1.4 and 1.5 eV are still somewhat underestimated. This can also be seen from Figure 5.5, where curves (c) and (d) correspond to consistently lower internal energies for a given $\log(k)$ value than the data based on the SID experiments.

Thirdly, the collision energy range in which the parent ion relative abundance decreases from 1 to 0 is narrower for the calculated ER-SID diagram. It has to be noted that in our reconstruction of the ER-SID diagram a single value has been used for the internal energy. Although the collisional activation in SID has been advertised as leading to

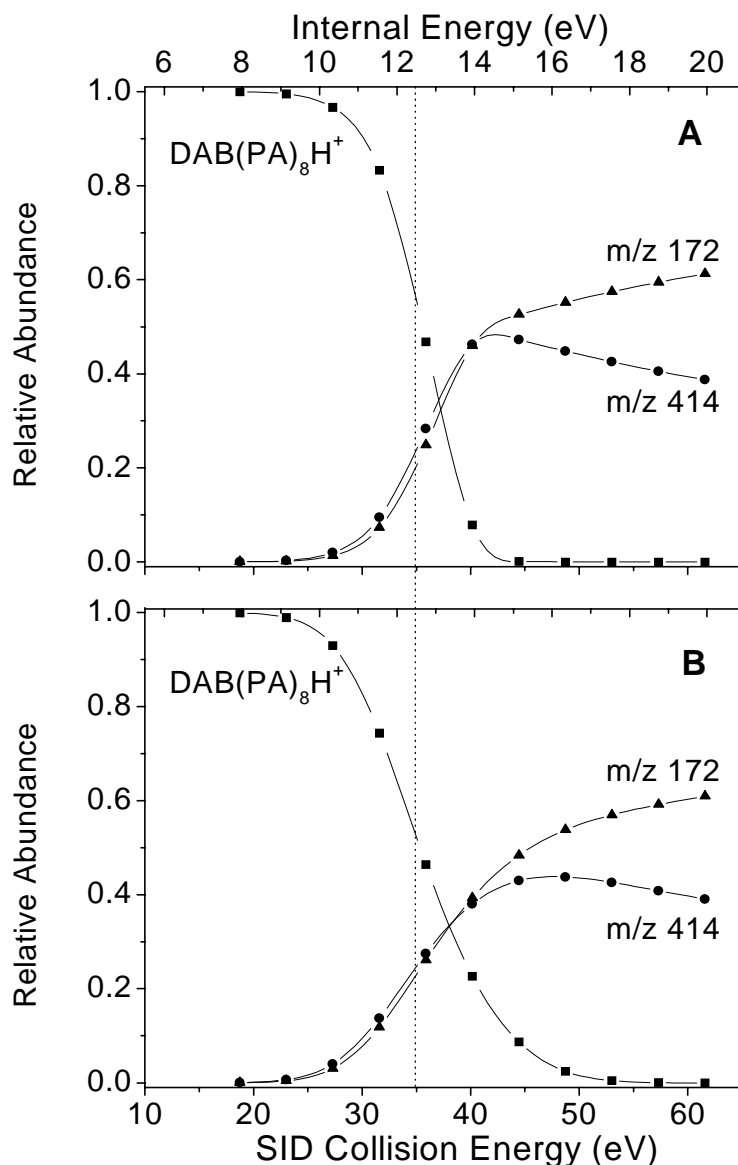


Figure 5.6: (a) calculated ER-SID diagram of $DAB(PA)_8H^+$ based on RRKM calculated $k(E)$ values. Each value of the SID collision energy on the x-axis corresponds to a single internal energy (the relation between internal energy and the SID collision energy is described by eq 5.4); (b) calculated ER-SID diagram of $DAB(PA)_8H^+$ based on RRKM calculated $k(E)$ values. Each value of the SID collision energy on the x-axis corresponds to the average of a Gaussian distribution of internal energies of which the FWHM is $0.5x$ the average.

narrow internal energy distributions, it is known from various experiments that the full width at half maximum of the internal energy distribution can be between 0.5 and 1 times the average of the internal energy [57]. To estimate the effect of an internal energy distribution on the SID results we have calculated once more the ER-SID diagram of $DAB(PA)_8H^+$ using Gaussian shaped internal energy distributions. The result for an internal energy distribution with a FWHM of half the average internal energy is shown in Figure 5.6(b). The

effect of this internal energy distribution is a smoothing of the ER-SID curves. This means that the dissociation threshold is at lower energies and 100% fragmentation efficiency is obtained at higher energies, whereas the energy at 50% fragmentation efficiency has not significantly changed. Note that for the used energy distribution the range over which the fragmentation efficiency changes between 0 and 100% is in good agreement with the experimental results (compare Figure 5.6 with Figure 5.4). Application of a wider internal energy distribution (e.g. with FWHM equal to the average) gives a range much larger than the experimental observation. We can take this as an indication that the distribution of internal energies of $\text{DAB(PA)}_8\text{H}^+$ upon SID, is not much wider than half the average internal energy.

5.4.4 Internal energies and dissociation rates in FTMS CID

General considerations

In classical high-energy CID experiments, the parent ion of interest is accelerated to a kinetic energy in the range of 1 to 10 keV and undergoes a single collision. Upon this collision the internal energy is increased instantaneously by a few eV, and the result of a subsequent unimolecular dissociation is observed in a time window of several microseconds, as defined by the experimental set-up. A large mass difference between the ion and the collision gas and the weak coupling between the translational and internal degrees of freedom of the ion result in an energy conversion of only tenths of a percent. In SID experiments a much more efficient conversion of kinetic to internal energy is obtained, efficiencies of the order of 10-30% are reported. From a conceptual point of view, a collision surface can be represented by a very dense collision gas and all atoms of the molecular ion collide simultaneously with a "collision gas" atom. In this way the "mass" of the collision gas (surface) scales with the molecular mass and consequently the energy conversion efficiency is not dependent on the mass for homologues series of molecules. In low-energy CID experiments the energy conversion ϵ_{CID} is increased by sequential collisions of the ions with the collision gas. This approach is applied in instruments where the ions cannot be accelerated to high kinetic energies, like quadrupole mass spectrometers and trapped ion mass spectrometers. The latter category also allows long dissociation times, so that relatively low internal energies are required to observe a given dissociation channel.

In the multiple collision regimes the modelling of the internal energy as a function of time is a difficult task. In the first part of the collision series the internal energy will increase stepwise until the kinetic and internal energy of the ion are in equilibrium. From that moment the kinetic and internal energy will both decrease until the full equilibrium with the collision gas is reached. The time scales for the "heating" and "cooling" phases of the ion depend on the collision frequency and the collision dynamics. Furthermore during the

process internal energy can be lost by infrared radiation of the ion. In this dynamic “heating and cooling” process the dissociation rate constants for the different dissociation channels also vary as function of time.

In this paragraph we will make an estimation of the order of magnitude of the variation of the internal energy of $\text{DAB}(\text{PA})_8\text{H}^+$ ions colliding with argon gas atoms. In this analysis a number of assumptions and approximations will be made. Recently, Heeren and Vékey have reported that in a resonant-excitation FTMS CID experiment 9.6% of the centre-of-mass energy per collision is converted to internal energy in the collision cascade [139]. In addition the authors reasoned that in each collision the kinetic energy of the ion is lowered by twice the centre-of-mass energy [139]. Thus the energetics of the collision is described by $\Delta E_{\text{lab}} = -2E_{\text{cm}}$ and $\Delta E_{\text{int}} = \epsilon_n E_{\text{cm}}$. Although these results were obtained for a specific collision system and at relatively low collision energies, we apply this model for a generalised analysis. The laboratory kinetic energy $E_{\text{lab}}(n)$ and the internal energy $E_{\text{int}}(n)$ after n collisions are given by:

$$E_{\text{lab}}(n) = E_{\text{lab}}(0) \times (1 - 2\mu)^n \quad (5.6)$$

$$E_{\text{int}}(n) = E_{\text{int}}(0) + \epsilon_n \mu E_{\text{lab}}(0) \sum_{l=0}^n (1 - 2\mu)^l \quad (5.7)$$

with $\mu = m_g / (m_i + m_g)$.

For small values of μ (< 0.5) the following approximations can be made:

$$E_{\text{lab}}(n) \cong E_{\text{lab}}(0) \times (1 - 2n\mu) \quad (5.8)$$

$$E_{\text{int}}(n) \cong E_{\text{int}}(0) + \epsilon_n \mu E_{\text{lab}}(0) \times (n - n\mu) \quad (5.9)$$

From these approximations it follows that for $n = 1/2\mu$

$$\begin{aligned} E_{\text{lab}}(n) &\cong 0 \\ E_{\text{int}}(n) &\cong E_{\text{int}}(0) + (\epsilon_n/2) E_{\text{lab}}(0) \end{aligned} \quad (5.10)$$

The number of collisions required to slow down the ion scales with the inverse of μ and the internal energy reaches a maximum value of $\epsilon_n \mu E_{\text{lab}}(0)$. Inserting $\mu = 0.049$ and $\epsilon_n = 0.096$ gives as a result that the kinetic energy is relaxed after about 10 collisions. The maximum internal energy is independent of μ and is about 4.8% of $E_{\text{lab}}(0)$. When these values are calculated more accurately, without the approximations introduced, about 40 collisions are needed to reduce the kinetic energy to 1% of the starting value $E_{\text{lab}}(0)$ and $E_{\text{int}} = 4.4 E_{\text{lab}}(0)$. In this analysis we neglect that after a number of collisions $E_{\text{int}}(n)$ can exceed the value which corresponds to the relative kinetic energy of the colliding particles. From this moment the internal energy is not increased any more by the collisions but instead is decreased. In the collisional “cooling” process we adopt that it takes also 40 collisions to cool down the active vibrational modes to the temperature of the collision gas. At a pressure of 10^{-7} mbar the collision frequency for the $\text{DAB}(\text{PA})_8\text{H}^+$ -Ar system at $E_{\text{lab}} = 100$ eV is in the order of 10 s^{-1} . This means that the time scale of the whole heating and cooling process is in the order of 10 s. To measure a reasonable degree of fragmentation within 10 s the reaction rate for dissociation must be equal or larger than

$k=0.1 \text{ s}^{-1}$. This imposes a minimum value on the kinetic energy of the $\text{DAB}(\text{PA})_8\text{H}^+$ ion at the start of the collision cascade. This minimum rate is represented by the lower dotted line in Figure 5.5. If the experiment is performed at a higher pressures, e.g. 10^{-5} mbar, the collisional relaxation times scale down with a factor of 100 and the effective dissociation reaction rate should be $k=10 \text{ s}^{-1}$. This requires a higher internal energy and thus a higher starting value for the kinetic energy of the ion. Another phenomenon is observed when the pressure is lowered to 10^{-9} mbar where the collision frequency is about 10^{-1} s^{-1} . Since in our FTMS experiment the dissociation reactions are monitored during 10 s this means that only the result of one collision can be observed. Under this “classical” one collision condition it will be clear that the kinetic energy of the molecular ion has to be raised to values in the keV range in order to observe a dissociation reaction. This analysis shows that at different collision gas pressures different internal energy domains and corresponding reaction rates are probed.

In the analysis given above we have neglected the loss of internal energy of the ions by emission of infrared radiation. From literature [73, 115] we estimate that the time scale for collisionless equilibration of the internal energy to the room temperature value is in the order of 10 s. This means that the radiation energy loss will influence in particular the measurements at relatively low pressures where reaction rates $k < 10^{-1} \text{ s}^{-1}$ are probed. So there are three timing effects which have to be taken into account in analysing the CID data resulting from multiple collision experiments: the collisional relaxation time, the radiative relaxation time and the time window used for the measurement. Thus the kinetic energy at the start of the collision cascade should be sufficiently high to give dissociation in the shortest of the three times discussed above.

For the SID experiments the concept of the characteristic dissociation energy E_{chr} was introduced. In practise for E_{chr} the laboratory collision energy E_{lab} is used at which the molecular ion intensity is reduced to half its original value. This concept worked well in studying the effect the number of degrees of freedom and the charge state of the ion on the dissociation efficiency. However from the analysis given above it will be clear that great caution has to be taken into account in the interpretation of E_{chr} values extracted from experiments where the internal energy is not increased instantaneously but is programmed in time.

In Figure 5.5 the estimated the internal energy of $\text{DAB}(\text{PA})_8\text{H}^+$ corresponding to 50% fragmentation efficiency is drawn with respect to the minimum rate $\Sigma k=0.1 \text{ s}^{-1}$. The arrow attached to this data point indicates that this energy is likely to correspond to a larger dissociation rate, in the light of the discussion above.

Internal energy simulations for multiple collision CID FTMS

The time-dependent internal energy ($E_{\text{int}}(t)$) for $\text{DAB}(\text{PA})_8 \text{H}^+$ is calculated via the stepwise changes:

$$t_n = t_{n-1} + kT/\sigma p v(t_{n-1}) \quad (5.11)$$

$$E_{\text{int}}(t_n) = E_{\text{int}}(t_{n-1}) + \epsilon_n [E_{\text{cm}}(t_n) - E_{\text{int}}(t_{n-1})/f] - \alpha[E_{\text{int}}(t_{n-1}) - E_{\text{int}}(t_\infty)](t_n - t_{n-1}) \quad (5.12)$$

$$E_{cm}(t_n) = \mu E_{lab}(t_n) \quad (5.13)$$

$$E_{lab}(t_n) = E_{lab}(t_{n-1}) - 2E_{cm}(t_{n-1}) \quad (5.14)$$

where ϵ_n is the energy conversion efficiency per collision, t_n is the time at which the n^{th} collision takes place, f is the number of active vibrational modes, α is the radiative rate constant, μ is the reduced mass of the collision system, σ the collision cross section, p the pressure of the collision gas and v the velocity of the ions.

The following values and start conditions for the various parameters were used:

$E_{int}(t_0) = E_{int}(t_\infty) = 0.98$ eV, $E_{lab}(t_0) = 75$ eV, $f = 30$, $\epsilon_n = 0.096$ (as determined by Heeren and Vékey [139]), $\alpha = 0$ and 10^{-1} , $T = 293$ K, $p = 10^{-7}$ mbar. The collisional cross section σ of $\text{DAB}(\text{PA})_8\text{H}^+$ is approximated by 13 times the collisional cross section of propane, giving 10.2 nm^2 [150].

Curve (a) in Figure 5.7 shows the increase of internal energy of the ions as a function of time neglecting any internal energy losses by collisions or radiation ($f=\infty$ and $\alpha=0$), for a laboratory kinetic energy of 75 eV. As a consequence of the choice for $\epsilon_n=0.096$ a maximum internal energy is obtained for $t \rightarrow \infty$ is 4.8% of $75 \text{ eV} + 0.98 = 4.58$ eV. Approximately 40 collisions are needed to increase the internal energy to 1% of this

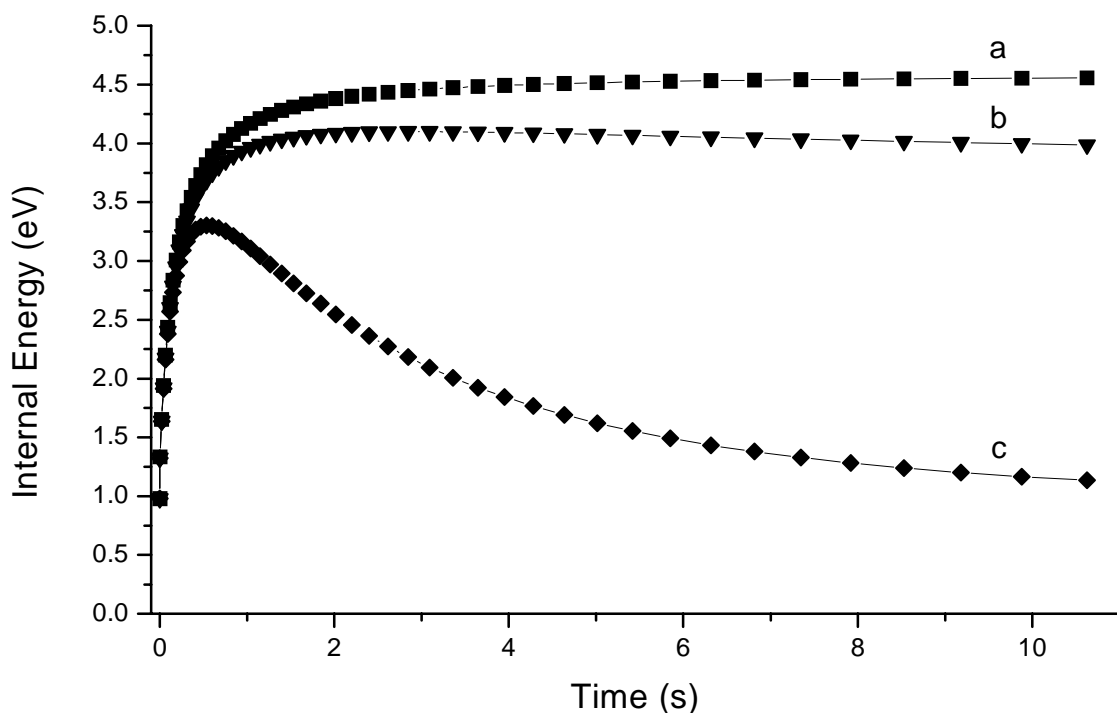


Figure 5.7: Time-dependent internal energy of $\text{DAB}(\text{PA})_8\text{H}^+$ based on the assumptions explained in the text. (a): effect of the finite rate of kinetic to internal energy conversion, curve (b) energy conversion and collisional cooling, (c) energy conversion, collisional and radiative (rate 0.1 s^{-1}) cooling.

maximum value, which occurs in ~ 5 s. For curve (b) in Figure 5.7 we have accounted for collisional energy loss ($f=30$) but neglected radiative energy loss ($\alpha=0$). In that case the maximum internal energy is obtained after 35 collisions ($t\sim 3$ s), where it is about 4.1 eV. Curve (c) is obtained accounting for both collisional loss of internal energy ($f=30$) and radiative energy loss at a rate of $\alpha=10^{-1} \text{ s}^{-1}$. This further decreases the maximum value for the internal energy to 3.3 eV, which is reached after 15 collisions in 0.5 s. From curve (c) we can see that within the 10.4 s delay between ion excitation and detection the internal energy has nearly relaxed to thermal the thermal value of 0.98 eV. The relative abundances of $\text{DAB}(\text{PA})_8\text{H}^+$ and its fragment ions can now be calculated by integration of the abundances over the time intervals, with the use of the reaction rates calculated based on RRKM theory. Figure 5.8 shows a reconstructed ER-CID diagram which we obtained by calculating the relative abundances for a series of laboratory kinetic energies $E_{\text{lab}}(t_0)$. Although this reconstruction compares well with the experimental data, one has to realize that many assumptions were involved in the reconstruction. The main issue is that the reaction rates determined from fitting the RRKM theory values to the experimental SID data, allows us to make a reasonable prediction for the multiple collision CID data obtained with the FTMS. It will be clear that a further test of the assumptions made on the energetics of the collisions and radiation losses should be tested more specifically in future.

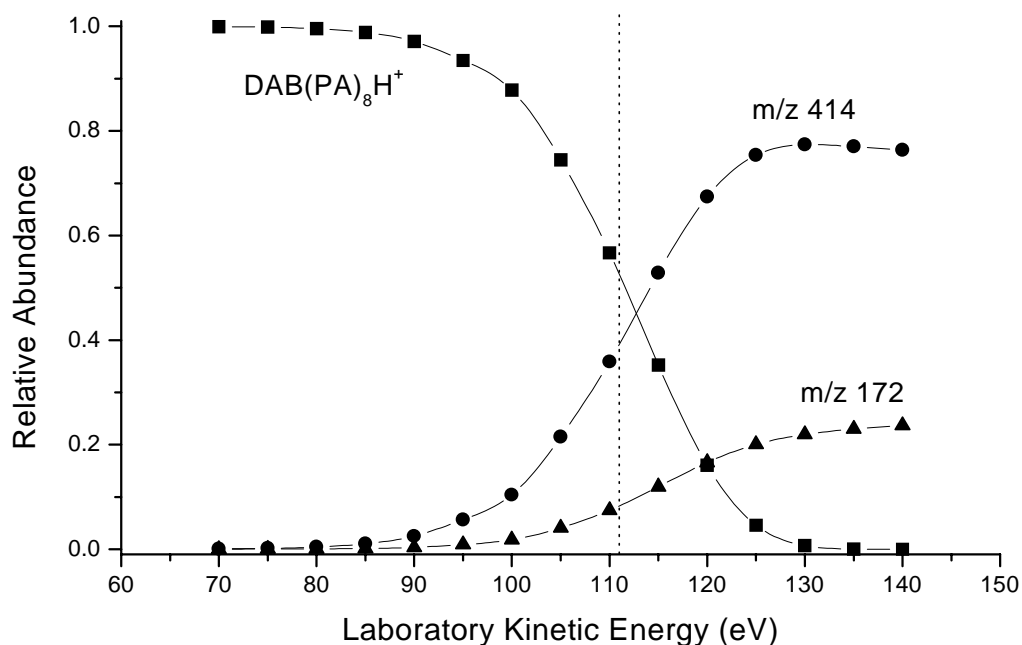


Figure 5.8: Reconstructed ER-CID diagram for $\text{DAB}(\text{PA})_8\text{H}^+$ with a dynamic internal energy profile accounting for energy conversion rate, collisional and radiative energy losses.

5.5. Conclusions

Tandem MS experiments with low-energy multiple collisional activation have been used to determine the order of appearance energies of the low-energy fragments of protonated polypropylenamine dendrimers at long observation times (10^{-3} -10s). For $\text{DAB(PA)}_8\text{H}^+$ the first fragment is m/z 414, followed by m/z 172. For $\text{DAB(PA)}_{16}\text{H}_2^{2+}$ m/z 172 is followed by m/z 400 as the internal energy of the parent ion is increased. Fragments can be formed by sequential fragmentation processes, as indicated by the formation of m/z 172 from m/z 414 (fragment of $\text{DAB(PA)}_8\text{H}^+$) in ITMS³ experiments. Direct formation of m/z 172 from $\text{DAB(PA)}_8\text{H}^+$ has not been achieved upon its resonant excitation in ITMS, even when Ar is used as the collision gas with the pressure as low as possible.

Calculations based on RRKM theory give frequency factors for the transition states in the range of 10^{12} - 10^{13} s^{-1} for the two lowest-energy fragmentation reactions. Based on a comparison between the RRKM calculated reaction rates and the experimental data obtained with SID, we conclude that the critical energies are in the range of 1.4-1.6 eV. We estimate that the critical energy for the reaction into the 5-membered ring fragment (m/z 414) is ~ 0.1 eV lower than that for 4-membered ring fragment (m/z 172).

We have argued that because of the dynamic behaviour of the internal energy of ions during the time of the FTMS CID experiments, these ions need to be activated to internal energies corresponding to dissociation rates of one over the time window during which the ion is internally activated. This time window can be defined by the rate of collisional cooling, infrared cooling or the experimentation time, depending on the experimental conditions. We have estimated that for $\text{DAB(PA)}_8\text{H}^+$ this time window is about 1-2 s. Calculation of a ER-CID diagram using dissociation rates corresponding to this time window gives results which are roughly comparable with the experimental data.

References

- [1] Vékey, K. Internal energy effects in mass spectrometry. *J. Mass Spectrom.* 1996, *31*, 445-463.
- [2] Cooks, R.G.; Ast, T., and Mabud, M.A. Collisions of polyatomic ions with surfaces. *Int. J. Mass Spectrom. Ion Proces.* 1990, *100*, 209-265.
- [3] Dongré, A.R.; Somogyi, Á., and Wysocki, V.H. Surface-induced dissociation: an effective tool to probe structure, energetics and fragmentation mechanisms of protonated peptides. *J. Mass Spectrom.* 1996, *31*, 339-350.
- [4] Carter, G. and Collignon, J.S., *Ion Bombardment of Solids*. 1968, London: Heineman Educational Books Ltd. 446.
- [5] Behrish, R., ed. *Sputtering by Particle Bombardment*. 1981, Springer-Verlag: Berlin Heidelberg New York.
- [6] Bitensky, I.S. and Parilis, E.S. Highest rotational and vibrational excitation of swift diatomic molecules scattered by a solid surface. *Surf. Sci.* 1985, *161*, L565.
- [7] Martin, J.S.; Feranchak, B.T.; Morris, J.R.; Greely, J.N., and Jacobs, D.C. Simplified classical trajectory model of dissociative scattering on surfaces: Role of incident vibrational and translational energies. *J. Phys. Chem.* 1996, *100*, 1689-1697.
- [8] Beuhler, R.J. and Friedman, L. Threshold studies of secondary electron emission induced by macro-ion impact on solid surfaces. *Nuclear Instruments and Methods* 1980, *170*, 309-315.
- [9] Beck, R.D.; St.John, P.; Alvarez, M.M.; Diederich, F., and Whetten, R.L. Resilience of all-carbon molecules C₆₀, C₇₀ and C₈₄: a surface scattering time-of-flight investigation. *J. Phys. Chem.* 1991, *95*, 8402.
- [10] Martens, J.; Ens, W.; Standing, K.G., and Verentchikov, A. Secondary-ion and electron production from surfaces bombarded by large polyatomic ions. *Rapid Commun. Mass Spectrom.* 1992, *6*, 147-157.
- [11] Verentchikov, A.; Ens, W.; Martens, J., and Standing, K.G. Detection of large molecular ions by secondary ion and secondary electron emission. *Int. J. Mass Spectrom. Ion Proces.* 1993, *126*, 75-83.
- [12] Demirev, P.L. Particle-induced desorption in mass spectrometry. Part II. Effects and applications. *Mass Spectrometry Reviews* 1995, *14*, 309-326.
- [13] Sullivan, P.A.; Axelsson, J., and Sundqvist, B.U.R. Light emission from impacts of energetic proteins on surfaces and light emission detector for MS. *Rapid Comm. Mass Spectrom.* 1995, *9*, 377.
- [14] Wu, Q. and Hanley, L. Reactive scattering, sputtering and dissociation of 32-eV pyridine ions colliding with clean and pyridine-covered Ag(111). *J. Phys. Chem.* 1993, *97*,

References

2677.

- [15] Somogyi, Á.; Kane, T.E.; Ding, J.-M., and Wysocki, V.H. Reactive collisions of $[C_6H_6]^+$ and $[C_6D_6]^+$ at self-assembled monolayer films prepared on gold from n-alkanethiols and a fluorinated alkanethiol: the influence of chain length on the reactivity of the films and the neutralisation of the projectile. *J. Am. Chem. Soc.* 1993, *115*, 5275.
- [16] Cooks, R.G.; Ast, T., and Beynon, J.H. Anomalous metastable peaks. *International Journal of Mass Spectrometry and Ion Physics* 1975, *16*, 348-352.
- [17] Cooks, R.G.; Terwilliger, D.H.; Ast, T.; Beynon, J.H., and Keough, T. Surface modified mass spectrometry. *J. Am. Chem. Soc.* 1975, *97*, 1583-1585.
- [18] Gandy, R.M.; Ampulski, R.; Prusaczyk, J., and Johnsen, R.H. Modification of a TOF-MS for studies in collisionally induced dissociations. *International Journal of Mass Spectrometry and Ion Physics* 1977, *24*, 363-371.
- [19] Mabud, M.A.; DeKrey, M.J., and Cooks, R.G. Surface-induced dissociation of molecular ions. *Int. J. Mass Spectrom. Ion Proces.* 1985, *67*, 285.
- [20] DeKrey, M.J.; Mabud, M.A., and Cooks, R.G. Applications of linked-scan procedures in investigating polyatomic ion/surface interactions. *Int. J. Mass Spectrom. Ion Proces.* 1985, *67*, 295.
- [21] Schey, K.; Cooks, R.G.; Grix, R., and Wöllnik, H. A tandem time-of-flight mass spectrometer for surface-induced dissociation. *Int. J. Mass Spectrom. Ion Proces.* 1987, *77*, 49.
- [22] Schey, K.L.; Cooks, R.G.; Kraft, A.; Grix, R., and Wöllnik, H. Ion/surface collision phenomena in an improved tandem time-of-flight instrument. *Int. J. Mass Spectrom. Ion Proces.* 1989, *94*, 1.
- [23] Bier, M.E.; Amy, J.W.; Cooks, R.G.; Syka, J.E.P.; Ceja, P., and Stafford, G. A tandem quadrupole mass spectrometer for the study of surface-induced dissociation. *Int. J. Mass Spectrom. Ion Proces.* 1987, *77*, 31-47.
- [24] Kaiser, J., R.E.; Cooks, R.G.; Syka, J.E.P., and Stafford, J., G.C. Collisionally activated dissociation of peptides using a QITMS. *Rapid Commun. Mass Spectrom.* 1990, *4*, 30-33.
- [25] Wright, A.D.; Despeyroux, D.; Jennings, K.R.; Evans, S., and Riddoch, A. Surface-induced dissociation mass spectra of protonated peptides using a four-sector mass spectrometer. *Organic Mass Spectrom.* 1992, *27*, 525.
- [26] Despeyroux, D.; Wright, A.D.; Jennings, K.R.; Evans, S., and Riddoch, A. The effect of collision energy and nature of the surface on the surface-induced dissociation mass spectra of fluorobenzene using a four-sector mass spectrometer. *Int. J. Mass Spectrom. Ion Proces.* 1992, *122*, 133-141.
- [27] Jackson, A.T.; Despeyroux, D., and Jennings, K.R. The observation of broad metastable ion peaks in the surface-induced dissociation mass spectra of protonated and cationated peptides. *Int. J. Mass Spectrom. Ion Proces.* 1995, *141*, 91.

- [28] James, C.F. and Wilkins, C.L. Surface-induced dissociation by Fourier transform mass spectrometry. *Anal. Chem.* 1990, *62*, 1295-1299.
- [29] Nuwaysir, L.M.; Castoro, J.A., and Wilkins, C.L. Combined photodissociation/surface-induced dissociation for multiple mass spectrometry (MS/MS/MS) studies using a FT-MS. *Org. Mass Spectrom.* 1991, *26*, 721.
- [30] Castoro, J.A.; Nuwaysir, L.M.; C.F., I., and Wilkins, C.L. Comparative study of photodissociation and surface-induced dissociation by laser desorption Fourier transform mass spectrometry. *Anal. Chem.* 1992, *64*, 2238-2243.
- [31] Williams, E.R.; Henry, K.D.; McLafferty, F.W.; Shabanowitz, J., and Hunt, D.F. Surface-induced dissociation of peptide ions in FT-MS. *J. Am. Soc. Mass Spectrom.* 1990, *1*, 413.
- [32] Chorush, R.A.; Little, D.P.; Beu, S.C.; Wood, T.D., and McLafferty, F.W. Surface-induced dissociation of multiply-protonated proteins. *Anal. Chem.* 1995, *67*, 1042.
- [33] Beck, R.D.; St.John, P.; Homer, M.C., and Whetten, R.L. Impact-induced cleaving and melting of alkali-halide nanocrystals. *Science* 1991, *253*, 879.
- [34] Beck, R.D.; St.John, P.; Homer, M.L., and Whetten, R.D. Demetallization of alkali/alkali-halide clusters: impact-induced fragmentation of cubic $\text{Na}_{14}\text{F}_{12}^+$. *Chem. Phys. Lett.* 1991, *187*, 122.
- [35] Yerezian, C.; Hansen, K.; Beck, R.D., and Whetten, R.L. Surface scattering of C_{60}^+ : recoil velocities and yield of C_{60}^+ . *J. Chem. Phys.* 1993, *98*, 7480.
- [36] Yerezian, C.; Beck, R.D., and Whetten, R.L. Cluster-surface scattering in a reflectron collider: probing fullerenes by surface impact. *Int. J. Mass Spectrom. Ion Proces.* 1994, *135*, 79.
- [37] Williams, E.R.; Jones, G.C.; Fang, L.; Zare, R.N.; Garrison, B.J., and Brenner, R.W. on-pickup of large, surface-adsorbed molecules: a demonstration of the Eley-Rideal mechanism. *J. Am. Chem. Soc.* 1992, *114*, 3207.
- [38] Williams, E.R.; Fang, L., and Zare, R.N. Surface-induced dissociation for tandem time-of-flight mass spectrometry. *Int. J. Mass Spectrom. Ion Proces.* 1993, *123*, 233.
- [39] Wysocki, V.H.; Ding, J.-M.; Jones, J.L.; Callahan, J.H., and King, F.L. Surface-induced dissociation in tandem quadrupole mass spectrometers: a comparison of three designs. *J. Am. Soc. Mass Spectrom.* 1992, *3*, 27-32.
- [40] Beck, R.D.; Weis, P.; Bräuchle, G., and Rockenberger, J. Tandem time-of-flight mass spectrometer for cluster-surface scattering experiments. *Rev. Sci. Instrum.* 1995, *66*, 4188-4197.
- [41] Winger, B.E.; R.K. Julian, J.; Cooks, R.G., and Chidsey, C.E.D. Surface reactions and surface-induced dissociation of polyatomic ions at self-assembled organic monolayer surfaces. *J. Am. Chem. Soc.* 1991, *113*, 8967.
- [42] Morris, M.R.; D.E. Riederer, J.; Winger, B.E.; Cooks, R.G.; Ast, T., and Chidsey,

References

- C.E.D. Ion/surface collisions at functionalized self-assembled monolayer surfaces. *Int. J. Mass Spectrom. Ion Proces.* 1992, *122*, 181.
- [43] Ast, T.; D.E. Riederer, J.; Miller, S.A.; Morris, M., and Cooks, R.G. Collisions of fluorocarbons at solid surfaces: electronic excitation, surface-induced dissociation and chemical sputtering. *Organic Mass Spectrometry* 1993, *28*, 1021-1033.
- [44] Pradeep, T.; Miller, S.A., and Cooks, R.G. Surface-induced dissociation from a liquid surface. *J. Am. Soc. Mass Spectrom.* 1993, *4*, 769.
- [45] Koppers, W.R.; Tsumori, K.; Beijersbergen, J.H.M.; Weeding, T.L.; Kistemaker, P.G., and Kleyn, A.W. Dissociative scattering of CF_3^+ from a barium covered Ag(111) surface. *Surf. Sci.* 1996, *357-358*, 678-683.
- [46] Koppers, W.R.; Tsumori, K.; Beijersbergen, J.H.M.; Weeding, T.L.; Kistemaker, P.G., and Kleyn, A.W. Dissociative scattering of polyatomic ions from metal surfaces: CF_3^+ on Ag(111) and Ba/Ag(111). *Int. J. Mass Spectrom. Ion Proces.* 1998, *174*, 11-34.
- [47] Koppers, W.R.; Beijersbergen, J.B.; Weeding, T.L.; Kistemaker, P.G., and Kleyn, A.W. Dissociative scattering of polyatomic ions from a liquid surface: CF_3^+ on a perfluoropolyether film. *J. Chem. Phys.* 1997, *107*, 10736.
- [48] Koppers, W.R.; Gleeson, M.; Lourenço, J.; Weeding, T.L.; Los, J., and Kleyn, A.W. Ion/liquid scattering: energy transfer to internal energy and to the surface. *J. Chem. Phys.* 1999, *110*, 2588-2596.
- [49] Mabud, M.A.; T.Ast, and Cooks, R.G. Surface-induced dissociation of isomeric $[\text{C}_5\text{H}_6]^+$ ions. *Organic Mass Spectrom.* 1987, *22*, 418.
- [50] Ast, T.; Mabud, M.A., and Cooks, R.G. Reactive collisions of polyatomic ions at solid surfaces. *Int. J. Mass Spectrom. Ion Proces.* 1988, *82*, 131.
- [51] Pradeep, T.; Riederer, D.E.; Ast, T., and Cooks, R.G. Reactions of low-energy ions with ferrocene self-assembled monolayer surfaces. *Rapid Commun. Mass Spectrom.* 1993, *7*, 711.
- [52] Pradeep, T.; D.E. Riederer, J.; S.H. Hoke, I.; T.Ast; Cooks, R.G., and Linford, M.R. Reactions of metal ions at fluorinated surfaces: formation of MF_n^+ (M = Ti, Cr, Fe, Mo and W; n = 1-5). *J. Am. Chem. Soc.* 1994, *116*, 8658.
- [53] Riederer, J., D.E. ; Cooks, R.G., and Linford, M.R. Abstraction of multiple surface atoms by pyrazine, pyrene and HC_2N ions on low-energy collisions with self-assembled monolayer surfaces. *J. Mass Spectrom.* 1995, *30*, 241.
- [54] Ast, T.; Pradeep, T.; Feng, B., and Cooks, R.G. Low-energy collisions of methane ions at a fluoroalkyl monolayer surface. *J. Mass Spectrom.* 1996, *31*, 791-801.
- [55] Kane, T.E.; Somogyi, Á., and Wysocki, V.H. Reactive ion-surface collisions: application of ionized acetone- d_6 , DMSO- d_6 and pyridine- d_5 as probes for the characterization of SAM films on gold. *Org. Mass Spectrom.* 1993, *28*, 1665-1673.

- [56] Somogyi, Á.; Kane, T.E., and Wysocki, V.H. Reactions between doubly charged $[C_6H_6]^{2+}$ ions and self-assembled monolayers. *Org. Mass Spectrom.* 1993, 28, 283.
- [57] Vékey, K.; Somogyi, Á., and Wysocki, V.H. Internal energy distribution of benzene molecular ion in surface-induced dissociation. *J. Mass Spectrom.* 1995, 30, 212-217.
- [58] Bente, I., P.F. ; McLafferty, F.W.; McAdoo, D.J., and Lifshitz, C. *J. Phys. Chem.* 1975, 79, 713.
- [59] Bier, M.E.; Schwartz, J.C.; Schey, K.L., and Cooks, R.G. Tandem mass spectrometry using an in-line ion/surface collision device. *Int. J. Mass Spectrom. Ion Proces.* 1990, 103, 1.
- [60] McCormack, A.L.; Jones, J.L., and Wysocki, V.H. Surface-induced dissociation of multiply protonated peptides. *J. Am. Soc. Mass Spectrom.* 1992, 3, 859-862.
- [61] McCormack, A.L.; Somogyi, Á.; Dongré, A.R., and Wysocki, V.H. Fragmentation of protonated peptides: surface-induced dissociation in conjunction with a quantum mechanical approach. *Anal. Chem.* 1993, 65, 2859-2872.
- [62] Jones, J.L.; Dongré, A.R.; Somogyi, Á., and Wysocki, V.H. Sequence dependence of peptide fragmentation efficiency curves determined by ESI/SID MS. *J. Am. Chem. Soc.* 1994, 116, 8368-8369.
- [63] Wysocki, V.H.; Jones, J.L.; Dongré, A.R.; Somogyi, Á., and McCormack, A., *Surface-induced dissociation of peptides*, in *Biological Mass Spectrometry: Present and Future*, T. Matsuo, *et al.*, Editors. 1994, John Wiley and Sons: New York. p. 249-254.
- [64] Bateman, R.H.; Green, M.R.; Scott, G., and Clayton, E. A combined magnetic sector-time-of-flight mass spectrometer for structural determination studies by tandem mass spectrometry. *Rapid Commun. Mass Spectrom.* 1995, 9, 1227-1233.
- [65] McLuckey, S.A.; Ouwerkerk, C.E.D.; Boerboom, A.J.H., and Kistemaker, P.G. *Int. J. Mass Spectrom. Ion Proces.* 1984, 59, 85.
- [66] Wysocki, V.H.; Kenttämaa, H.I., and Cooks, R.G. Internal energy distributions of isolated ions after activation by various methods. *Int. J. Mass Spectrom. Ion Proces.* 1987, 75, 181.
- [67] Todd, P.J. and McLafferty, F.W., *Collisionally activated dissociation of high kinetic energy ions*, in *Tandem Mass Spectrometry*, F.W. McLafferty, Editor. 1983, John Wiley & Sons: New York. p. 149-174.
- [68] Covey, T., *Liquid chromatography/MS for the analysis of protein digests*, in *Protein and Peptide analysis by Mass Spectrometry*, J.R. Chapman, Editor. 1996, Humana Press Inc.: Totowa. p. 83-99.
- [69] Speir, J.P.; Senko, M.W.; Little, D.P.; Loo, J.A., and McLafferty, F.W. High-resolution tandem mass spectra of 37-67 kDa proteins. *J. Mass Spectrom.* 1995, 30, 39-42.
- [70] O'Connor, P.B.; Speir, J.P.; Senko, M.W.; Little, D.P., and McLafferty, F.W. Tandem mass spectrometry of carbonic anhydrase. *J. Mass Spectrom.* 1995, 30, 88-93.

References

- [71] McIver, J., R.T.; Bowers, W.D.; Delbert, S.-S., and Hunter, R.L. ?Peptide dissociation by excimer laser? *J. Am. Chem. Soc.* 1984, *106*, 7288.
- [72] Little, D.P.; Speir, J.P.; Senko, M.W.; O'Connor, P.B., and McLafferty, F.W. Infrared multiphoton dissociation of large multiply charged ions for biomolecule sequencing. *Anal. Chem.* 1994, *66*, 2809.
- [73] Price, W.D.; Schnier, P.D.; Jockusch, R.A.; Strittmatter, E.F., and Williams, E.R. Unimolecular reaction kinetics in the high-pressure limit without collisions. *J. Am. Chem. Soc.* 1996, *118*, 10640-10644.
- [74] McLafferty, F.W.; Zubarev, R.A., and Kelleher, N.L., *Gaseous conformations of Cytochrome c probed by electron capture dissociation*, in *47th ASMS Conference on Mass Spectrometry and Allied Topics*. 1998.
- [75] Sheil, M.M. and Derrick, P.J. Tandem MS of peptides. Relationship between translational energy loss and fragment ion mass. *Org. Mass Spectrom.* 1988, *23*, 429.
- [76] Busmann, H.-G.; Lill, T., and Hertel, I.V. Near specular reflection of C₆₀ ions in collisions with an HOPG graphite surface. *Chem. Phys. Lett.* 1991, *187*, 459-465.
- [77] Wysocki, V.H.; Jones, J.L., and Ding, J.-M. Polyatomic ion/surface collisions at self-assembled monolayer films. *J. Am. Chem. Soc.* 1991, *113*, 8969.
- [78] Dagan, S. and Amirav, A. High-efficiency surface-induced dissociation on a rhenium-oxide surface. *J. Am. Soc. Mass Spectrom.* 1993, *4*, 869.
- [79] Hayward, M.J.; Mabud, M.A., and Cooks, R.G. Ion/surface collisions for distinction of isomeric [C₆H₆]⁺ and [C₆H₆]²⁺ ions. *J. Am. Chem. Soc.* 1988, *110*, 1343.
- [80] Johnson, P.M. The multiphoton ionisation spectrum of benzene. *J. Chem. Phys.* 1976, *64*, 4143.
- [81] Steenvoorden, R.J.J.M.; Vasconcelos, M.H.; Kistemaker, P.G., and Weeding, T.L. Rotational band analysis of vibrational modes 6 and 7 of benzene isotopomers using REMPI and TOF-MS. *J. Mol. Spectros.* 1993, *161*, 17.
- [82] Eland, J.H.D.; Frey, R.; Schulte, H., and Brehm, B. New results on the fragmentation of the benzene ion. *Int. J. Mass Spectrom. Ion Phys.* 1976, *21*, 209.
- [83] Konijn, S.W.; Steenvoorden, R.J.J.M.; Kistemaker, P.G., and Weeding, T.L. *J. Phys. Chem.* 1994, *98*, 5399.
- [84] Neusser, H.J. Multi-photon mass spectrometry and unimolecular ion decay. *Int. J. Mass Spectrom. Ion Proces.* 1987, *79*, 141.
- [85] Wiley, W.C. and McLaren, I.H. Time-of-flight mass spectrometer with improved resolution. *Rev. Sci. Instr.* 1955, *26*, 1150.
- [86] Boesl, U.; Weinkauff, R., and Schlag, E.W. Reflectron time-of-flight mass spectrometry and laser excitation for the analysis of neutrals, ionised molecules and secondary fragments. *Int. J. Mass Spectrom. Ion Proces.* 1992, *112*, 121.
- [87] Wu, Q. and Hanley, L. Pyridine ion collisions with pyridine-d₅ multilayers on Ag(111):

- new scattered ions and neutralisation quenching. *J. Phys. Chem.* 1993, *97*, 8021.
- [88] Weast, R.C., ed. *CRC Handbook of Chemistry and Physics*. 1994, CRC Press: Boca Raton. .
- [89] McLafferty, F.W. and Stauffer, D.B., eds. *The Wiley/NBS Registry of Mass Spectral Data*. 1989, John Wiley and Sons: New York. .
- [90] Rosenstock, H.M.; Dannacher, J., and Liebman, J.F. The role of excited electronic states in ion fragmentation: $C_6H_6^+$. *Radiat. Phys. Chem.* 1982, *20*, 7.
- [91] van Tilborg, M.W.E.M. and Thuijl, J.v. A relation between ion structures and experimental overall cross-sections for collisionally activated decomposition. *Org. Mass Spectrom.* 1984, *19*, 217.
- [92] van den Hoek, P.J. and Kleyn, A.W. *J. Chem. Phys.* 1989, *91*, 4318.
- [93] Winger, B.E.; Laue, H.-J.; Horning, S.R.; R.K. Julian, J.; Lammert, S.A.; Riederer, D.E., and Cooks, R.G. Hybrid BEEQ tandem mass spectrometer for the study of ion/surface collision processes. *Rev. Sci. Instrum.* 1992, *63*, 5613.
- [94] Lammert, S.A. and Cooks, R.G. Surface-induced dissociation of molecular ions in a quadrupole ion trap mass spectrometer. *J. Am. Soc. Mass Spectrom.* 1991, *2*, 487.
- [95] Zhong, W.; Nikolaev, E.; Futrell, J.H., and Wysocki, V.H. Tandem FTMS studies of SID of benzene monomer and dimer ions on a self-assembled fluorinated alkanethiolate monolayer surface. *Anal. Chem.* 1997, *69*, 2496.
- [96] de Maaijer-Gielbert, J.; Beijersbergen, J.H.M.; Kistemaker, P.G., and Weeding, T.L. Surface-induced dissociation of benzene on a PFPE liquid insulator in a time-of-flight mass spectrometer. *Int. J. Mass Spectrom. Ion Proces.* 1996, *153*, 119-128.
- [97] Brown, P. Kinetic studies in MS-VII: competing cleavage and rearrangement processes in molecular ion decomposition reactions. *Org. Mass Spectrom.* 1970, *3*, 1175.
- [98] Stiller, S.W. and Johnston, M.V. Competitive fragmentation processes in multiphoton ionization: the role of ladder switching. *J. Phys. Chem.* 1985, *89*, 2717-2719.
- [99] Miller, S.A.; D.E. Riederer, J.; Cooks, R.G.; Cho, W.R.; Lee, H.W., and Kang, H. Energy disposal and target effects in hyperthermal collisions of ferrocene molecular ions at surfaces. *J. Phys. Chem.* 1994, *98*, 245.
- [100] Paiva, A., *Photoionization and dissociation of diphenyl ether*. 1998, Universidad de Lisboa: Lisboa.
- [101] Experiments have been also performed on PFPE in the tandem quadrupole yielding similar relative intensities for the same collision energies.
- [102] Meot-Ner (Mautner), M.; Dongré, A.R.; Somogyi, Á., and Wysocki, V.H. Thermal decomposition kinetics of protonated peptides and peptide dimers, and comparison with surface-induced dissociation. *Rapid Commun. Mass Spectrom.* 1995, *9*, 829-836.
- [103] Dole, M.; Mack, L.L.; Hines, R.L.; Mobley, R.C.; Ferguson, L.D., and Alice, M.B. Molecular beams of macroions. *Chem. Phys.* 1968, *49*, 2240-2249.

References

- [104] Yamashita, M. and Fenn, J.B. Electrospray ion source. Another variation on the free jet theme. *J. Phys. Chem.* 1984, *88*, 4451-4459.
- [105] Barinaga, C.J.; Edmonds, C.G.; Udseth, H.R., and Smith, R.D. Sequence determination of multiply charged peptide molecular ions by electrospray ionization tandem mass spectrometry. *Rapid Commun. Mass Spectrom.* 1989, *3*, 160-164.
- [106] Hunt, D.F.; Henderson, R.A.; Shabanowitz, J.; Sakaguchi, K.; Michel, H.; Sevilir, N.; Cox, A.L.; Apella, E., and Engelhard, V.H. Characterization of peptides bound to the Class I MHC molecule HLA-A2.1 by mass spectrometry. *Science* 1992, *255*, 1261-1263.
- [107] Loo, J.A.; Edmonds, C.G., and Smith, R.D. Tandem mass spectrometry of very large molecules: serum albumin sequence information from multiply charged ions formed by electrospray ionization. *Anal. Chem.* 1991, *63*, 2488-2499.
- [108] Smith, R.D. and Barinaga, C.J. Internal energy effects in the collision-induced dissociation of large biopolymer molecular ions produced by electrospray ionization tandem mass spectrometry of cytochrome c. *Rapid Commun. Mass Spectrom.* 1990, *4*, 54-57.
- [109] Senko, M.W.; Speir, J.P., and McLafferty, F.W. Collisional activation of large multiply charged ions using Fourier transform mass spectrometry. *Anal. Chem.* 1994, *66*, 2801-2808.
- [110] Bulet, O.; Orkiszewski, R.S.; Ballard, K.D., and Gaskell, S.J. Charge promotion of low-energy fragmentations of peptide ions. *Rapid Commun. Mass Spectrom.* 1992, *6*, 658-662.
- [111] Tang, X.-J.; Thibault, P., and Boyd, R.K. Fragmentation reactions of multiply protonated peptides and implications for sequencing by tandem mass spectrometry with low-energy collision induced dissociation. *Anal. Chem.* 1993, *65*, 2824-2834.
- [112] Dongré, A.R.; Jones, J.L.; Somogyi, Á., and Wysocki, V.H. Influence of peptide composition, gas-phase basicity, and chemical modification on fragmentation efficiency: evidence for the mobile proton model. *J. Am. Chem. Soc.* 1996, *118*, 8365-8374.
- [113] Nair, H.; Somogyi, Á., and Wysocki, V.H. Effect of alkyl substitution at the amide nitrogen on amide bond cleavage: electrospray ionization/surface-induced dissociation fragmentation of Substance P and two alkylated analogs. *J. Mass Spectrom.* 1996, *31*, 1141-1148.
- [114] Smith, R.D.; Loo, J.A.; Barinaga, C.J.; Edmonds, C.G., and Udseth, H.R. Collisional activation and collision-activated dissociation of large multiply charged polypeptides and proteins produced by electrospray ionization. *J. Am. Soc. Mass Spectrom.* 1990, *1*, 53-65.
- [115] Jockush, R.A.; Schnier, P.D.; Price, W.D.; Strittmatter, E.F.; Demirev, P.A., and Williams, E.R. Effects of charge state on fragmentation pathways, dynamics and activation energies of ubiquitin ions measured by BIRD. *Anal. Chem.* 1997, *69*, 1119-1126.
- [116] Cox, K.A.; Gaskell, S.J.; Morris, M., and Whiting, A. Role of the site of protonation in the low-energy decompositions of gas-phase peptide ions. *J. Am. Soc. Mass Spectrom.*

1996, 7, 522-531.

[117] Somogyi, Á.; Wysocki, V.H., and Mayer, I. The effect of protonation site on bond strengths in simple peptides: application of ab initio and MNDO bond orders and MNDO energy partitioning. *J. Am. Soc. Mass Spectrom.* 1994, 5, 704-717.

[118] Yalcin, T.; Csizmadia, I.G.; Peterson, M.R., and Harrison, A.G. The structure and fragmentation of B_n ($n \geq 3$) ions in peptide spectra. *J. Am. Soc. Mass Spectrom.* 1996, 7, 233-242.

[119] Rockwood, A.L.; Busman, M., and Smith, R.D. Coulombic effects in the dissociation of large highly charged ions. *Int. J. Mass Spectrom. Ion Proces.* 1991, 111, 103-129.

[120] Vékey, K. and Gömör, Á. Theoretical modelling of mass spectrometric behaviour of peptides: singly and doubly protonated glycine. *Rapid Commun. Mass Spectrom.* 1996, 10, 1485-1496.

[121] Mengerink, Y.; Mure, M.; Brabander, E.M.M.d., and Wal, S.v.d. Exclusion chromatography of polypropylenamine dendrimers. *J. Chrom. A* 1996, 730, 75-81.

[122] Yamdagni, R. and Kebarle, P. Gas-phase basicities of amines. Hydrogen bonding in proton-bound amine dimers and proton-induced cyclization of α,ω -diamines. *J. Am. Chem. Soc.* 1973, 95, 3504-3510.

[123] Whitney, T.A.; Klemann, L.P., and Field, F.H. Investigation of polytertiary alkylamines using chemical ionization mass spectrometry. *Anal. Chem.* 1971, 43, 1048-1052.

[124] Weener, J.W.; Van Dongen, J.L.J.; Hummelen, J.C., and Meijer, E.W. Fragmentation studies of poly(propylene imine) dendrimers in the gas-phase by using electrospray ionization mass spectrometry (ESI-MS). *Polym. Mater. Sci. Eng.* 1997, 77, 147-148.

[125] de Maaijer-Gielbert, J.; Gu, C.G.; Somogyi, Á.; Wysocki, V.H.; Kistemaker, P.G., and Weeding, T.L. ESI/SID of POPAM dendrimers. *Adv. Mass Spectrom.* 1998, 14.

[126] de Maaijer-Gielbert, J.; Somogyi, Á.; Wysocki, V.H.; Kistemaker, P.G., and Weeding, T.L. Surface-induced dissociation of diphenyl ether. *Int. J. Mass Spectrom. Ion Proces.* 1997, 174, 81-94.

[127] Chowdhury, S.K.; Katta, V., and Chait, B.T. An electrospray-ionization mass spectrometer with new features. *Rapid Commun. Mass Spectrom.* 1990, 4, 81-87.

[128] Papac, D.I.; Schey, K.L., and Knapp, D.R. Combination electrospray-liquid secondary ion mass spectrometry ion source. *Anal. Chem.* 1991, 63, 1658-1660.

[129] de Maaijer, J.; Heeren, R.M.; Kistemaker, P.G., and Weeding, T.L. *in preparation* 1998.

[130] Lias, S.G.; Bartmess, J.E.; Liebman, J.F.; Holmes, J.L.; Levin, R.D., and Mallard, W.G. Gas-phase ion and neutral thermochemistry. *J. Phys. Chem. Ref. Data* 1988, 17, Suppl. 1.

[131] Meot-Ner (Mautner), M.; Hamlet, P.; Hunter, E.P., and Field, F.H. Internal and external solvation of polyfunctional ions. *J. Am. Chem. Soc.* 1980, 102, 6393-6399.

References

- [132] Schnier, P.D.; Gross, D.S., and Williams, E.R. On the maximum charge state and proton transfer reactivity of peptide and protein ions formed by electrospray ionization. *J. Am. Soc. Mass Spectrom.* 1995, *6*, 1086-1097.
- [133] Schnier, P.D.; Price, W.D., and Williams, E.R. Modeling the maximum charge state of arginine-containing peptide ions formed by electrospray ionization. *J. Am. Soc. Mass Spectrom.* 1996, *7*, 972-976.
- [134] Beck, R.D.; Rockenberger, J.; Weis, P., and Kappes, M.M. Fragmentation of C₆₀⁺ and higher fullerenes by surface impact. *J. Chem. Phys.* 1996, *104*, 3638-3650.
- [135] Schlag, E.W. and Levine, R.D. On the unimolecular dissociation of large molecules. *Chem. Phys. Lett.* 1989, *163*, 523-530.
- [136] Vékey, K.; Somogyi, Á., and Wysocki, V.H. Average activation energies of low-energy fragmentation processes of protonated peptides determined by a new approach. *Rapid Commun. Mass Spectrom.* 1996, *10*, 911-918.
- [137] de Maaijer-Gielbert, J.; Gu, C.; Somogyi, Á.; Wysocki, V.H.; Kistemaker, P.G., and Weeding, T.L. Surface-induced dissociation of singly and multiple protonated POPAM dendrimers. *J. Am. Soc. Mass Spectrom.* 1999, 414-422.
- [138] McLuckey, S.A. Principles of collisional activation in analytical mass spectrometry. *J. Am. Soc. Mass Spectrom.* 1992, *3*, 599-614.
- [139] Heeren, R.M.A. and Vékey, K. A novel method to determine collisional energy transfer efficiency by FTICR-MS. *Rapid Commun. Mass Spectrom.* 1998, *12*, 1175-1181.
- [140] van Rooij, G. and Heeren, R.M.A. *To be published* 1998.
- [141] Heeren, R.M.A. and Boon, J.J. Rapid microscale analyses with an external ion source FT-ICR-MS. *Int. J. Mass Spectrom. Ion Proces.* 1997, *157/158*, 391-403.
- [142] March, R.E. and Todd, J.F.J., eds. *Practical Aspects of Ion Trap Mass Spectrometry Vol.III.* 1995, CRC Press: Boca Raton. .
- [143] Goeringer, D.E. and McLuckey, S.A., *Computer simulation of ion internal cooling rates in the RF quadrupole ion trap*, in *45th ASMS Conference on Mass Spectrometry and Allied Topics.* 1997. Palm Springs.
- [144] Sievers, H.L.; Grutzmacher, H.F., and Caravatti, P. *Int. J. Mass Spectrom. Ion Proces.* 1996, *157/158*, 233-247.
- [145] Heck, A.J.R.; de Koning, L.J.; Pinkse, F.A., and Nibbering, N.M.M. Mass-specific selection of ions in FT-ICR-MS. Unintentional off-resonance cyclotron excitation of selected ions. *Rapid Commun. Mass Spectrom.* 1991, *5*, 406-414.
- [146] Drahos, L. and Vékey, K., *The meaning of effective temperature in the kinetic method*, in *46th ASMS Conference on Mass Spectroscopy and Allied Topics.* 1998. Orlando, Florida.
- [147] Drahos, L. and Vékey, K. Determination of the thermal energy and its distribution in peptides. *J. Am. Soc. Mass Spectrom.* 1999, *10*.

References

- [148] Drahos, L. and Vékey, K. How closely related are the effective and the real temperature. *J. Mass Spectrom.* 1999, 34, 79-84.
- [149] Gronowska, J.; Paradisi, C.; Traldi, P., and Vettori, U. A study of relevant parameters in collisional activation of ions in the ITMS. *Rapid Commun. Mass Spectrom.* 1990, 4, 306-315.
- [150] Johnston, H.S., *Gas-phase Reaction Rate Theory*. 1966, New York: The Ronald Press Company. 362.

Summary

This thesis contains a study on the applicability of surface-induced dissociation (SID) for mass spectrometric (MS) analysis. In the past decade, several research groups have made significant progress in the use of SID in mass spectrometry. The application of SID is especially promising for MS/MS of large molecules. It is assumed that internal energy is distributed statistically over the degrees of freedom of a molecule or rather, its ion. The larger an ion, the more degrees of freedom it has, and the more energy is required to make it dissociate in the limited time available in the mass spectrometer. Especially for ions of large molecules, kinetic energy is more efficiently converted to internal energy by the collision of an ion with a solid surface, compared to a collision with a gas phase compound.

In Chapter 2 of this thesis the implementation of SID in a tandem linear time-of-flight (TOF) instrument is described. We have chosen this instrument since TOF has an in principle unlimited mass range. However, for this initial study a relatively small ion, the radical cation of benzene, is used. The intention of this study is to elucidate the properties of a tandem TOF-SID mass analyzer with respect to ion yield and resolution, rather than to obtain high mass limits for SID. The fragmentation of the benzene radical cation by SID has been well characterized by others. To obtain a high fragment ion yield from the collision surface we have used a perfluorinated polyether liquid surface. This surface causes less neutralization of ions than a metal surface, while at the same time charging of the collision surface does not occur. We have determined the conversion efficiency of kinetic to internal energy by deconvolution of the SID fragment spectra as $30\pm 7\%$. This is comparable to the efficiency determined by others for a similar surface. To optimize both resolution in parent ion selection and fragment ion resolution we have implemented a pulsed voltage on the collision surface, so that ions with a mass-to-charge smaller than the parent ion are removed from the spectrum. With the time-focus at the collision surface we could optimize both the resolution for parent ion selection and the starting conditions for optimal resolution of the fragment ion spectrum. In spite of this, the SID spectrum in Chapter 2 demonstrates that the resolution in our tandem linear TOF set-up remains limited. In Chapter 2 we give an inventory of factors which are known to limit resolution. We have convoluted these factors to calculate their cumulative effect. It appears that the recoil kinetic energy distribution of fragments from the collision surface can not completely account for the low resolution, but that there must also be effects due to misalignment of the ion optics.

In Chapter 3 a comparative study between the tandem TOF SID set-up and a tandem quadrupole SID set-up is described. We have used the diphenyl ether radical cation as a model compound because it is somewhat larger than benzene but also volatile and can be photo ionized. We have applied a similar deconvolution as for benzene in

References

Chapter 2, to the SID fragment spectra of diphenyl ether. We have found that fundamental aspects such as internal energy deposition efficiency are, within the uncertainty of the experiments, independent of the configuration of the mass spectrometers when similar collision surfaces are used. In addition, we demonstrated that for the tandem TOF set-up an optimized fragment ion yield leads to limitations in observation of rearrangement fragmentation channels, because of competitive shift. Namely, in the TOF set-up sufficient fragment ion yields are obtained only with high acceleration fields after the collision surface. This reduces the time available for fragmentation to less than a microsecond and gives a different ratio of rearrangement fragments to direct cleavage fragments, compared to the tandem quadrupole instrument where the time available for fragmentation is approximately 5 microseconds. With perdeuterated diphenyl ether, ion/surface reaction products are observed. In addition, we investigated the ion/surface reactions upon collision of the rearrangement fragments of diphenyl ether.

In Chapter 4, we have applied SID as a tool to study the fragmentation behavior of various sizes and charge states of a new class of synthetic polymers: dendrimers. This study has been carried out with ESI/tandem quadrupole SID set-up of Wysocki and coworkers. The fragmentation efficiency of the protonated polypropylenamine (POPAM) dendrimers appeared to be independent of the charge state for the charge states studied. This indicates that destabilization by Coulomb repulsion is not important for the fragmentation of these dendrimer ions. The dendrimer result is in contrast with results obtained with peptides, for which dissociation is generally facilitated with higher charge state. In Chapter 4 we explain this contrast based on the absence of the need to 'mobilize' the charges to positions where they can initiate the low-energy charge-directed fragmentation reactions. In the POPAM dendrimers, the protons are already on positions where they can initiate fragmentation, because these positions have the lowest effective gas-phase basicity. For peptides the positions with the lowest gas-phase basicity are different from the positions where protons need to be to initiate low-energy fragmentations.

In the last chapter of this thesis, Chapter 5, we have determined the lowest-energy fragmentation channel of $\text{DAB}(\text{PA})_8\text{H}^+$ by collision-induced dissociation (CID) in an ion trap mass spectrometer (ITMS). In addition, we have used ITMS³ experiments to demonstrate that sequential fragmentation can occur. Energy-resolved CID fragment spectra of the POPAM dendrimer ions are measured in a Fourier transform ion cyclotron resonance mass spectrometer (FTMS). By comparing the SID experimental results with RRKM calculated dissociation rates, critical energies of 1.4-1.6 eV are estimated for the fragmentation of the POPAM dendrimers. Since the time available for dissociation in the CID experiments is much longer than the time available in the SID experiments (seconds compared to microseconds), the internal energy needed for fragmentation of the dendrimers with FTMS CID is lower than with quadrupole SID. From the RRKM calculated dissociation rates the FTMS energy-resolved CID diagrams were reconstructed. We have reasoned that, because the energy conversion occurs at a finite rate, and the ions are subject to collisional and radiative cooling processes, the internal energy of the

DAB(PA)₈H⁺ ions varies during the experiment. We have estimated a time-dependent internal energy profile of DAB(PA)₈H⁺ ions during the FTMS experiments and based on this we have calculated relative fragment ion abundances for a range of kinetic energies. Since the time during which the ion has a high level of internal energy is shorter than the duration of the FTMS experiment, more energy is needed to obtain fragmentation compared to when the internal energy of the ions would be constant.

In all chapters, the fragment spectra have been recorded over a range of collision energies. Energy-resolved fragment spectra of compounds of known activation energies have been used for the characterization of the energy deposition during SID in Chapters 2 and 3. In Chapter 4 and 5 energy-resolved fragmentation has been applied for the clarification of fragmentation behavior of the dendrimer quasi-molecular ion.

Samenvatting

Dit proefschrift behandelt de toepassing van oppervlaktegeïnduceerde dissociatie (SID) voor massaspectrometrische analyse. Onder massaspectrometrie (MS) verstaan we het bepalen van de component(en) uit een monster aan de hand van de verhouding tussen de massa en de elektrische lading. Elektrische lading hebben we door “ioniseren” aan deze componenten gegeven. Moleculen die uit verschillende aantallen atomen of uit verschillende soorten atomen bestaan, hebben een verschillende massa. Omdat ze een lading hebben, kunnen de elektrisch geladen moleculen, d.w.z. ionen, makkelijk in het luchtledige van de massaspectrometer gemanipuleerd, gescheiden en waargenomen worden. In een massaspectrometer kan de verhouding tussen massa en lading van een ion gemeten worden, en zodoende worden de moleculen “gewogen”. Nu is het mogelijk dat ionen verschillende structuren maar dezelfde massa-ladingsverhouding (m/z) hebben. Het wegen van fragmenten van die ionen kan dan helpen. Om ionen te laten fragmenteren moeten we geweld gebruiken om de ionen van binnen warm te maken, zodat ze makkelijk uit elkaar vallen. Een veelgebruikte methode hiervoor is het laten botsen van ionen met gasvormige atomen (CID). Voor grote moleculen is echter meestal meer inwendige energie nodig om ze kapot te maken dan voor kleine moleculen. In de in dit proefschrift beschreven experimenten worden fragmenten gevormd door het botsen van ionen op een vast oppervlak. SID is halverwege de jaren '80 geïntroduceerd als alternatieve methode om fragmenten te maken. Deze methode wordt echter nog niet routinematig toegepast zoals bij gasfasebotsingen het geval is. In tegenstelling tot bij CID groeit bij SID de grootte van hetgeen waarmee gebotst wordt, mee met het botsende ion. SID wordt vooral als interessante methode gezien om ionen gemaakt van grote moleculen, zoals synthetische polymeren en eiwitten, te fragmenteren.

In hoofdstuk 2 van dit proefschrift wordt de implementatie beschreven van SID in een vluchttijdmassaspectrometer (TOF-MS). Een TOF-MS geeft de m/z van ionen weer doordat verschillen in m/z resulteren in verschillen in vluchttijd. We hebben voor een TOF-MS gekozen omdat deze in principe een onbeperkt massabereik heeft. Met deze eerste studie wilden we voornamelijk de eigenschappen van onze TOF-MS aangaande ionenopbrengst en oplossend vermogen onderzoeken. Derhalve hebben we voor deze verkennende studie voor een ion van een vrij klein molecuul gekozen, namelijk het positief geladen ion van benzeen. De fragmentatie van dit “radicaalkation” met SID is reeds goed gekarakteriseerd door anderen. Om een hoge opbrengst aan fragmenten vanaf het oppervlak te krijgen, hebben we een oppervlak gebruikt bestaande uit een vloeibare, geperfluoreerde polyether. Het was bekend dat met een dergelijk oppervlak de neutralisatie van de ionen beperkt is. Bovendien treedt geen oplading van dit oppervlak op door de botsingen van de geladen deeltjes. Uit de SID-fragmentspectra van benzeen hebben we de omzetting van botsingsenergie naar inwendige energie met dit oppervlak in

References

de tandem lineaire TOF-MS bepaald. Deze bedraagt 30 ± 7 %. Dit is vergelijkbaar met de omzetting die door anderen was bepaald voor een gefluoreerd "self-assembled monolayer" oppervlak in een tandem quadropoolmassaspectrometer (QMS). Deze energieomzetting is veel hoger dan die verkregen met gasfasebotsingen. We hebben ernaar gestreefd om zowel de selectie van het te botsen molecuul als de onderscheidbaarheid van de fragmenten in het fragmentspectrum optimaal te maken. Daartoe hebben we de elektrische spanning op het botsoppervlak gepulst gemaakt. Hierdoor kunnen ionen met een m/z lager dan die van het gewenste ion uit het SID-fragmentspectrum verwijderd worden. Dankzij de gepulste spanning botsen ze namelijk veel harder met het oppervlak. De te fragmenteren ionen worden om twee redenen in de tijd gefocusseerd op het botsoppervlak. Ten eerste willen we een zo goed mogelijke scheiding krijgen tussen alle ionen die bij ionisatie zijn ontstaan, opdat de gepulste selectie optimaal is. Ten tweede willen we de fragmenten zo veel mogelijk op hetzelfde tijdstip laten ontstaan. Zo kunnen vluchttijden van fragmenten met verschillende massa zo goed mogelijk gescheiden worden. Desondanks laat het SID-spectrum zien dat scheiding tussen de fragmenten niet zo goed is vergeleken met wat er met andere massaspectrometers bereikt kan worden. Daarom hebben we een inventarisatie gemaakt van de factoren die in onze massaspectrometer de resolutie kunnen beperken. We hebben de gezamenlijke invloed van deze factoren berekend. Hieruit bleek dat de verdeling van snelheden waarmee de fragmenten van het botsoppervlak terugkaatsen niet helemaal de lage resolutie kon verklaren. Er zijn waarschijnlijk ook onvolmaaktheden in de ionenoptiek.

Hoofdstuk 3 behelst een vergelijkende studie tussen de tandem lineaire TOF-MS en een tandem QMS. In deze studie hebben we het radicaalkation van difenylether gebruikt als modelverbinding. Dit is iets groter dan benzeen maar ook vluchtig en kan met laserlicht geïoniseerd worden. Om de omzetting van kinetische naar interne energie te bepalen, hebben we eenzelfde deconvolutie van het fragmentspectrum gedaan als voor benzeen. Ons is gebleken dat fundamentele aspecten zoals omzetting van energie onafhankelijk zijn van de configuratie van de massaspectrometers, mits vergelijkbare botsoppervlakken gebruikt worden. Daarbij hebben we laten zien dat voor de tandem TOF-MS de geoptimaliseerde opbrengst aan fragmenten leidt tot beperkte waarneming van omleggingsfragmenten, vanwege competitieve verschuiving. Dit houdt in dat een fragment dat een lage activeringsenergie nodig heeft maar een lange tijd nodig heeft om gevormd te worden (dit is meestal het geval bij de zogenaamde omleggingsfragmenten), altijd maar in zeer beperkte mate waargenomen wordt indien de beschikbare tijd kort is, ook al is de inwendige energie hoog. Fragmenten waarvoor de benodigde inwendige energie hoger is, maar waarvan de vorming veel sneller is (meestal het geval bij directe-breekfragmenten), worden in grotere mate waargenomen. Om de opbrengst aan fragmenten in de TOF-MS hoog genoeg te maken, hebben we namelijk de versnelvelden in de massaspectrometer sterker gemaakt. Hierdoor is ook de snelheid van de ionen groter geworden en de beschikbare tijd voor fragmenteren korter (minder dan een miljoenste

seconde). Hierdoor wordt een andere verhouding gevonden tussen omleggingsfragmenten en de directe-breukfragmenten met de TOF-MS, dan met de tandem QMS, waar de tijd beschikbaar voor fragmentatie ongeveer vijf maal een miljoenste seconde is. Met behulp van difenylether waarvan alle waterstofatomen vervangen zijn door deuteriumatomen, die per atoom twee maal zo zwaar zijn, hebben we reacties tussen de ionen van difenylether en het oppervlak waar kunnen nemen. Deze reacties konden worden aangetoond doordat er fragmenten in het SID spectrum verschenen met een massa die niet overeenkwam met een mogelijke combinatie van de deuteriumatomen van het gebotste ion, maar een massa tussen deze mogelijke waarden in. Dit duidt aan dat er tijdens de botsing waterstofatomen, afkomstig van een gekozen waterstofbevattend oppervlak, meegegaan zijn met het botsende ion. Daarnaast hebben we, op dezelfde manier, de ion-oppervlakreacties bestudeerd van de omleggingsfragmenten van het radicaalkation van difenylether.

In Hoofdstuk 4 hebben we SID toegepast om het fragmentatiegedrag van verschillende groottes en ladingstoestanden te bestuderen van een nieuwe klasse van synthetische polymeren: dendrimeren. Deze studie is uitgevoerd met behulp van de elektropray/tandem QMS van Wysocki en medewerkers. Het gemak van fragmentatie van de geprotoneerde polypropylenamine (POPAM) dendrimeren bleek onafhankelijk te zijn van de ladingstoestand, althans voor de bestudeerde ladingstoestanden. Dit geeft aan dat destabilisatie door Coulombrepulsie binnen het ion niet belangrijk is voor de fragmentatie van deze ionen. Dit resultaat met de dendrimeren staat in contrast met eerder verkregen resultaten voor peptiden. Voor peptiden wordt de dissociatie over het algemeen wel vergemakkelijkt door een hogere ladingstoestand. Bij de POPAM dendrimeren is de noodzaak niet aanwezig om de protonen te 'mobiliseren' naar plaatsen waar ze laagenergetische fragmentatiereacties kunnen bevorderen. Hier zitten de protonen reeds op plaatsen waar ze de fragmentatie kunnen bevorderen, omdat deze posities de laagste gasfasebasiciteit hebben binnen het ion. Bij peptiden zijn de plaatsen met de laagste gasfasebasiciteit verschillend van de plaatsen waar de protonen nodig zijn om de laagenergetische fragmentatiereacties te bevorderen. Hierbij geldt dat hoe meer protonen er aanwezig zijn (hoe hoger de ladingstoestand), hoe makkelijker de protonen naar de plaatsen met lagere gasfasebasiciteit gebracht kunnen worden. Daarom bevordert een hogere ladingstoestand het gemak van dissociëren wel voor peptiden.

In Hoofdstuk 5 hebben we vastgesteld wat het laagstenergetische fragmentatiekanaal van het geprotoneerde POPAM dendrimeer $\text{DAB(PA)}_8\text{H}^+$ is door CID in een ionenvalmassaspectrometer (ITMS). Daarnaast hebben we de fragmenten weer laten fragmenteren (ITMS³) om te laten zien dat fragmenten mogelijk sequentieel gevormd kunnen worden. Met behulp van een Fourier-transform ion-cyclotronresonantie massaspectrometer (FTMS) hebben we de ionen van de POPAM dendrimeren laten fragmenteren na meervoudige laagenergetische gasfasebotsingen. Dit proces hebben we als functie van de botsingsenergie van de ionen bekeken en vergeleken met SID. Op basis van de experimentele resultaten met SID hebben we een schatting gemaakt van de relatie tussen de inwendige energie en de fragmentatiesnelheid van de ionen. Ook hebben we

References

theoretische berekeningen gedaan aangaande de relatie tussen inwendige energie en fragmentatiesnelheid voor het dendrimeer $\text{DAB}(\text{PA})_8\text{H}^+$. Deze resultaten zijn redelijk in overeenstemming. Doordat de beschikbare tijd voor fragmentatie in de FTMS CID experimenten veel langer is dan die in de SID-experimenten (10 seconden tegenover een paar miljoenste van een seconde) is de benodigde inwendige energie om de ionen te laten fragmenteren, lager. De hoeveelheden fragmentionen bij een bepaalde botsingsenergie met CID hebben we ook op grond van de theoretische berekeningen bepaald. In eerste benadering lijken deze resultaten minder goed in overeenstemming: in de praktijk is veel meer interne energie nodig in de FTMS dan volgens de berekening. Ter verklaring hebben we beredeneerd, dat in de FTMS CID experimenten de ionen binnen de tijd van het experiment met een bepaalde snelheid hun inwendige energie verkrijgen en weer verliezen. Dit is anders dan bij de QMS SID experimenten, waarbij de bewegingsenergie onmiddellijk naar inwendige energie omgezet wordt en de tijd te kort is voor de ionen om af te kunnen koelen. Door het proces van opwarmen en afkoelen in de FTMS hebben de ionen korter de tijd om uit elkaar te vallen dan het experiment duurt. Daardoor moet de inwendige energie waarbij de fragmentatie verloopt hoger zijn dan verwacht op grond van de tijdsduur van het experiment.

In alle hoofdstukken zijn de fragmentspectra opgenomen over een bepaald gebied van botsingsenergieën. Energieopgeloste fragmentspectra van verbindingen met bekende activeringsenergieën zijn gebruikt voor de karakterisering van de energieomzetting door SID in de Hoofdstukken 2 en 3. In Hoofdstukken 4 en 5 wordt energieopgeloste fragmentatie toegepast om fragmentatiegedrag van de quasi-moleculaire ionen van dendrimeren op te helderen.

Nawoord

Allereerst wil ik mijn promotor Piet Kistemaker en mijn copromotor Tina Weeding bedanken voor hun inzet en begeleiding bij de totstandkoming van dit proefschrift. Tina, ik heb er veel van geleerd dat je mij steeds gedwongen hebt mijn relatieve begrippen te concretiseren. Piet, je hebt mij door telkens weer de zaken om te draaien laten inzien dat het resultaat vaak verbeterd kan worden als dingen van de andere kant bekeken worden. Hoewel ik altijd heb geprobeerd zo eigenwijs mogelijk te zijn, moest ik toch vaak gehoor geven aan jullie adviezen. Regelmatig heb ik jullie in gedachten mijn wetenschappelijke ouders genoemd. Streng, maar altijd het beste met mij voor hebbend. Voor het beschrijven van de waardevolle bijdragen die jullie aan de totstandkoming van dit proefschrift hebben geleverd, is dit nawoord eigenlijk te kort.

Jaap Beijersbergen, dank voor de bergen die je me hebt helpen verzetten in de eerste jaren van mijn promotieonderzoek. Of waren het windmolens waar we destijds de strijd mee aanbonden? Ron, Sander en Marc wil ik bedanken voor hun hulp bij het FTMS-werk. Laszlo Drahos and Karoly Vékey, thank you for the RRKM calculations (Chapter 5) and the helpful and stimulating discussions. De mensen van andere groepen, hier wil ik met name Aart Kleyn en Wim Koppers bedanken, die eveneens aan SID hebben gewerkt maar met een andere invalshoek.

I would like to thank the members of the Wysocki Vultures from Tucson: Chuck thank you for repeating the data acquisition for me with much higher accuracy than what I was able to obtain in the few weeks that I could work with the instrumentation. Árpád thank you for your help, friendship and hospitality during and after my stay in Tucson, Vicki for your hospitality, help and advice, and also Hari, Ashok, Vince, Norman, Wendy for giving me an enjoyable stay. Also thanks go to my roommates during my second stay in Tucson, for making me feel at home. Some thanks go without saying.

De leden van de gebruikerscommissie van het SID-project wil ik bedanken voor hun goede suggesties en adviezen.

Mijn groepsgenoten en oud-groepsgenoten (en dat zijn er intussen heel wat in de vijfentwintig jaar die ik op Amolf heb doorgebracht) bedank ik in willekeurige volgorde voor de prettige samenwerking en samen-ontspanning: António, Oscar, Gisela, Jos P. Peter A., Erik v/d H, Ivana, Gert (bedankt voor alle hulp bij problemen met de computer), Chris, Gerard, Ron, Jan, Marc, Annebeth, Jerre, Nicholas, Jorrit, Georgiana, Leo, Inez, Linda, Klaas-Jan, Vincent, Jaap, Jaap, Liz, Muriël, Marike.

Overige Amolf-medewerkers met wie ik het contact als aangenaam heb ervaren zijn er te veel om op te noemen. Ik wil ook de ondersteunende groepen van Amolf bedanken, ten eerste zijn daar de groepstechnici, Ilja, Michel, Ad, die mij bij grote en kleine problemen hebben bijgestaan, de technische ondersteuning in het algemeen heel E&I en

References

met name Dennis en Idsart, de tekenkamer, de mechanische werkplaats, de administratieve ondersteuning en de huishoudelijke dienst o.a. voor het schoonhouden van mijn werkplekken. Henk Sodenkamp wil ik bedanken voor de grafische ondersteuning bij het vervaardigen van de kaft voor mijn proefschrift. Ook speciaal wil ik de toenmalige leden van de instituuts-personeelsraad van AMOLF (Tine, René, Wim, Oscar, Liesbeth, Dick) en de centrale ondernemingsraad van FOM bedanken voor de leerzame samenwerking in mijn medezeggenschapsjaren. Ook de opposenten van deze raden hebben bijgedragen hieraan, waarvoor mijn dank.

Ed, je hebt mij zeer vaak en met plezier geholpen om Wendelien op tijd van de crèche te halen, en mij in vele zaken met raad en daad ondersteund. Hierbij is ook de bijdrage van Helen niet onbelangrijk geweest.

Mijn ouders, jullie hebben mij altijd de mogelijkheid gegeven om de richting te kiezen die ik op wilde, en me daarbij van harte gesteund. Mijn schoonouders wil ik ook bedanken voor alle hulp met wat dan ook.

Wendelien, omdat je mij amper slapeloze nachten maar wel heel veel moedergeluk hebt bezorgd heb je onmetelijk veel bijgedragen aan mijn geestelijk welbevinden. Hierdoor waren er voor mij niet veel excuses om niet aan mijn proefschrift te werken, behalve dat jij ook af en toe wat aandacht wilde.

Remco, je was in het algemeen mijn steun en toeverlaat. Mijn dank voor het nog in de kleine uurtjes op de laatste dag corrigeren van de concept-samenvatting.

Ik hoop dat ik nu niemand ben vergeten.

